

DESIGN, CONTROL AND OPTIMIZATION OF VEHICLE SUSPENSIONS WITH
INERTERS

A THESIS SUBMITTED TO
THE GRADUATE SCHOOL OF NATURAL AND APPLIED SCIENCES
OF
MIDDLE EAST TECHNICAL UNIVERSITY

BY

OZAN GERGER

IN PARTIAL FULFILLMENT OF THE REQUIREMENTS
FOR
THE DEGREE OF MASTER OF SCIENCE
IN
MECHANICAL ENGINEERING

SEPTEMBER 2013

Approval of the thesis:

**DESIGN, CONTROL AND OPTIMIZATION OF VEHICLE SUSPENSIONS WITH
INERTERS**

submitted by **OZAN GERGER** in partial fulfillment of the requirements for the degree of
**Master of Science in Mechanical Engineering Department, Middle East Technical Uni-
versity** by,

Prof. Dr. Canan Özgen
Dean, Graduate School of **Natural and Applied Sciences**

Prof. Dr. Suha Oral
Head of Department, **Mechanical Engineering**

Assist. Prof. Dr. Ender Ciğeroğlu
Supervisor, **Mechanical Engineering Dept., METU**

Inst. Dr. Çağlar Başlamışlı
Co-supervisor, **Mechanical Engineering Dept., Hacettepe University**

Examining Committee Members:

Prof. Dr. Y. Samim Ünlüsoy
Mechanical Engineering Department, METU

Assist. Prof. Dr. Ender Ciğeroğlu
Mechanical Engineering Department, METU

Inst. Dr. Çağlar Başlamışlı
Mechanical Engineering Department, Hacettepe University

Assist. Prof. Dr. Gökhan O. Özgen
Mechanical Engineering Department, METU

Prof. Dr. M. Kemal Leblebicioğlu
Electrical and Electronics Department, METU

Date:

I hereby declare that all information in this document has been obtained and presented in accordance with academic rules and ethical conduct. I also declare that, as required by these rules and conduct, I have fully cited and referenced all material and results that are not original to this work.

Name, Last Name: OZAN GERGER

Signature :

ABSTRACT

DESIGN, CONTROL AND OPTIMIZATION OF VEHICLE SUSPENSIONS WITH INERTERS

Gerger, Ozan

M.S., Department of Mechanical Engineering

Supervisor : Assist. Prof. Dr. Ender Cigeroğlu

Co-Supervisor : Inst. Dr. Çağlar Başlamışlı

September 2013, 97 pages

Inerter is proposed as a mechanical equivalent of the capacitors available in electric circuits. The main advantage of the inerter is to provide a wider design space for a vehicle suspension by adding another suspension element next to spring and damper. Therefore, fine tuning of a suspension performance can be made without subjected to heavy trade-offs. The effect of the addition of inerter to a vehicle suspension and performance of the selected suspension arrangements with passive and semi-active inerters are investigated in this study by using ISO standards.

At first, mathematical models of the suspension systems are constructed. In this scope, configurations that are analyzed in this study which are quarter-car model of standard suspension, passive parallel inerter, passive serial inerter and semi-active serial inerter; half-car model of standard suspension, passive serial inerter and semi-active serial inerter are explained with schematics and equations. New type of semi-active inerter control method is proposed based on a sky-hook damping control system. Furthermore, the effect of the inerter on the vertical vehicle dynamics in frequency domain is explained by using the quarter-car models.

In the second part of the study, ISO-8608 road profiles are constructed for optimization and performance evaluation purposes. Optimization of the passive suspension parameters are made. Before proceeding into the optimizations, the effect of the inertance, inerter stiffness and suspension damping on the performance of the suspension with passive serial inerter are presented. After the parameters are chosen, the performance of the suspension systems with passive serial inerter and semi-active serial inerter are compared with the standard suspension by using the ISO-2631 ride comfort evaluation methods. Performance evaluations are

based on ride quality, tire deflection and suspension deflection in time domain, ride quality in frequency domain. Furthermore, suspension performance when the vehicle passing over a standard hump profiles are also evaluated.

Finally, using standard bump profiles and ISO-8608 road profiles simulations are made and the results are presented.

Keywords: Inerter, Passive Serial Inerter, Semi-Active Serial Inerter, Semi-Active Suspension, Passive Suspension, Mathematical Modeling, ISO-8608 Road Profiles, ISO-2631 Ride Comfort Analysis

ÖZ

İNERTER İÇEREN ARAÇ SÜSPANSİYONLARININ TASARIMI, KONTROLÜ VE OPTİMİZASYONU

Gerger, Ozan

Yüksek Lisans, Makina Mühendisliği Bölümü

Tez Yöneticisi : Yrd. Doç. Dr. Ender Cigeroğlu

Ortak Tez Yöneticisi : Öğr. Gör. Dr. Çağlar Başlamışlı

Eylül 2013 , 97 sayfa

İnerter elemanı, elektronik devrelerdeki kapasitörün eşleniği olarak sunulmuştur. İnerterin getirdiği esas avantaj, yay ve sönümleyici süspansiyon elemanlarının yanına yeni bir eleman eklenmesi sonucunda tasarım düzleminin genişlemesidir. Böylelikle süspansiyon performansının ikilemlere maruz kalmadan daha ince bir şekilde ayarlanabilmektedir. Bu çalışmada, araç süspansiyonuna inerter eklenmesinin etkileri, pasif ve yarı-aktif inertere sahip belirli süspansiyon konfigürasyonlarının performansı, ISO standartları kullanılarak incelenmiştir.

Öncelikle süspansiyon sistemlerinin matematiksel modelleri oluşturulmuştur. Bu kapsamda, çeyrek araç modeli şeklinde standard süspansiyon, pasif paralel inerter, pasif seri inerter ve yarı-aktif seri inerter; yarım araç modeli şeklinde standard süspansiyon, pasif seri inerter ve yarı-aktif seri inerter, şemalar ve denklemlerle açıklanmıştır. Yeni tip yarı-aktif inerter kontrol metodu önerilmiştir. Bunlara ek olarak, inerterin dikey araç dinamikleri(frekans düzleminde) üzerindeki etkileri, çeyrek araç modelleri kullanılarak açıklanmıştır.

Çalışmanın ikinci bölümünde, optimizasyon ve performanse değerlendirme amaçları için ISO-8608 yol profilleri oluşturulmuştur. Pasif süspansiyon parametrelerinin optimizasyonları yapılmıştır. Optimizasyonlara başlanmadan önce, inerter efektif kütlelerinin, inerter direngenliğinin ve süspansiyon sönümleme katsayısının, pasif seri inerter içeren süspansiyonun performansı üzerindeki etkileri gösterilmiştir. Parametreler seçildikten sonra ise pasif seri ve yarı-aktif seri inerter içeren süspansiyonların performansları, ISO-2631 sürüş konforu değerlendirme yöntemleri kullanılarak, standard süspansiyonun performansı ile karşılaştırılmıştır. Performans değerlendirmeleri zaman düzleminde sürüş kalitesine, teker deplasmanına ve süspansiyon deplasmanına, frekans düzleminde ise sürüş kalitesine bakılarak yapılmıştır. Bunlara ek

olarak, standart kasis profillerinden geçen aracın süspansiyon performansları da değerlendirilmiştir.

Son kısımda ise standart kasis profilleri ve ISO-8608 yol profilleri kullanılarak simülasyonlar yapılmış ve sonuçlar verilmiştir.

Anahtar Kelimeler: Inerter, Pasif Seri Inerter, Yarı-Aktif Seri Inerter, Pasif Süspansiyon, Yarı-Aktif Süspansiyon, Matematiksel Modelleme, ISO-8608 Yol Profilleri, ISO-2631 Sürüş Konforu Analizi

To My Father and Mother

ACKNOWLEDGMENTS

First of all, I want to express my sincere appreciation to Asst. Prof. Dr. Ender CİĞEROĞLU and Inst. Dr. Çağlar S. BAŞLAMIŞLI for their support, guidance, helpful and positive comments throughout the progress of my thesis study.

I would like to thank my colleague Gökhan YAŞAR in ASELSAN Inc. for his support and friendship.

I would like to express my special thanks to my father, mother and cousin for their endless love, patience and support.

Also thanks to ASELSAN Inc. for giving the opportunity of this study by providing necessary permissions.

TABLE OF CONTENTS

ABSTRACT	v
ÖZ	vii
ACKNOWLEDGMENTS	x
TABLE OF CONTENTS	xi
LIST OF TABLES	xiv
LIST OF FIGURES	xv
LIST OF ABBREVIATIONS	xxii
CHAPTERS	
1 INTRODUCTION	1
1.1 Literature Review	8
1.2 Scope of Thesis	11
1.3 Outline	12
2 MATHEMATICAL MODELING OF VEHICLE SUSPENSIONS	15
2.1 Passive Quarter-Car Models	15
2.1.1 Quarter-Car Model of Standard Suspension	16
2.1.2 Quarter-Car Model of Passive Serial Inerter	16
2.1.3 Quarter-Car Model of Passive Parallel Inerter	17
2.1.4 Semi-Active Inerter	18

2.1.5	Quarter Car Model of Semi-Active Serial Inerter	19
2.2	Semi-Active Quarter Car Models	19
2.2.1	Quarter Car Model of Semi-Active Parallel Inerter	20
2.3	Half-Car Models	20
2.3.1	Pitch-Oriented Half-Car Model of Passive Standard Suspension	21
2.3.2	Pitch-Oriented Half-Car Model of Passive Serial Inerter	22
2.3.3	Pitch-Oriented Half-Car Model of Semi-Active Parallel Inerter	23
2.3.4	Pitch-Oriented Half-Car Model of Semi-Active Serial Inerter	24
2.4	Parameters Used in Mathematical Models	25
3	FREQUENCY RESPONSES OF VEHICLE SUSPENSIONS	27
3.1	Introduction	27
3.2	State-Space Models of Vehicle Suspensions	27
3.2.1	State-Space Model of Passive Serial-Inerter	27
3.2.2	State-Space Model of Passive Standard Suspension	28
3.2.3	Transfer Functions of the Vehicle Suspensions	29
3.2.4	Frequency Responses	29
4	RANDOM ROAD PROFILE MODELING	35
4.1	ISO-8608 Road Profiles	35
5	OPTIMIZATION	41
5.1	Introduction	41
5.2	Optimization with ISO Roads	42
5.3	Semi-Active Suspension comparison with Passive Suspensions	46

5.4	The Effect of Change of Suspension Damping on Inerter Performance	49
6	RIDE COMFORT EVALUATION	63
6.1	ISO-2631 Comfort Frequency Weightings	63
7	SIMULATIONS	73
7.1	ISO-8608 Road Simulations	73
7.2	Hump Simulations	79
7.2.1	Standard Circular Hump	79
7.2.2	Standard Trapezoidal Hump	84
8	CONCLUSION AND FUTURE WORK	91
8.1	Conclusion	91
8.2	Future Work	92
	REFERENCES	93
	APPENDICES	
A	SIMULINK MODELS OF HALF-CAR MODELS	95

LIST OF TABLES

TABLES

Table 2.1	Parameters Kept Constant and Used in Pre-Optimized Analysis'	25
Table 3.1	Inerter Parameters used in ADAMS® Inerter Model	32
Table 4.1	Road Roughness Classification	35
Table 4.2	Road Generation Parameters	37
Table 5.1	Parameters Used in Optimization	57
Table 5.2	Lower and Upper Bounds of Parameters to be Optimized	57
Table 5.3	Optimized Parameters	60
Table 5.4	Constant Vehicle Parameters	60
Table 6.1	ISO 2631 Frequency Weightings for Vertical Vibrations[11]	64
Table 6.2	ISO 2631 Comfort Ratings [3]	68
Table 7.1	Parameters Used in Half-Car Models	73

LIST OF FIGURES

FIGURES

Figure 1.1 Influence of parameter change on suspension performance[1]	2
Figure 1.2 Ideal inerter	3
Figure 1.3 Rack and pinion type mechanical inerter prototype developed in Cambridge University Engineering Department[4]	4
Figure 1.4 Screw-ball type mechanical inerter prototype developed in Cambridge University Engineering Department[5]	4
Figure 1.5 Schematic of mechanical inerters	5
Figure 1.6 Inerter in series with spring and damper[4]	5
Figure 1.7 Schematic of inerter in series with spring and damper	6
Figure 1.8 Parallel inerter-spring-damper[6]	6
Figure 1.9 Parallel inerter-spring-damper schematic	6
Figure 1.10 Hydraulic inerter prototype developed in National Taiwan University[3] . .	7
Figure 1.11 Schematic of hydraulic inerter	7
Figure 1.12 Analogy between mechanical and electrical elements	8
Figure 1.13 Fluid inerter with damping schematic proposed by Cambridge Enterprise and Penske Racing Shocks[9]	9
Figure 1.14 Fluid inerter schematic proposed by Lotus-Renault GP LTD[10]	9
Figure 1.15 Semi-Active sky-hook inerter schematic	11
Figure 2.1 Quarter-car model of standard suspension	16
Figure 2.2 Quarter-car model of passive serial inerter	17
Figure 2.3 Quarter-Car Model of Passive Parallel Inerter	17

Figure 2.4 Sky-hook serial inerter schematic	18
Figure 2.5 Actuator model in Simulink® environment	19
Figure 2.6 Quarter-car model of semi-active serial inerter	19
Figure 2.7 Quarter-car model of semi-active parallel inerter	20
Figure 2.8 Pitch-oriented half-car model of passive standard suspension	21
Figure 2.9 Pitch-oriented half-car model of passive serial inerter	22
Figure 2.10 Pitch-oriented half-car model of semi-active parallel inerter	23
Figure 2.11 Pitch-oriented half-car model of semi-active serial inerter	24
Figure 3.1 Frequency response of the systems obtained by transfer functions of quarter-car models	30
Figure 3.2 Frequency response estimation of the systems modeled with quarter-car models (Sprung mass acceleration)	30
Figure 3.3 Frequency response estimation of the systems modeled with quarter-car models (Suspension deflection)	31
Figure 3.4 Frequency response estimation of the systems modeled with quarter-car models (Tire deflection)	31
Figure 3.5 Detailed view of the inerter modeled in ADAMS®	32
Figure 3.6 Suspension systems modeled in ADAMS®/View	33
Figure 3.7 Frequency response of the sprung mass accelerations obtained by ADAMS®/Vibration	33
Figure 3.8 Superposed frequency responses of sprung mass acceleration	34
Figure 4.1 ISO-8608 PSD Lines	36
Figure 4.2 Generated B-class ISO-8608 road profile for $V=30$ kph	37
Figure 4.3 PSD lines of B-class ISO-8608 road profile for $V=30$ kph	38
Figure 4.4 Generated B-class ISO-8608 road profile for $V=60$ kph	38
Figure 4.5 PSD lines of B-class ISO-8608 road profile for $V=60$ kph	39
Figure 4.6 Generated B-class ISO-8608 road profile for $V=90$ kph	39
Figure 4.7 PSD lines of B-class ISO-8608 road profile for $V=90$ kph	40

Figure 5.1 J_3 vs. J_1 with different inertance values at $V=30\text{kph}$ (Passive serial inerter, $k_{inrt} = 35000N/m$, $c_{inrt} = 2000Ns/m$, $k_s = 15000N/m$, $c_s = 900Ns/m$) . .	43
Figure 5.2 J_3 vs. J_2 with different inertance values at $V=30\text{kph}$ (Passive serial inerter, $k_{inrt} = 35000N/m$, $c_{inrt} = 2000Ns/m$, $k_s = 15000N/m$, $c_s = 900Ns/m$) . .	43
Figure 5.3 J_3 vs. J_1 with different inertance values at $V=60\text{kph}$ (Passive serial inerter, $k_{inrt} = 35000N/m$, $c_{inrt} = 2000Ns/m$, $k_s = 15000N/m$, $c_s = 900Ns/m$) . .	44
Figure 5.4 J_3 vs. J_2 with different inertance values at $V=60\text{kph}$ (Passive serial inerter, $k_{inrt} = 35000N/m$, $c_{inrt} = 2000Ns/m$, $k_s = 15000N/m$, $c_s = 900Ns/m$) . .	44
Figure 5.5 J_3 vs. J_1 with different inertance values at $V=90\text{kph}$ (Passive serial inerter, $k_{inrt} = 35000N/m$, $c_{inrt} = 2000Ns/m$, $k_s = 15000N/m$, $c_s = 900Ns/m$) . .	45
Figure 5.6 J_3 vs. J_2 with different inertance values at $V=90\text{kph}$ (Passive serial inerter, $k_{inrt} = 35000N/m$, $c_{inrt} = 2000Ns/m$, $k_s = 15000N/m$, $c_s = 900Ns/m$) . .	45
Figure 5.7 J_3 vs J_1 with different inertance values at $V=30\text{kph}$ (Passive serial inerter and semi-active serial inerter, $k_{inrt} = 35000N/m$, $c_{inrt} = 2000Ns/m$, $k_s =$ $15000N/m$, $c_s = 900Ns/m$)	46
Figure 5.8 J_3 vs J_2 with different inertance values at $V=30\text{kph}$ (Passive serial inerter and semi-active serial inerter, $k_{inrt} = 35000N/m$, $c_{inrt} = 2000Ns/m$, $k_s =$ $15000N/m$, $c_s = 900Ns/m$)	46
Figure 5.9 J_3 vs J_1 with different inertance values at $V=60\text{kph}$ (Passive serial inerter and semi-active serial inerter, $k_{inrt} = 35000N/m$, $c_{inrt} = 2000Ns/m$, $k_s =$ $15000N/m$, $c_s = 900Ns/m$)	47
Figure 5.10 J_3 vs J_2 with different inertance values at $V=60\text{kph}$ (Passive serial inerter and semi-active serial inerter, $k_{inrt} = 35000N/m$, $c_{inrt} = 2000Ns/m$, $k_s =$ $15000N/m$, $c_s = 900Ns/m$)	47
Figure 5.11 J_3 vs J_1 with different inertance values at $V=90\text{kph}$ (Passive serial inerter and semi-active serial inerter, $k_{inrt} = 35000N/m$, $c_{inrt} = 2000Ns/m$, $k_s =$ $15000N/m$, $c_s = 900Ns/m$)	48
Figure 5.12 J_3 vs J_2 with different inertance values at $V=90\text{kph}$ (Passive serial inerter and semi-active serial inerter, $k_{inrt} = 35000N/m$, $c_{inrt} = 2000Ns/m$, $k_s =$ $15000N/m$, $c_s = 900Ns/m$)	48
Figure 5.13 J_3 vs J_1 with different inertance values at $V=30\text{kph}$ (Passive serial inerter and semi-active serial inerter, $k_{inrt} = 35000N/m$, $c_{inrt} = 2000Ns/m$, $k_s =$ $15000N/m$, $c_s = 1500Ns/m$)	49

Figure 5.14 J_3 vs J_2 with different inertance values at $V=30\text{kph}$ (Passive serial inerter and semi-active serial inerter, $k_{inrt} = 35000\text{N/m}$, $c_{inrt} = 2000\text{Ns/m}$, $k_s = 15000\text{N/m}$, $c_s = 1500\text{Ns/m}$)	49
Figure 5.15 J_3 vs J_1 with different inertance values at $V=60\text{kph}$ (Passive serial inerter and semi-active serial inerter, $k_{inrt} = 35000\text{N/m}$, $c_{inrt} = 2000\text{Ns/m}$, $k_s = 15000\text{N/m}$, $c_s = 1500\text{Ns/m}$)	50
Figure 5.16 J_3 vs J_2 with different inertance values at $V=60\text{kph}$ (Passive serial inerter and semi-active serial inerter, $k_{inrt} = 35000\text{N/m}$, $c_{inrt} = 2000\text{Ns/m}$, $k_s = 15000\text{N/m}$, $c_s = 1500\text{Ns/m}$)	50
Figure 5.17 J_3 vs J_1 with different inertance values at $V=90\text{kph}$ (Passive serial inerter and semi-active serial inerter, $k_{inrt} = 35000\text{N/m}$, $c_{inrt} = 2000\text{Ns/m}$, $k_s = 15000\text{N/m}$, $c_s = 1500\text{Ns/m}$)	51
Figure 5.18 J_3 vs J_2 with different inertance values at $V=90\text{kph}$ (Passive serial inerter and semi-active serial inerter, $k_{inrt} = 35000\text{N/m}$, $c_{inrt} = 2000\text{Ns/m}$, $k_s = 15000\text{N/m}$, $c_s = 1500\text{Ns/m}$)	51
Figure 5.19 J_3 vs J_1 with different inertance values at $V=30\text{kph}$ (Passive serial inerter and semi-active serial inerter, $k_{inrt} = 35000\text{N/m}$, $c_{inrt} = 2000\text{Ns/m}$, $k_s = 15000\text{N/m}$, $c_s = 1800\text{Ns/m}$)	52
Figure 5.20 J_3 vs J_2 with different inertance values at $V=30\text{kph}$ (Passive serial inerter and semi-active serial inerter, $k_{inrt} = 35000\text{N/m}$, $c_{inrt} = 2000\text{Ns/m}$, $k_s = 15000\text{N/m}$, $c_s = 1800\text{Ns/m}$)	52
Figure 5.21 J_3 vs J_1 with different inertance values at $V=60\text{kph}$ (Passive serial inerter and semi-active serial inerter, $k_{inrt} = 35000\text{N/m}$, $c_{inrt} = 2000\text{Ns/m}$, $k_s = 15000\text{N/m}$, $c_s = 1800\text{Ns/m}$)	53
Figure 5.22 J_3 vs J_2 with different inertance values at $V=60\text{kph}$ (Passive serial inerter and semi-active serial inerter, $k_{inrt} = 35000\text{N/m}$, $c_{inrt} = 2000\text{Ns/m}$, $k_s = 15000\text{N/m}$, $c_s = 1800\text{Ns/m}$)	53
Figure 5.23 J_3 vs J_1 with different inertance values at $V=90\text{kph}$ (Passive serial inerter and semi-active serial inerter, $k_{inrt} = 35000\text{N/m}$, $c_{inrt} = 2000\text{Ns/m}$, $k_s = 15000\text{N/m}$, $c_s = 1800\text{Ns/m}$)	54
Figure 5.24 J_3 vs J_2 with different inertance values at $V=90\text{kph}$ (Passive serial inerter and semi-active serial inerter, $k_{inrt} = 35000\text{N/m}$, $c_{inrt} = 2000\text{Ns/m}$, $k_s = 15000\text{N/m}$, $c_s = 1800\text{Ns/m}$)	54
Figure 5.25 J_4 vs. inertance, b_{inrt} at $V=30\text{kph}$ (Passive serial inerter, $k_{inrt} = 35000\text{N/m}$, $c_{inrt} = 2000\text{Ns/m}$)	55

Figure 5.26 J_4 vs. inertance, b_{inrt} at $V=60\text{kph}$ (Passive serial inerter, $k_{inrt} = 35000\text{N/m}$, $c_{inrt} = 2000\text{Ns/m}$)	55
Figure 5.27 J_4 vs. inertance, b_{inrt} at $V=90\text{kph}$ (Passive serial inerter, $k_{inrt} = 35000\text{N/m}$, $c_{inrt} = 2000\text{Ns/m}$)	56
Figure 5.28 Inertance trade-off curves for suspension with inerter	56
Figure 5.29 J_1 at $V=60\text{kph}$, A class road	57
Figure 5.30 J_2 at $V=60\text{kph}$, A class road	58
Figure 5.31 J_3 at $V=60\text{kph}$, A class road	58
Figure 5.32 J_4 at $V=60\text{kph}$, A class road	59
Figure 5.33 Optimization algorithm flowchart	59
Figure 5.34 Reduction in sprung mass acceleration RMS (J_1)	60
Figure 5.35 Reduction in sprung mass acceleration PSD (J_2)	61
Figure 5.36 Reduction in tire deflection RMS (J_3)	61
Figure 5.37 Reduction in overall cost function $\rho_1 J_1 + \rho_2 J_2 + \rho_3 J_3 + \rho_4 J_4$	62
Figure 6.1 Typical frequency ranges and magnitudes of interest for the study of motion sickness, whole-body vibration, and hand-transmitted vibration	64
Figure 6.2 Frequency weightings for vertical vibrations	66
Figure 6.3 Weighted PSDs of sprung mass acceleration for $V=30\text{kph}$ on B class road	67
Figure 6.4 Weighted PSDs of sprung mass acceleration for $V=60\text{kph}$ on B class road	67
Figure 6.5 Weighted PSDs of sprung mass acceleration for $V=90\text{kph}$ on B class road	68
Figure 6.6 Weighted sprung mass acceleration RMS values for $V=30\text{kph}$	69
Figure 6.7 Weighted sprung mass acceleration RMS values for $V=60\text{kph}$	69
Figure 6.8 Weighted sprung mass acceleration RMS values for $V=90\text{kph}$	70
Figure 6.9 Percentage reduction in passive serial inerter SMA RMS with respect to standard suspension	70
Figure 6.10 Percentage reduction in semi-active serial inerter SMA RMS with respect to standard suspension	71

Figure 6.11 Percentage reduction in semi-active serial inerter SMA RMS with respect to passive serial inerter	71
Figure 7.1 Simulation for standard suspension and passive serial inerter at $V=30\text{kph}$, B-class road	74
Figure 7.2 Simulation for standard suspension and semi-active serial inerter at $V=30\text{kph}$, B-class road	74
Figure 7.3 Simulation for standard suspension and passive serial inerter at $V=60\text{kph}$, B-class road	75
Figure 7.4 Simulation for standard suspension and semi-active serial inerter at $V=60\text{kph}$, B-class road	75
Figure 7.5 Simulation for standard suspension and passive serial inerter at $V=90\text{kph}$, B-class road	76
Figure 7.6 Simulation for standard suspension and semi-active serial inerter at $V=90\text{kph}$, B-class road	76
Figure 7.7 Force applied by inerter on the sprung mass at $V=30\text{kph}$, B-class road (passive serial inerter)	77
Figure 7.8 Force applied by spring-damper-inerter on the sprung mass at $V=30\text{kph}$, B-class road (passive serial inerter)	77
Figure 7.9 Force applied by inerter on the sprung mass at $V=30\text{kph}$, B-class road (semi-active serial inerter)	78
Figure 7.10 Force applied by spring-damper-inerter on the sprung mass at $V=30\text{kph}$, B-class road (semi-active serial inerter)	78
Figure 7.11 Force applied by spring-damper-inerter on the sprung mass at $V=30\text{kph}$, B-class road (semi-active serial inerter)	79
Figure 7.12 Standard circular hump profile	80
Figure 7.13 Peak sprung mass acceleration for different vehicle speeds	80
Figure 7.14 Vehicle passing over standard circular hump	81
Figure 7.15 Standard circular hump simulation for $V=20\text{kph}$	81
Figure 7.16 Standard circular hump simulation for $V=25\text{kph}$	82
Figure 7.17 Standard circular hump simulation for $V=30\text{kph}$	82

Figure 7.18 Standard circular hump simulation for $V=35\text{kph}$	83
Figure 7.19 Standard circular hump simulation for $V=40\text{kph}$	83
Figure 7.20 Standard circular hump simulation for $V=45\text{kph}$	84
Figure 7.21 Standard trapezoidal hump profile	84
Figure 7.22 Peak sprung mass acceleration for different vehicle speeds	85
Figure 7.23 Vehicle passing over standard trapezoidal hump	85
Figure 7.24 Standard trapezoidal hump simulation for $V=20\text{kph}$	86
Figure 7.25 Standard trapezoidal hump simulation for $V=25\text{kph}$	86
Figure 7.26 Standard trapezoidal hump simulation for $V=30\text{kph}$	87
Figure 7.27 Standard trapezoidal hump simulation for $V=35\text{kph}$	87
Figure 7.28 Standard trapezoidal hump simulation for $V=40\text{kph}$	88
Figure 7.29 Standard trapezoidal hump simulation for $V=45\text{kph}$	88
Figure A.1 Overview of half-car model of standard suspension	95
Figure A.2 Heave block of half-car model of standard suspension	95
Figure A.3 Pitch block of half-car model of standard suspension	96
Figure A.4 Front unsprung mass block of of half-car model of standard suspension	96
Figure A.5 Geometric relations block of of half-car model of standard suspension	96
Figure A.6 Overview of half-car model of semi-active serial inerter	97
Figure A.7 Controller block of half-car model of semi-active serial inerter	97

LIST OF ABBREVIATIONS

RMS	Root mean square
PSD	Power spectral density
SMA	Sprung mass acceleration

CHAPTER 1

INTRODUCTION

Road irregularities are the main source of the discomfort for the automobile users. Vehicle suspension systems are introduced as a mechanical filter to isolate the passengers from the effects of the road irregularities, humps and other external disturbances. According to [1], there are 4 basic functions of the suspension system:

1. Providing good ride quality by isolating the vehicle body from road disturbances:
In general, ride quality can be evaluated by measuring the vertical vehicle body accelerations. Well-designed suspension system should provide an isolation from vibratory forces caused by road irregularities.
2. Providing good road holding ability by keeping the tires in contact with the road:
Cornering, braking and traction abilities can be used for characterization of road holding performance of a vehicle. Road holding is improved by minimizing the variations in tire deflection. Since the tire is modeled as a linear spring, its deflection can be considered as a performance measure and must be minimized.
3. Providing good road holding by reducing roll and pitch acceleration during cornering, braking and traction:
Roll and pitch motions are the measures for good road holding during those actions. Therefore, roll and pitch motions should be minimized as much as possible.
4. Supporting the vehicle's static weight:
This function is related with the rattle space requirements of the vehicle. Suspension deflection is used for defining this requirement. Therefore, suspension deflection should also be reduced by the suspension.

The design and the tuning of the vehicle suspension parameters is the critical part for satisfying ride comfort without deteriorating the other performance metrics mentioned above. In Figure 1.1, effects of a change of parameter in a traditional suspension system are shown.

Suspension Change	Influence	Impact on Ride Quality	Impact on Rattle Space
Reduced suspension stiffness k_s	Decrease in the value of the first natural frequency ω_1	GOOD Improved sprung mass acceleration transfer function at high frequencies	BAD Increased suspension deflection at low frequencies
Increased suspension damping b_s	Better damping at the first natural frequency ω_1	GOOD Reduces or eliminates the first resonant peak resulting in highly improved ride quality at the first resonant frequency. BAD Deteriorates ride quality at high frequencies by causing a slower roll-off and resulting in high frequency "harshness"	GOOD Reduces or eliminates the first resonant peak in the suspension deflection transfer function resulting in improved suspension deflection performance at the first resonant frequency. BAD This change has no detrimental effects on the suspension deflection transfer function

Figure 1.1: Influence of parameter change on suspension performance[1]

With the introduction of the inerter concept, the parameters affecting the suspension performance increased by one, thus, providing flexibility to the designers. The main reason why the inerters are applicable is that the additional mass to the system is significantly smaller than its equivalent mass.

In [2], it is stated that the inerter applications consist of a vibration absorption problems, suspension strut design and simulating a mass element. In common, a spring and damper type struts are generally used in the strut design and force elements' magnitudes are proportional to relative displacement and velocity between the sprung mass and unsprung mass for linearized case. However, there is also an acceleration difference between two masses, and it is started to be used in suspension design. The inerter, whose terminals connected to two different masses, applies a force proportional to acceleration difference across its terminals, and stores energy proportional to square of the acceleration difference.

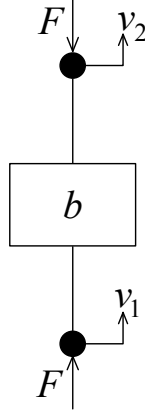


Figure 1.2: Ideal inerter

In [2] force and energy storage equations are written for the ideal inerter which is a mechanical one-port device shown in Figure 1.2. Those equations are given in equation 1.1 and 1.2.

$$F = b (\dot{v}_2 - \dot{v}_1), \quad (1.1)$$

$$E = \frac{1}{2} b (v_2 - v_1)^2, \quad (1.2)$$

where the constant b is called the inertance whose units are in kilograms.

In terms of mechanical parameters, the equation of motion of the inerter is given in equation 1.3. The corresponding system is shown in Figure 1.5.

$$F = (m \alpha_1^2 \alpha_2^2) (\dot{v}_2 - \dot{v}_1), \quad (1.3)$$

where

r_1 = radius of rack pinion,

r_2 = radius of gear wheel,

r_3 = radius of wheel pinion,

γ = radius of gyration of wheel,

m = mass of the wheel,

$\alpha_1 = \gamma / r_3$,

$\alpha_2 = r_2 / r_1$.

In [2] and [3], it is shown that the inerter is not just a conceptual device. It is stated in [4] that the mechanical rack and pinion type prototype built has a flywheel with 0.225 kg mass and creates the inertance effect equivalent to 726 kg and it also improves the phase characteristics are improved. This device is shown in Figure 1.3. As reported by [5], a prototype screw-ball type mechanical inerter having 240kg inertance constant is also developed and manufactured. Figure 1.4 shows the screw-ball type inerter. In Figure 1.5, schematic of these inerters are shown.

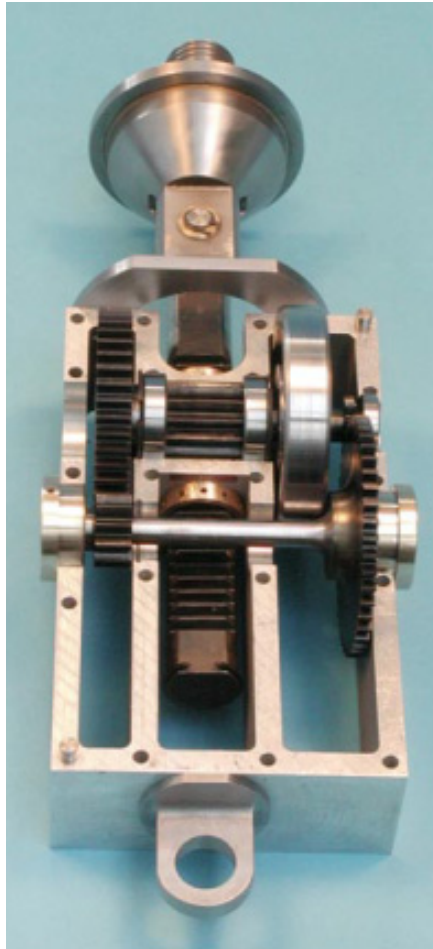


Figure 1.3: Rack and pinion type mechanical inerter prototype developed in Cambridge University Engineering Department[4]

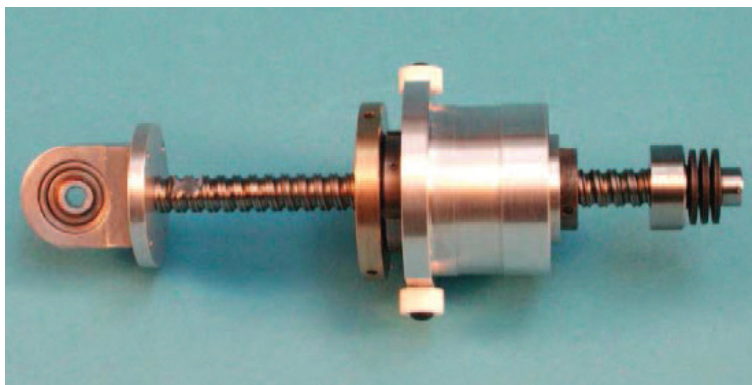


Figure 1.4: Screw-ball type mechanical inerter prototype developed in Cambridge University Engineering Department[5]

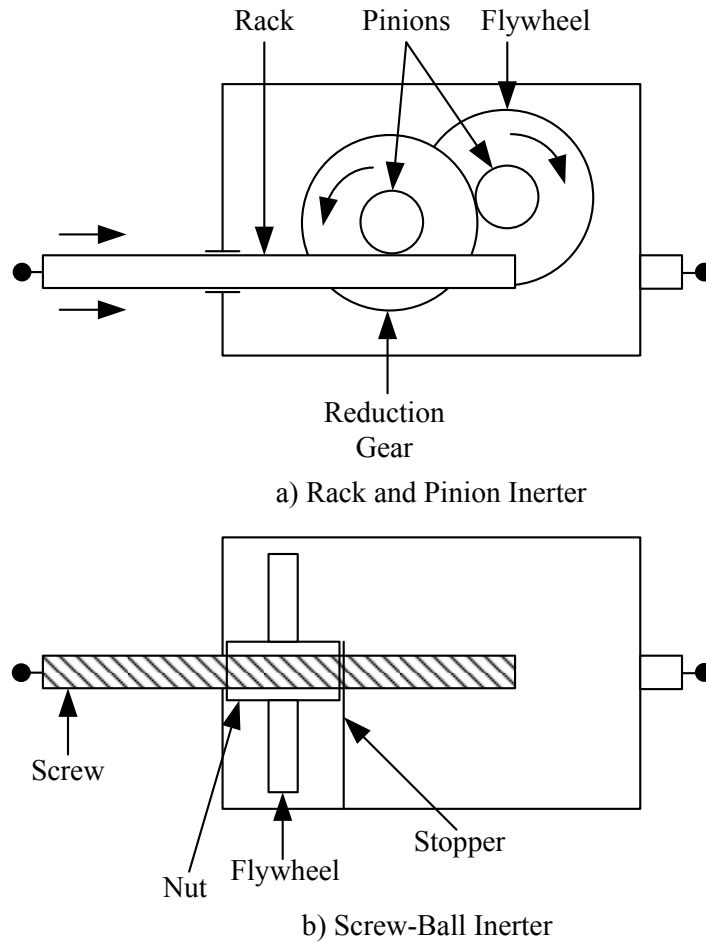


Figure 1.5: Schematic of mechanical inerter

Furthermore, inerter in serial combination with spring and dampers [4] is built in the same department and it is shown in Figure 1.6.

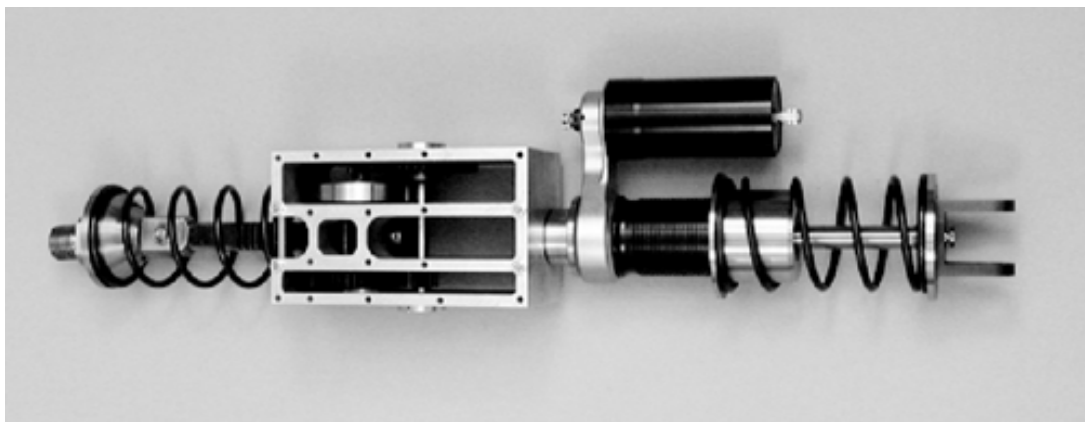


Figure 1.6: Inerter in series with spring and damper[4]

This is the most closest arrangement available in the literature to the one which is investigated in this thesis. It's schematic is given in Figure 1.7.

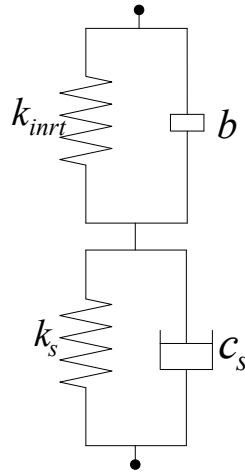


Figure 1.7: Schematic of inerter in series with spring and damper

Another solution for parallel spring-damper-inerter arrangement is presented in [6]. In order to apply the inerter to train suspensions, parallel arrangement of an inerter is realized. It is shown in Figure 1.8.



Figure 1.8: Parallel inerter-spring-damper[6]

Schematic of parallel spring-damper-inerter arrangement is given in Figure 1.9.

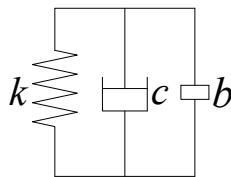


Figure 1.9: Parallel inerter-spring-damper schematic

The working principle of the mechanical inerter is basically converting the linear motion into rotational motion and storing energy into flywheel using its inertia. The relative acceleration between two terminals creates a force in the opposite direction of the motion, proportional to the inertance constant. In [3], a hydraulic type inerter with a two action piston is built and tested. Both of them are applicable to current suspension systems.

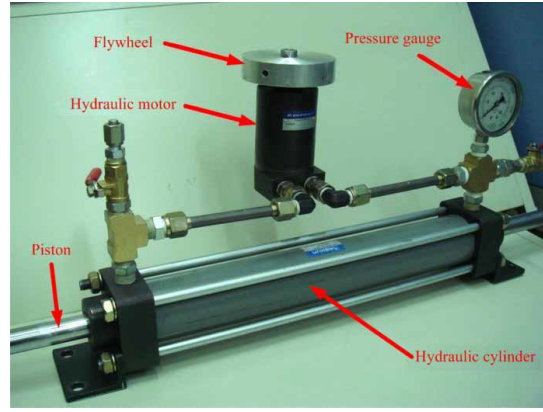


Figure 1.10: Hydraulic inerter prototype developed in National Taiwan University[3]

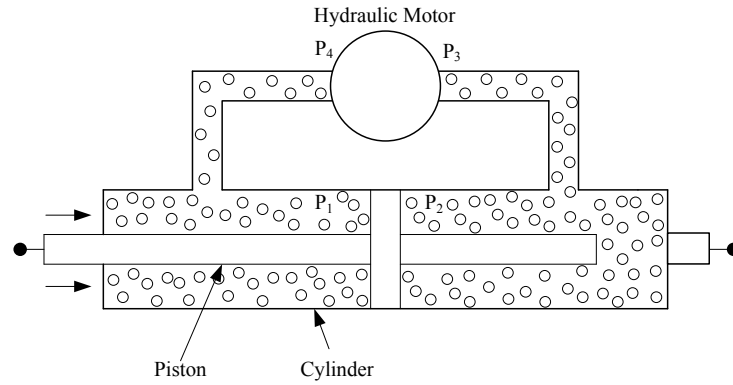


Figure 1.11: Schematic of hydraulic inerter

The working principle of the hydraulic inerter [3] is similar to mechanical inerter, as shown in Figure 1.11. Hydraulic cylinder and the piston are the two terminals of the hydraulic inerter. Hydraulic motor connected in series with the two chambers of the piston creates an effect like hydro-power generator. When force is applied on the piston, the pressure difference between two terminals of the hydraulic motor results in a rotational motion. A flywheel attached to the shaft of the motor and stores energy using the rotational motion. In this case, inertance given in terms of system parameters is represented by equation 1.4.

$$b = I \left(\frac{A}{D} \right)^2, \quad (1.4)$$

where,

I = flywheel attached to hydraulic motor,

A = area of the piston,

D = displacement of the hydraulic motor.

1.1 Literature Review

In [4], as a substitute for the traditional mass element which is the equivalent of the capacitance in mechanical systems, a new mechanical element called the inerter is introduced. The main working principle of this element is that the force applied to the system is proportional to the relative acceleration between the terminals. It is also argued that dynamic characteristics of the standard suspension arrangement which employs spring and damper only and not including the mass element is not offering enough variety. Inerter element gives opportunity to designers to enhance the vertical dynamics of the vehicle with spring - damper - inerter combination struts.

Between mechanical and electrical systems, so-called force-current analogy made such that [4]:

- force - current,
- velocity - voltage,
- mechanical ground - electrical ground,
- spring - inductor,
- damper - resistor.

The analogy is shown in Figure 1.12.

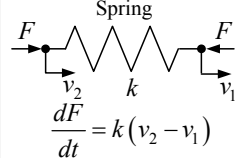
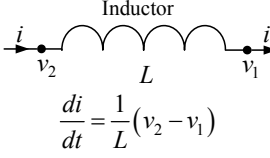
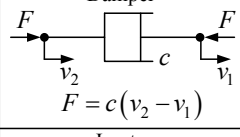
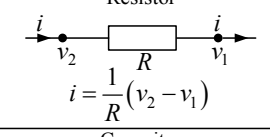
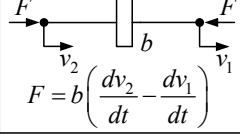
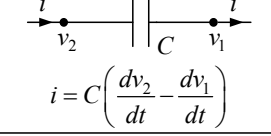
Mechanical	Electrical
<p>Spring</p>  $\frac{dF}{dt} = k(v_2 - v_1)$	<p>Inductor</p>  $\frac{di}{dt} = \frac{1}{L}(v_2 - v_1)$
<p>Damper</p>  $F = c(v_2 - v_1)$	<p>Resistor</p>  $i = \frac{1}{R}(v_2 - v_1)$
<p>Inerter</p>  $F = b\left(\frac{dv_2}{dt} - \frac{dv_1}{dt}\right)$	<p>Capacitor</p>  $i = C\left(\frac{dv_2}{dt} - \frac{dv_1}{dt}\right)$

Figure 1.12: Analogy between mechanical and electrical elements

In 2008, inerter has become very popular among the formula 1(F1) teams. As reported by [7], McLaren F1 team exploited this technology in 2005 Spanish Grand Prix and won the

championship. What is more interesting is that the Lotus Renault somehow acquired the technical drawings of the inerter device but they could not figure out the working mechanism of the device at that time (FIA World Motor Sport Council Decision, 7 December 2007) [8]. Commercially, Cambridge Enterprise had an agreement with Penske Racing Shocks company. They applied for a patent together that was published in 2011 [9]. In this patent, the arrangement and the working mechanism of the device utilized in F1 cars are shown.

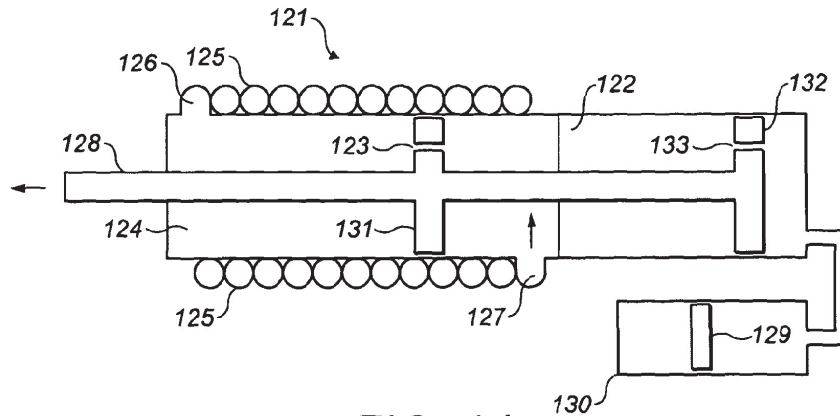


Figure 1.13: Fluid inerter with damping schematic proposed by Cambridge Enterprise and Penske Racing Shocks[9]

Furthermore, Lotus Renault was also published a patent in 2011 [10], explaining the working principle of their fluid inerter.

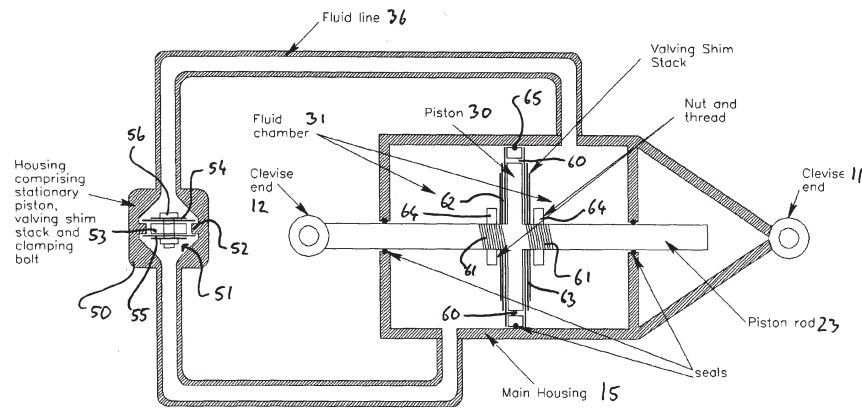


Figure 1.14: Fluid inerter schematic proposed by Lotus-Renault GP LTD[10]

In order to apply such a complicated device to passenger cars, however; more work has to be done. In this thesis, more feasible and applicable solutions are offered for inerter devices and their effects are investigated thoroughly. Even semi-active inerter concept is introduced and control algorithm for semi-active suspension is adopted from suspension systems with semi-active dampers. Before proceeding further into those studies, research currently available in literature will be summarized. Currently, very few publications are available in the literature that discuss the effect of inerters on the vehicle dynamics, especially on the ride quality. In addition to that, practical suspension arrangements with inerters are not considered and an-

alyzed. Generally, there are some physical limitations or problems such as vertical spacing, drift or indeterminacy in steady-state operation of the suspension with the proposed suspension arrangements.

With all the flexibilities and advantages that inerter offers to designers, it has not been widely investigated especially in terms of vehicle dynamics aspects such as ride comfort. For proper and valid evaluation, methods given in [11] are used for investigating the effect of inerter on ride comfort with the proposed suspension arrangements. The main reason behind the study is to show the suitability of inerter applications on passenger vehicles. Such applications have not been revealed up to now. Considering that the first inerter patent was published in 2002 [12], in 10 years it could somehow be applied those type of vehicles. Instead, it went through a long development stage in a competitive environment, which is nothing but the F1 races. In terms of focus, the main difference between F1 racing cars and passenger cars is that for F1 cars road holding is the most important performance measure, whereas, for passenger cars ride quality is more important. Road holding ability of a vehicle allows it to grip the road at higher speeds. Therefore, formula 1 teams (firstly, McLaren) equipped the vehicles with the inerters and involved in developing stage of the device by providing valuable feedback. In this thesis, both road holding and ride quality effect of the inerter device is investigated. However, the main focus of the study is on the effect of inerter on the ride quality. The critical point of the study is to improve ride quality of the vehicle without deteriorating the road holding ability too much.

Inerter concept is also applied to the building and train suspensions. In [13], it is argued that the vertical vibrations induced by traffic or earth quakes can be decreased by 30 percent with 2 different suspension arrangements in frequency domain. Those improvements are obtained as a result of optimization processes and results are relative to the standard suspension. One of the arrangements is the parallel inerter to spring-damper and the other one is the inerter serial to damper and parallel to the spring. By using the same arrangements, in [6] inerters are applied to train suspensions. It is argued that up to 12 percent improvement can be achieved by application of inerters to the train suspensions in time domain.

In order to increase the efficiency of the inerter on the ride comfort, semi-active sky-hook damping strategy will be adopted to inerters in the following chapters. Before proceeding further into the proposed method for semi-active inerter, semi-active suspension concept will be explained. Normally, semi-active damper system consists of an electronic shock absorber with a variable damping in a relatively large bandwidth around 30–40Hz [14]. The main advantage for this system is the force delivered into the system follows the passivity constraint of the damper. The meaning of this is that no additional energy is supplied into the system. Therefore, the power required while working is relatively low compared to active suspensions. It is stated in [14] that the power required will be around tens of Watts. From that point of view, the most suitable inerter structure for the implementation of semi-active concept is the fluid inerter. It allows the usage of rheological fluid in this device, like the ones in magnetorheological dampers. By changing the viscosity of the fluid, inertance constant can be controlled. In Figure 1.13, suitable structure for this method is shown. Sky-hook inerter schematic is given in Figure 1.15.

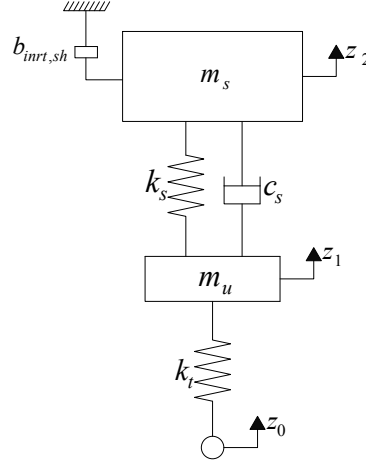


Figure 1.15: Semi-Active sky-hook inerter schematic

The logic behind the semi-active inerter control is nothing but the balance logic and it is explained in [15] as “a spring force cancellation strategy”. In this logic, semi-active damper force is generated such that it cancels the spring force of the strut. The sky-hook control strategy is effective and simple approximation of the balance logic. Body bounce motion can be effectively controlled by using this strategy, therefore, acceleration of the sprung mass is reduced. In sky-hook control, sprung mass velocity is used for generating the damping force. Even though the sky-hook control is an excellent strategy reducing the road based vibrations at the sprung mass, it is applied at the expense of a increased vibration in unsprung mass due to the fact that more damping is added to sprung mass while removing damping effect from the unsprung mass. Another and obvious effect of the semi-active dampers is on the region between the two natural frequencies of the vehicle in terms of the body acceleration. Likewise, with the implementation of semi-active sky-hook inerter concept to vehicle suspensions, body acceleration is successfully decreased in this region. In this strategy, sprung mass acceleration is used for generating the inerter force.

1.2 Scope of Thesis

The purpose in this study, is to investigate the effect of the inerter on the ride comfort and road holding performance. Suspension systems with parallel and serial inerter configurations with different inertance constants are investigated and their efficiencies of the ride comfort improvement are compared through the thesis. Moreover, since the additional mass that inerter device brings on the unsprung mass is not desired and the working space is limited, the optimization of the inerters are needed. With the optimization process, both ride comfort and physical requirements are satisfied in a reasonable way. Before the optimization process, firstly, the effect of inerter on the passive systems are investigated. During that phase, passive parallel inerter configuration is left out of the optimization process, due to the severe increase on magnitude of the wheel hop motion. Due to the lack of performances and the semi-active

modeling in the literature, the sky-hook inerter concept is introduced. When the semi-active concept is investigated, the parallel inerter arrangement is included in the analysis with the serial inerter configuration. All of the analysis are made by using ISO-2631 ride comfort evaluation methods [11] and ISO 8608 random road profiles [16]. Finally, simulations are also included in the thesis using ISO 8608 random road profiles and standard hump profiles. To sum up:

- passive and semi-active serial inerter concept to suspension system is modeled with quarter-car and half-car models,
- suspension parameters are optimized with single-objective optimization using A to E-class ISO-8608 random road profiles at 3 different vehicle speeds,
- ride comfort according to ISO 2631 criteria is evaluated,
- semi-active sky-hook inerter concept is introduced and its performance is investigated,
- both performance of passive and semi-active suspensions with inerters are compared with standard suspension,
- the effect of variation of inertance is shown clearly on the suspension performance.

1.3 Outline

In Chapter 1, literature review of the topics investigated in the thesis is given.

In Chapter 2, mathematical models of the suspension systems that are used in the simulations and analysis are given with the figures and equations clearly.

In Chapter 3, frequency responses of the the suspension systems which are used in the frequency domain analysis and the methods used when calculating the responses are explained.

In Chapter 4, the mathematical models used for generation of the ISO 8608 random road profiles, the methods and the samples generated are provided.

In Chapter 5, the optimization process with genetic algorithm is explained and the results for the passive serial inerter is given. The inerter effects on the ride comfort and road holding are discussed. The performances of passive and semi-active systems are compared.

In Chapter 6, the methods for ride comfort evaluation using the ISO 2631 criteria is explained. The ride comfort analysis are made for all the suspension systems that are considered in previous chapters.

In Chapter 7, simulation results using the half-car models with ISO 8608 random road profiles

and standard hump profiles are given.

In Chapter 8, discussions and conclusion are made, future work is given.

CHAPTER 2

MATHEMATICAL MODELING OF VEHICLE SUSPENSIONS

2.1 Passive Quarter-Car Models

Quarter-car model is often used when suspension modeling is considered. Vertical behavior of a vehicle can be studied in a simplified manner with this model. The accuracy of the model is surprisingly close to half-car or full-car models. The only drawback of this model is that the pitch and the roll motions of the body cannot be studied.

The quarter-car model can basically represented by four elements:

1. The sprung mass which represents the body.
2. The unsprung mass which takes masses of the elements such as the wheel, the brake, the caliper, etc. into account.
3. Spring as an elastic element.
4. Damper as a dissipative element.

Both effects of the elastic and dissipative elements are assumed to be additive. Other assumptions made are listed below as:

1. The tire is modeled by a linear spring.
2. Suspension spring and damping forces are considered to be linear.
3. Tire damping factor is assumed to be zero.
4. Small displacements are assumed around the nominal load point. In other words, road disturbances are small enough such that they do not cause any non-linearity to the suspension system. In addition to that, the only input to the system is road disturbance.
5. The tire is always in contact with the road.

2.1.1 Quarter-Car Model of Standard Suspension

Standard suspension will be used as a reference in order to evaluate the performance of the proposed suspension systems. Standard suspension configuration can be found in Figure 2.1.

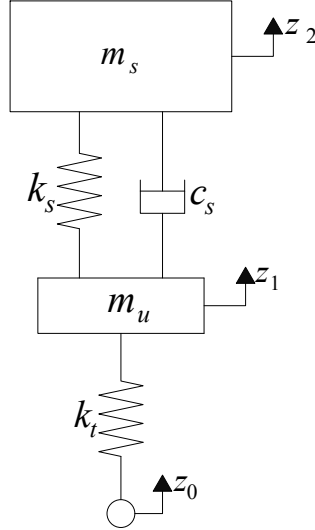


Figure 2.1: Quarter-car model of standard suspension

The equations of motion of the standard suspension are represented by equation (2.1). Road input, z_0 is given to the system in the form of displacement in all cases.

$$\begin{aligned} m_s \ddot{z}_2 &= k_s (z_1 - z_2) + c_s (\dot{z}_1 - \dot{z}_2) \\ m_u \ddot{z}_1 &= k_s (z_2 - z_1) + c_s (\dot{z}_2 - \dot{z}_1) + k_t (z_0 - z_1). \end{aligned} \quad (2.1)$$

2.1.2 Quarter-Car Model of Passive Serial Inerter

A serial combination of a parallel spring – damper and parallel spring – damper – inerter is the configuration of the passive serial inerter system. By placing the spring of the strut, parallel to inerter spring and still getting equivalent stiffness equal to the standard suspension, one can significantly decrease the required vertical space to accommodate the suspension. In this way, the vertical space of the suspension is decreased by at least free length of the spring, and as a result, the suspension deflection of the passive serial inerter will not be deteriorated. However, it is important to keep the minimum required distance between m_p and m_u , in order to prevent any collision under extreme cases. Passive serial inerter configuration is shown in Figure 2.2.

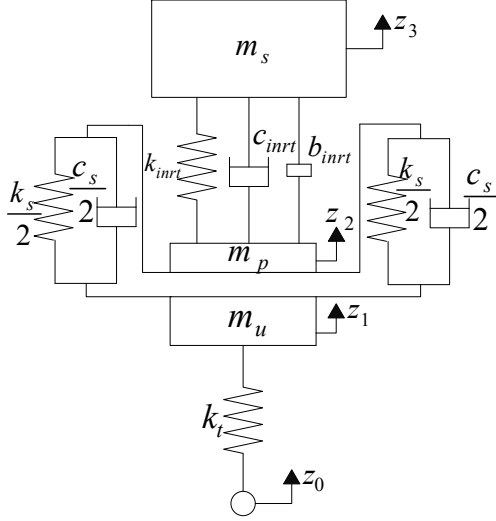


Figure 2.2: Quarter-car model of passive serial inerter

The equations of motion of the passive serial inerter are expressed by equation (2.2).

$$\begin{aligned}
 m_s \ddot{z}_3 &= F_{inrt} \\
 m_p \ddot{z}_2 &= k_s (z_1 - z_2) + c_s (\dot{z}_1 - \dot{z}_2) - F_{inrt} \\
 m_u \ddot{z}_1 &= k_s (z_2 - z_1) + c_s (\dot{z}_2 - \dot{z}_1) + k_t (z_0 - z_1) \\
 F_{inrt} &= b_{inrt} (\ddot{z}_2 - \ddot{z}_3) + c_{inrt} (\dot{z}_2 - \dot{z}_3) + k_{inrt} (z_2 - z_3) .
 \end{aligned} \tag{2.2}$$

2.1.3 Quarter-Car Model of Passive Parallel Inerter

Passive parallel inerter, as the name implies, consists of an inerter connected parallel to spring-damper. In terms of vertical space requirements, it is an advantageous system. This arrangement is shown in Figure 2.3.

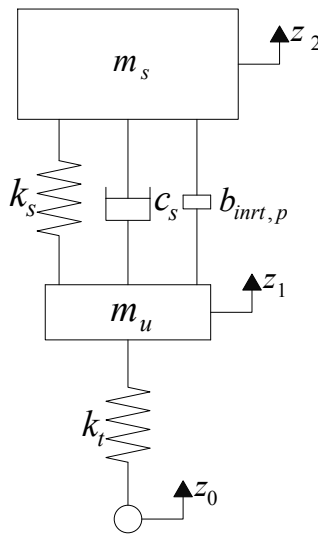


Figure 2.3: Quarter-Car Model of Passive Parallel Inerter

The equations of motion of the passive serial inerter are defined by equation (2.3).

$$\begin{aligned} m_s \ddot{z}_2 &= k_s (z_1 - z_2) + c_s (\dot{z}_1 - \dot{z}_2) + b_{inrt,p} (\ddot{z}_1 - \ddot{z}_2) \\ m_u \ddot{z}_1 &= k_s (z_1 - z_2) + c_s (\dot{z}_1 - \dot{z}_2) + b_{inrt,p} (\ddot{z}_1 - \ddot{z}_2) + k_t (z_0 - z_1). \end{aligned} \quad (2.3)$$

2.1.4 Semi-Active Inerter

In semi-active inerter system, spring and damper force cancellation strategy is adopted. As the name implies, inerter force is used for cancellation of both damper and spring. As a result, sprung mass acceleration is reduced. The quarter car model of the semi-active inerter system used in this thesis is given in Figure 2.4.

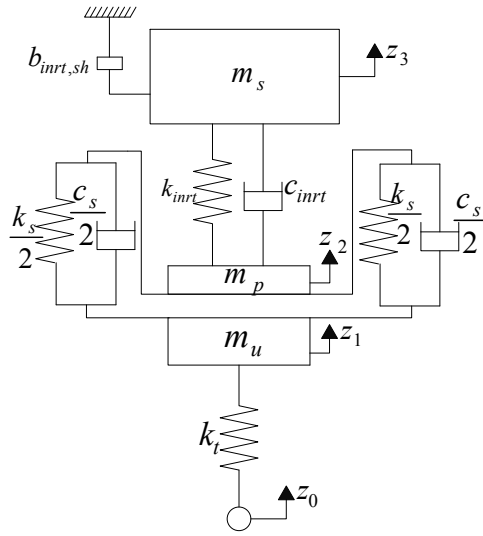


Figure 2.4: Sky-hook serial inerter schematic

The actuator dynamics are necessary to simulate the realistic conditions of the actuators used in the suspension systems. The main reason is that the actuators cannot work in a infinitely wide-band; instead, they have limited bandwidth characteristics. b_{min} is the minimum inerance of the inerter when the electronic command is off; b_{max} is the maximum inerance of the inerter when the electronic command is on, the positive constant β represents the bandwidth of the electric subsystem. The equation that represents the actuator dynamics is as follows [14]:

$$\dot{b}_{in} = \beta (b_{inrt,in} - b(t)). \quad (2.4)$$

During the analysis, the bandwidth of the actuator is selected to be 15Hz. The reason for this bandwidth selection is that the actuators having 15Hz bandwidth are available in the market and can be found rather easily with a reasonable price. Actuator model developed in Simulink® environment is shown in Figure 2.5. This model will be used with all of the semi-active vehicle models with inerter.

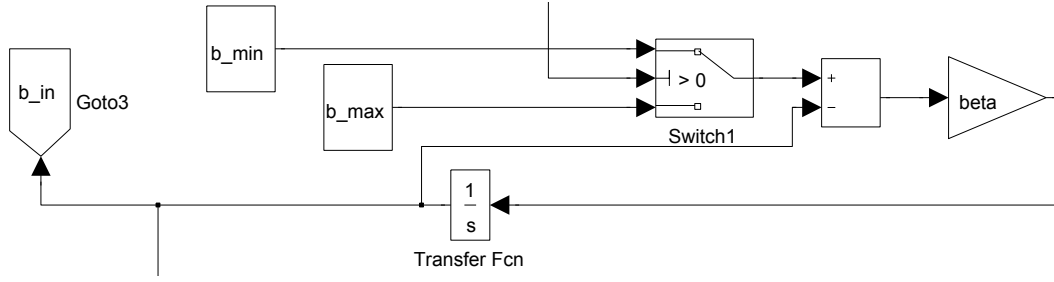


Figure 2.5: Actuator model in Simulink® environment

2.1.5 Quarter Car Model of Semi-Active Serial Inerter

2.2 Semi-Active Quarter Car Models

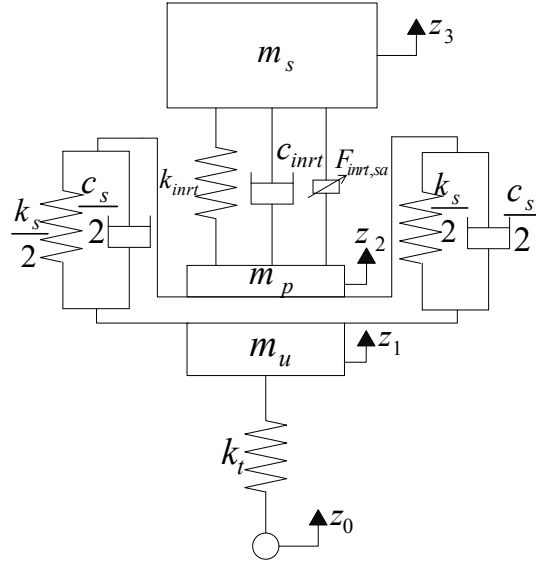


Figure 2.6: Quarter-car model of semi-active serial inerter

By applying the sky-hook damping control logic to inerters, semi-active serial inerter model is constructed. This configuration is shown in Figure 2.6. Equations of motion of semi-active serial inerter are expressed in equation 2.5. Controller equations obtained by using the balance logic are defined by equation 2.6.

$$\begin{aligned}
 F_{inrt} &= F_{inrt,sa} + c_{inrt} (\dot{z}_2 - \dot{z}_3) + k_{inrt} (z_2 - z_3) \\
 m_s \ddot{z}_3 &= F_{inrt} \\
 m_p \ddot{z}_2 &= k_s (z_1 - z_2) + c_s (\dot{z}_1 - \dot{z}_2) - F_{inrt} \\
 m_u \ddot{z}_1 &= k_s (z_2 - z_1) + c_s (\dot{z}_2 - \dot{z}_1) + k_t (z_0 - z_1)
 \end{aligned} \tag{2.5}$$

where

$$\begin{aligned} b_{inrt,in} &= b_{\max} \text{ if } \ddot{z}_3 (\ddot{z}_3 - \ddot{z}_2) > 0 \\ b_{inrt,in} &= b_{\min} \text{ if } \ddot{z}_3 (\ddot{z}_3 - \ddot{z}_2) \leq 0 \\ F_{inrt,sa} &= b_{inrt,in} (\ddot{z}_2 - \ddot{z}_3). \end{aligned} \quad (2.6)$$

2.2.1 Quarter Car Model of Semi-Active Parallel Inerter

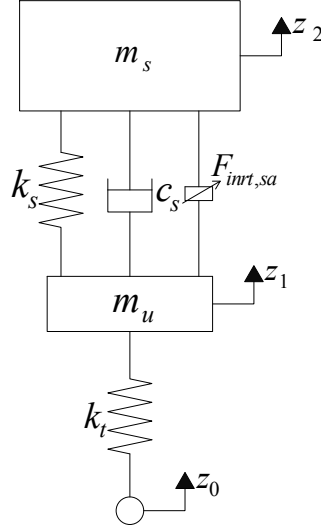


Figure 2.7: Quarter-car model of semi-active parallel inerter

By applying same control logic explained in semi-active serial inerter subsection, semi-active parallel inerter model is constructed. This configuration is shown in Figure 2.7.

$$\begin{aligned} m_s \ddot{z}_2 &= k_s (z_1 - z_2) + c_s (\dot{z}_1 - \dot{z}_2) + F_{inrt,sa} \\ m_u \ddot{z}_1 &= k_s (z_1 - z_2) + c_s (\dot{z}_1 - \dot{z}_2) - F_{inrt,sa} + k_t (z_0 - z_1) \end{aligned} \quad (2.7)$$

where

$$\begin{aligned} b_{inrt,sa} &= b_{\max} \text{ if } \ddot{z}_2 (\ddot{z}_2 - \ddot{z}_1) > 0 \\ b_{inrt,sa} &= b_{\min} \text{ if } \ddot{z}_2 (\ddot{z}_2 - \ddot{z}_1) \leq 0 \\ F_{inrt,sa} &= b_{inrt,sa} (\ddot{z}_1 - \ddot{z}_2). \end{aligned} \quad (2.8)$$

2.3 Half-Car Models

The quarter-car models can only be used to study the vertical behavior of the vehicle. In addition to vertical motion, roll and pitch motions can be investigated by using the half-car models. In other words, half-car models contain roll and pitch motions beneath the heave motion. They are constructed by connecting the two quarter-car models with a vehicle body.

2.3.1 Pitch-Oriented Half-Car Model of Passive Standard Suspension

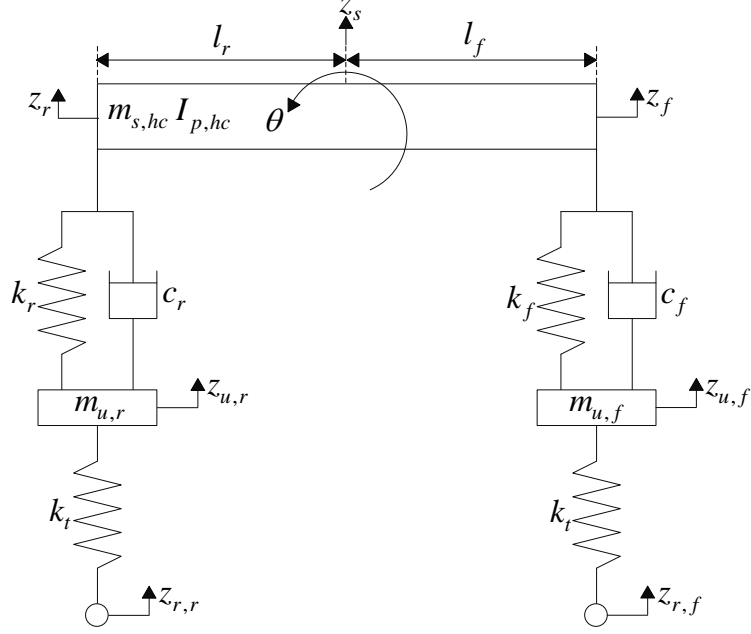


Figure 2.8: Pitch-oriented half-car model of pssive standard suspension

$$\begin{aligned}
 m_{s,hc} \ddot{z}_s &= k_r (z_{u,r} - z_r) + k_f (z_{u,f} - z_f) + c_r (\dot{z}_{u,r} - \dot{z}_r) + c_f (\dot{z}_{u,f} - \dot{z}_f) \\
 m_{u,f} \ddot{z}_{u,f} &= k_f (z_f - z_{u,f}) + c_f (\dot{z}_f - \dot{z}_{u,f}) + k_t (z_{r,f} - z_{u,f}) \\
 m_{u,r} \ddot{z}_{u,r} &= k_r (z_r - z_{u,r}) + c_r (\dot{z}_r - \dot{z}_{u,r}) + k_t (z_{r,r} - z_{u,r}) \\
 I_{p,hc} \ddot{\theta} &= l_r (k_r (z_r - z_{u,r}) + c_r (\dot{z}_r - \dot{z}_{u,r})) - l_f (k_f (z_f - z_{u,f}) + c_f (\dot{z}_f - \dot{z}_{u,f}))
 \end{aligned} \tag{2.9}$$

where the geometric relationships are,

$$\begin{aligned}
 z_f &= z_s + l_f \sin(\theta) \\
 z_r &= z_s - l_r \sin(\theta) \\
 \dot{z}_f &= \dot{z}_s + l_f \dot{\theta} \cos(\theta) \\
 \dot{z}_r &= \dot{z}_s - l_r \dot{\theta} \cos(\theta) .
 \end{aligned} \tag{2.10}$$

2.3.2 Pitch-Oriented Half-Car Model of Passive Serial Inerter

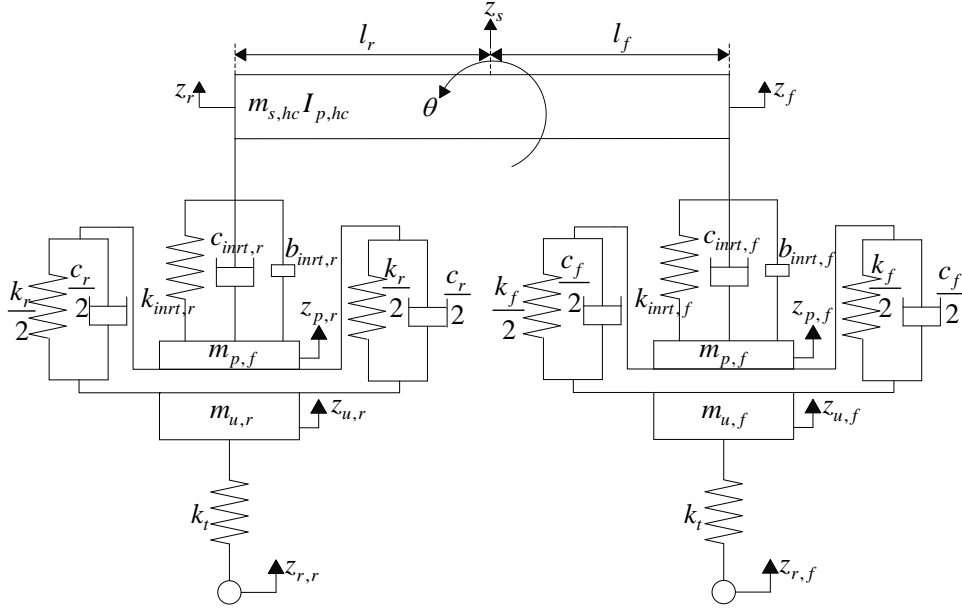


Figure 2.9: Pitch-oriented half-car model of passive serial inerter

$$\begin{aligned}
 m_{s,hc} \ddot{z}_s &= -F_{inrt,r} - F_{inrt,f} \\
 m_{p,r} \ddot{z}_{p,r} &= k_r (z_{u,r} - z_{p,r}) + c_r (\dot{z}_{u,r} - \dot{z}_{p,r}) + F_{inrt,r} \\
 m_{p,f} \ddot{z}_{p,f} &= k_f (z_{u,f} - z_{p,f}) + c_f (\dot{z}_{u,f} - \dot{z}_{p,f}) + F_{inrt,f} \\
 m_{u,r} \ddot{z}_{u,r} &= k_r (z_{p,r} - z_{u,r}) + c_r (\dot{z}_{p,r} - \dot{z}_{u,r}) + k_t (z_{r,r} - z_{u,r}) \\
 m_{u,f} \ddot{z}_{u,f} &= k_f (z_{p,f} - z_{u,f}) + c_f (\dot{z}_{p,f} - \dot{z}_{u,f}) + k_t (z_{r,f} - z_{u,f}) \\
 I_{p,hc} \ddot{\theta} &= l_r F_{inrt,r} - l_f F_{inrt,f} \\
 F_{inrt,r} &= k_{inrt,r} (z_r - z_{p,r}) + c_{inrt,r} (\dot{z}_r - \dot{z}_{p,r}) + b_{inrt,r} (\ddot{z}_r - \ddot{z}_{p,r}) \\
 F_{inrt,f} &= k_{inrt,f} (z_f - z_{p,f}) + c_{inrt,f} (\dot{z}_f - \dot{z}_{p,f}) + b_{inrt,f} (\ddot{z}_f - \ddot{z}_{p,f})
 \end{aligned} \tag{2.11}$$

where the geometric relationships are,

$$\begin{aligned}
 z_f &= z_s + l_f \sin(\theta) \\
 z_r &= z_s - l_r \sin(\theta) \\
 \dot{z}_f &= \dot{z}_s + l_f \dot{\theta} \cos(\theta) \\
 \dot{z}_r &= \dot{z}_s - l_r \dot{\theta} \cos(\theta) \\
 \ddot{z}_f &= \ddot{z}_s + l_f \ddot{\theta} \cos(\theta) - l_f \dot{\theta}^2 \sin(\theta) \\
 \ddot{z}_r &= \ddot{z}_s - l_f \ddot{\theta} \cos(\theta) + l_f \dot{\theta}^2 \sin(\theta) .
 \end{aligned} \tag{2.12}$$

2.3.3 Pitch-Oriented Half-Car Model of Semi-Active Parallel Inerter

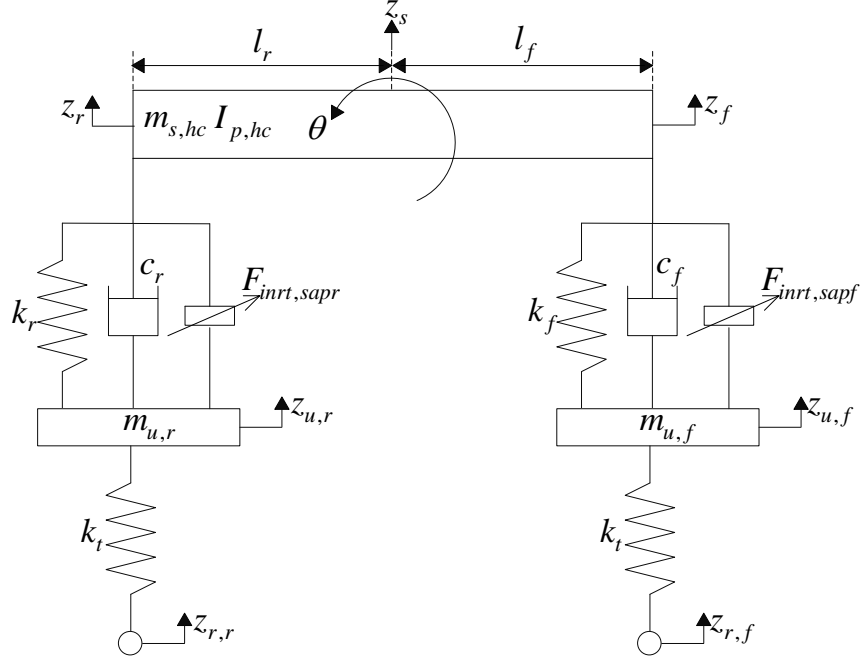


Figure 2.10: Pitch-oriented half-car model of semi-active parallel inerter

$$\begin{aligned}
 m_{s,hc}\ddot{z}_s &= k_r(z_{u,r} - z_r) + k_f(z_{u,f} - z_f) + c_r(\dot{z}_{u,r} - \dot{z}_r) + c_f(\dot{z}_{u,f} - \dot{z}_f) \\
 &\quad + F_{inrt,sapf} + F_{inrt,sapr} \\
 m_{u,f}\ddot{z}_{u,f} &= k_f(z_f - z_{u,f}) + c_f(\dot{z}_f - \dot{z}_{u,f}) + k_t(z_{r,f} - z_{u,f}) - F_{inrt,sapf} \\
 m_{u,r}\ddot{z}_{u,r} &= k_r(z_r - z_{u,r}) + c_r(\dot{z}_r - \dot{z}_{u,r}) + k_t(z_{r,r} - z_{u,r}) - F_{inrt,sapr} \\
 I_{p,hc}\ddot{\theta} &= l_r(k_r(z_r - z_{u,r}) + c_r(\dot{z}_r - \dot{z}_{u,r}) - F_{inrt,sapr}) \\
 &\quad - l_f(k_f(z_f - z_{u,f}) + c_f(\dot{z}_f - \dot{z}_{u,f}) - F_{inrt,sapf})
 \end{aligned} \tag{2.13}$$

where the control laws are,

$$\begin{aligned}
 b_{inrt,inf} &= b_{\max} \text{ if } \ddot{z}_s(\ddot{z}_f - \ddot{z}_{uf}) > 0 \\
 b_{inrt,inf} &= b_{\min} \text{ if } \ddot{z}_s(\ddot{z}_f - \ddot{z}_{uf}) \leq 0 \\
 F_{inrt,sapf} &= b_{inrt,inf}(\ddot{z}_{uf} - \ddot{z}_f) \\
 b_{inrt,inr} &= b_{\max} \text{ if } \ddot{z}_s(\ddot{z}_r - \ddot{z}_{ur}) > 0 \\
 b_{inrt,inr} &= b_{\min} \text{ if } \ddot{z}_s(\ddot{z}_r - \ddot{z}_{ur}) \leq 0 \\
 F_{inrt,sapr} &= b_{inrt,inr}(\ddot{z}_{ur} - \ddot{z}_r)
 \end{aligned} \tag{2.14}$$

and the geometric relationships are,

$$\begin{aligned}
 z_f &= z_s + l_f \sin(\theta) \\
 z_r &= z_s - l_r \sin(\theta) \\
 \dot{z}_f &= \dot{z}_s + l_f \dot{\theta} \cos(\theta) \\
 \dot{z}_r &= \dot{z}_s - l_r \dot{\theta} \cos(\theta) \\
 \ddot{z}_f &= \ddot{z}_s + l_f \ddot{\theta} \cos(\theta) - l_f \dot{\theta}^2 \sin(\theta) \\
 \ddot{z}_r &= \ddot{z}_s - l_f \ddot{\theta} \cos(\theta) + l_f \dot{\theta}^2 \sin(\theta) .
 \end{aligned} \tag{2.15}$$

2.3.4 Pitch-Oriented Half-Car Model of Semi-Active Serial Inerter

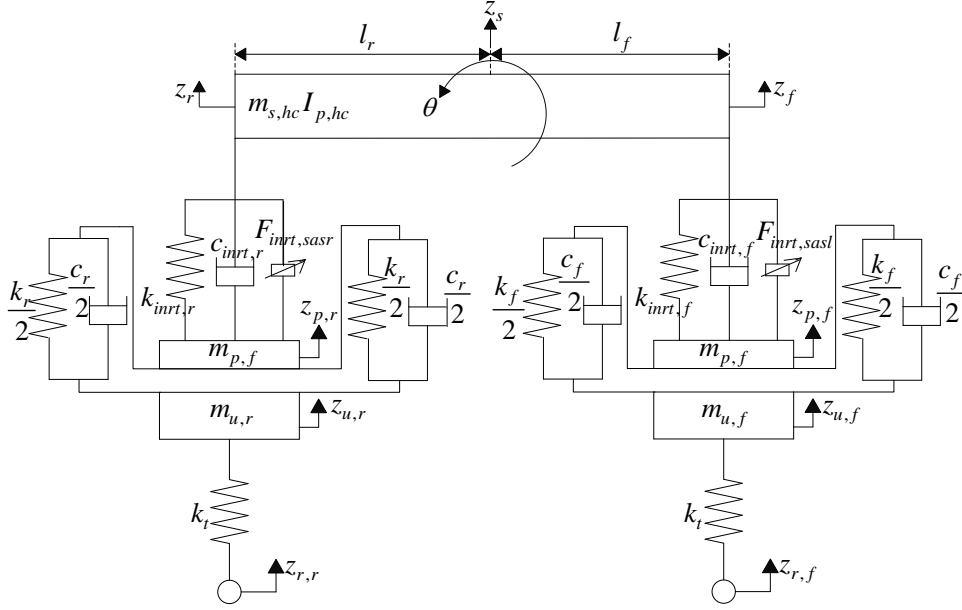


Figure 2.11: Pitch-oriented half-car model of semi-active serial inerter

$$\begin{aligned}
 m_{s,hc} \ddot{z}_s &= -F_{inrt,r} - F_{inrt,f} \\
 m_{p,r} \ddot{z}_{p,r} &= k_r (z_{u,r} - z_{p,r}) + c_r (\dot{z}_{u,r} - \dot{z}_{p,r}) + F_{inrt,r} \\
 m_{p,f} \ddot{z}_{p,f} &= k_f (z_{u,f} - z_{p,f}) + c_f (\dot{z}_{u,f} - \dot{z}_{p,f}) + F_{inrt,f} \\
 m_{u,r} \ddot{z}_{u,r} &= k_r (z_{p,r} - z_{u,r}) + c_r (\dot{z}_{p,r} - \dot{z}_{u,r}) + k_t (z_{r,r} - z_{u,r}) \\
 m_{u,f} \ddot{z}_{u,f} &= k_f (z_{p,f} - z_{u,f}) + c_f (\dot{z}_{p,f} - \dot{z}_{u,f}) + k_t (z_{r,f} - z_{u,f}) \\
 I_{p,hc} \ddot{\theta} &= l_r F_{inrt,r} - l_f F_{inrt,f} \\
 F_{inrt,r} &= k_{inrt,r} (z_r - z_{p,r}) + c_{inrt,r} (\dot{z}_r - \dot{z}_{p,r}) + F_{inrt,sasr} \\
 F_{inrt,f} &= k_{inrt,f} (z_f - z_{p,f}) + c_{inrt,f} (\dot{z}_f - \dot{z}_{p,f}) + F_{inrt,sasf}
 \end{aligned} \tag{2.16}$$

where the control laws are,

$$\begin{aligned}
 b_{inrt,inf} &= b_{\max} \text{ if } \ddot{z}_s (\ddot{z}_f - \ddot{z}_{uf}) > 0 \\
 b_{inrt,inf} &= b_{\min} \text{ if } \ddot{z}_s (\ddot{z}_f - \ddot{z}_{uf}) \leq 0 \\
 F_{inrt,sapf} &= b_{inrt,inf} (\ddot{z}_{uf} - \ddot{z}_f) \\
 b_{inrt,inr} &= b_{\max} \text{ if } \ddot{z}_s (\ddot{z}_r - \ddot{z}_{ur}) > 0 \\
 b_{inrt,inr} &= b_{\min} \text{ if } \ddot{z}_s (\ddot{z}_r - \ddot{z}_{ur}) \leq 0 \\
 F_{inrt,sapr} &= b_{inrt,inr} (\ddot{z}_{ur} - \ddot{z}_r)
 \end{aligned} \tag{2.17}$$

and the geometric relationships are,

$$\begin{aligned}
 z_f &= z_s + l_f \sin(\theta) \\
 z_r &= z_s - l_r \sin(\theta) \\
 \dot{z}_f &= \dot{z}_s + l_f \dot{\theta} \cos(\theta) \\
 \dot{z}_r &= \dot{z}_s - l_r \dot{\theta} \cos(\theta) \\
 \ddot{z}_f &= \ddot{z}_s + l_f \ddot{\theta} \cos(\theta) - l_f \dot{\theta}^2 \sin(\theta) \\
 \ddot{z}_r &= \ddot{z}_s - l_f \ddot{\theta} \cos(\theta) + l_f \dot{\theta}^2 \sin(\theta) .
 \end{aligned} \tag{2.18}$$

2.4 Parameters Used in Mathematical Models

During the analysis, some parameters are kept constant in order to simplify the analysis' and compare the systems. Those parameters are given in Table 2.1. In Chapter 5, inerter stiffness, damping and inertance will be replaced by optimized parameters. Standard suspension parameters will be kept constant in all cases. Furthermore, in Chapter 3, these parameters will be used for plotting the frequency responses of the systems for an initial assessment.

Table 2.1: Parameters Kept Constant and Used in Pre-Optimized Analysis'

Parameter	Value
m_s	240kg
m_p	3kg
m_u	30kg
k_s	15000N/m
c_s	900N.s/m
k_t	190000N/m
k_{inrt}	35000N/m
c_{inrt}	2000N.s/m
$b_{inrt,p}$	400kg
b_{inrt}	400kg

CHAPTER 3

FREQUENCY RESPONSES OF VEHICLE SUSPENSIONS

3.1 Introduction

In order to determine the frequency domain characteristics, or draw the Bode plots of the systems, equations of motions given in previous chapter are used to obtain the transfer functions. The method used in obtaining the transfer functions is Laplace transformation of the equation of motions. In addition to this method, the following state-space models of the quarter car models can also be used to determine the transfer functions.

3.2 State-Space Models of Vehicle Suspensions

3.2.1 State-Space Model of Passive Serial-Inerter

State-space model of the quarter-car model of a passive serial inerter will be used for determining the frequency response of the system, and for time-domain simulations. State-space equation of the quarter car model with serial inerter is given in eq(3.1).

$$\dot{\underline{x}} = \underline{A} \underline{x} + \underline{B} u \quad (3.1)$$

States are chosen as following:

$$\underline{x} = \begin{bmatrix} z_1 \\ z_2 \\ z_3 \\ \dot{z}_1 \\ \dot{z}_2 \\ \dot{z}_3 \end{bmatrix}, \quad z_o(t) = u. \quad (3.2)$$

State-space matrices derived from equation of motions are given in eq(3.3) and eq(3.4).

$$\underline{A} = \begin{bmatrix} 0 & 0 & 0 \\ 0 & 0 & 0 \\ 0 & 0 & 0 \\ -\frac{k_s+k_t}{m_u} & \frac{k_s}{m_u} & 0 \\ \frac{(m_s+b_{inrt})k_s}{D_{qcar}} & -\frac{(m_s k_{inrt}+(m_s+b_{inrt})k_s)}{D_{qcar}} & \frac{m_s k_{inrt}}{D_{qcar}} \\ \frac{b_{inrt}k_s}{D_{qcar}} & \frac{k_{inrt}m_p-b_{inrt}k_s}{D_{qcar}} & -\frac{k_{inrt}m_p}{D_{qcar}} \\ 1 & 0 & 0 \\ 0 & 1 & 0 \\ 0 & 0 & 1 \\ \dots & -\frac{c_s}{m_u} & 0 \\ \frac{(m_s+b_{inrt})c_s}{D_{qcar}} & -\frac{(m_s c_{inrt}+(m_s+b_{inrt})c_s)}{D_{qcar}} & \frac{m_s c_{inrt}}{D_{qcar}} \\ \frac{b_{inrt}c_s}{D_{qcar}} & \frac{c_{inrt}m_p-b_{inrt}c_s}{D_{qcar}} & -\frac{c_{inrt}m_p}{D_{qcar}} \end{bmatrix}. \quad (3.3)$$

$$\underline{B} = \begin{bmatrix} 0 \\ 0 \\ 0 \\ \frac{k_t}{m_u} \\ 0 \\ 0 \end{bmatrix}, \quad \underline{C} = \begin{bmatrix} 1 & 0 & 0 & 0 & 0 & 0 \\ 0 & 1 & 0 & 0 & 0 & 0 \\ 0 & 0 & 1 & 0 & 0 & 0 \\ 0 & 0 & 0 & 1 & 0 & 0 \\ 0 & 0 & 0 & 0 & 1 & 0 \\ 0 & 0 & 0 & 0 & 0 & 1 \end{bmatrix}, \quad \underline{D} = \begin{bmatrix} 0 \\ 0 \\ 0 \\ 0 \\ 0 \\ 0 \end{bmatrix} \quad (3.4)$$

where,

$$D_{qcar} = (m_s m_p + b_{inrt} m_s + b_{inrt} m_p). \quad (3.5)$$

3.2.2 State-Space Model of Passive Standard Suspension

For the same reason explained in previous section, state-space model of passive standard suspension will be used. States are chosen as following:

$$\underline{x} = \begin{bmatrix} z_2 \\ \dot{z}_2 \\ z_1 \\ \dot{z}_1 \end{bmatrix}, \quad z_o(t) = u. \quad (3.6)$$

With the chosen states, state-space model of this suspension system is given in eq(3.7).

$$\underline{A} = \begin{bmatrix} 0 & 1 & 0 & 0 \\ -\frac{k_s}{m_s} & -\frac{c_s}{m_s} & \frac{k_s}{m_s} & \frac{c_s}{m_s} \\ 0 & 0 & 0 & 1 \\ \frac{k_s}{m_u} & \frac{c_s}{m_u} & -\frac{k_s+k_t}{m_u} & -\frac{c_s}{m_u} \end{bmatrix}, \quad \underline{B} = \begin{bmatrix} 0 \\ 0 \\ 0 \\ \frac{k_t}{m_u} \end{bmatrix}, \quad (3.7)$$

$$\underline{C} = \begin{bmatrix} 1 & 0 & 0 & 0 \\ 0 & 1 & 0 & 0 \\ 0 & 0 & 1 & 0 \\ 0 & 0 & 0 & 1 \end{bmatrix}, \quad \underline{D} = \begin{bmatrix} 0 \\ 0 \\ 0 \\ 0 \end{bmatrix}.$$

3.2.3 Transfer Functions of the Vehicle Suspensions

In order to find the transfer functions between the defined states and the input, equation (3.8) is used.

$$\underline{G}(s) = \underline{C}(s\underline{I} - \underline{A})^{-1}\underline{B} + \underline{D}. \quad (3.8)$$

In the case of quarter car with serial inerter, $\underline{G}(s)$ will consist of:

$$\underline{G}(s) = \begin{bmatrix} \frac{Z_1(s)}{Z_0(s)} & \frac{Z_2(s)}{Z_0(s)} & \frac{Z_3(s)}{Z_0(s)} & \frac{\dot{Z}_1(s)}{Z_0(s)} & \frac{\dot{Z}_2(s)}{Z_0(s)} & \frac{\dot{Z}_3(s)}{Z_0(s)} \end{bmatrix}^T. \quad (3.9)$$

With the proper manipulation of the found transfer functions, other transfer functions needed for evaluation of ride comfort and road holding can be obtained. Those transfer functions are given in equation (3.10), respectively, sprung mass acceleration, suspension deflection(rattle space) and tire deflection.

$$\begin{aligned} G_{sma}(s) &= \frac{\ddot{Z}_3(s)}{Z_0(s)} \\ G_{rs}(s) &= \frac{Z_3(s) - Z_1(s)}{Z_0(s)} \\ G_{td}(s) &= \frac{Z_1(s)}{Z_0(s)} - 1 \end{aligned} \quad (3.10)$$

After necessary arrangements and combinations of eq(2.3), the following transfer function for standard suspension with parallel inerter relating the road profile displacement to sprung mass acceleration is found as:

$$\frac{\ddot{Z}_2(s)}{Z_0(s)} = \frac{N_p}{D_{4p}s^4 + D_{3p}s^3 + D_{2p}s^2 + D_{1p}s + D_{0p}} \quad (3.11)$$

where

$$\begin{aligned} N_p &= k_t (b_{inrt,p}s^4 + c_s s^3 + k_s s^2) \\ D_{4p} &= (b_{inrt,p}m_s + b_{inrt,p}m_u + m_s m_u) \\ D_{3p} &= (m_s c_s + m_u c_s) \\ D_{2p} &= (b_{inrt,p}k_t + m_s k_s + m_s k_t + m_u k_s) \\ D_{1p} &= k_t c_s \\ D_{0p} &= k_s k_t \end{aligned} \quad (3.12)$$

3.2.4 Frequency Responses

Frequency response obtained by using linear transfer functions are shown in Figure 3.1.

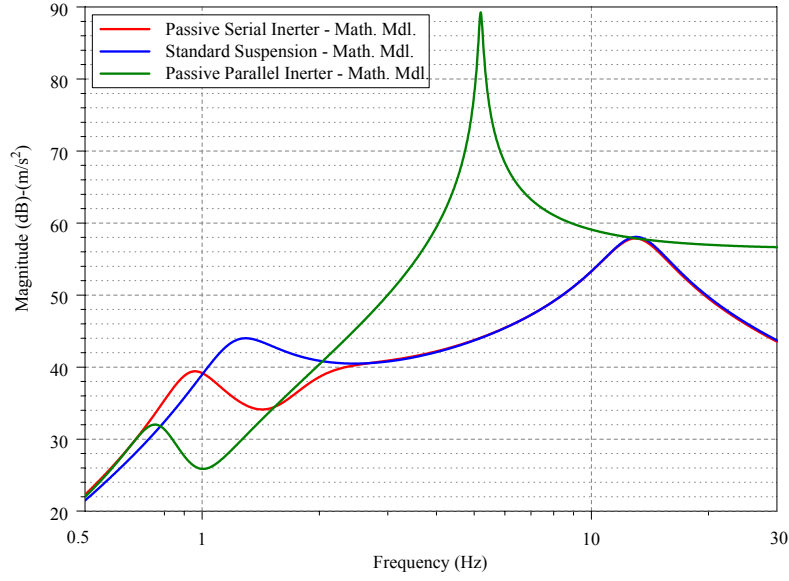


Figure 3.1: Frequency response of the systems obtained by transfer functions of quarter-car models

Frequency responses of the semi-active quarter car models cannot be obtained by linear transfer functions due to discontinuous equations used in semi-active controller. Therefore, the frequency response estimation of the 3 quarter-car models are obtained by using the “Frequency Response Estimation” toolbox of the MATLAB® software, which analyzes the systems with FFT algorithms excited by chirp or sweeping sine inputs. All of the car models are modeled in Simulink® environment.

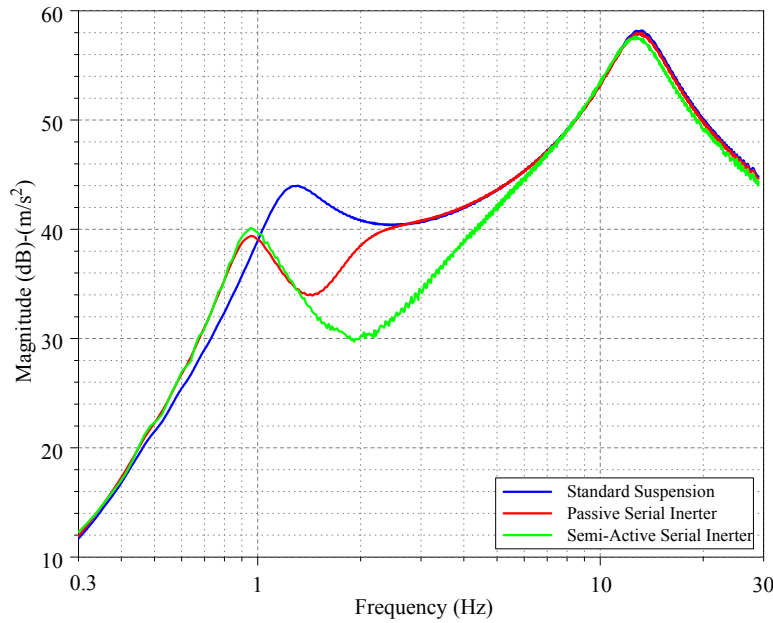


Figure 3.2: Frequency response estimation of the systems modeled with quarter-car models (Sprung mass acceleration)

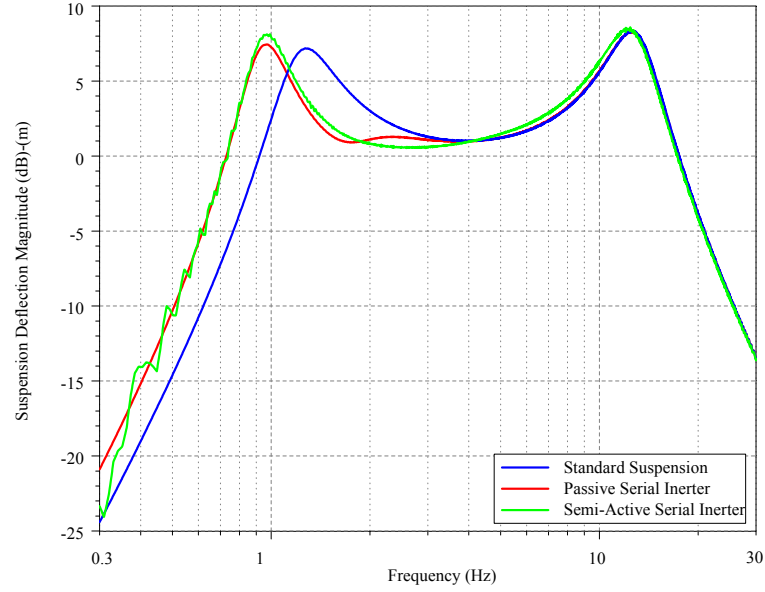


Figure 3.3: Frequency response estimation of the systems modeled with quarter-car models (Suspension deflection)

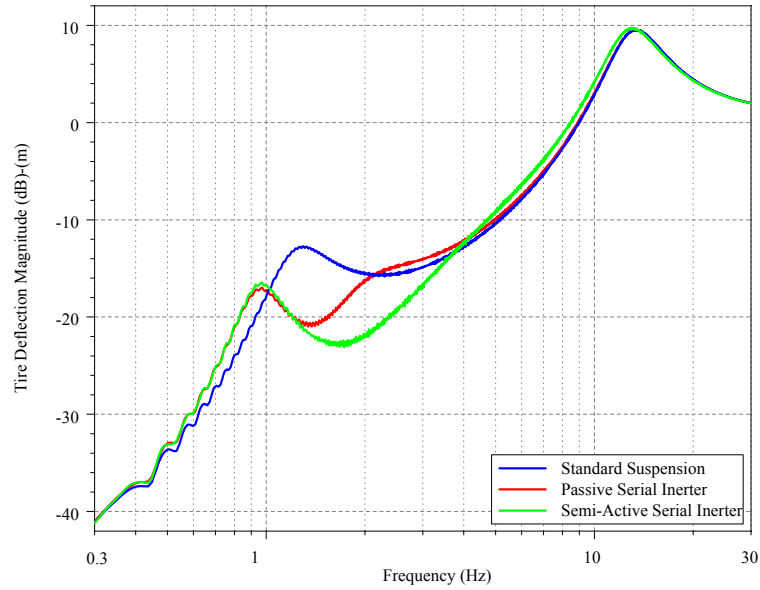


Figure 3.4: Frequency response estimation of the systems modeled with quarter-car models (Tire deflection)

In this thesis, physical realization of the suspensions with inerters will not be made by manufacturing a prototype. However, those systems will be simulated by using a CAE software. For that purpose, 3 quarter car models are modeled in ADAMS®/View module. Furthermore, frequency response of the systems are obtained by using ADAMS®/Vibration module. Since rack and pinion type inerter is rather hard to model, screw-ball type inerter will be used. The inerter is modeled with a flywheel, screw-ball type joint and a revolute joint. Revolute joint is used for connection of flywheel to the mass in the middle and screw-ball joint is used for

creating the inertance effect. The detailed view of the model is shown in Figure 3.5

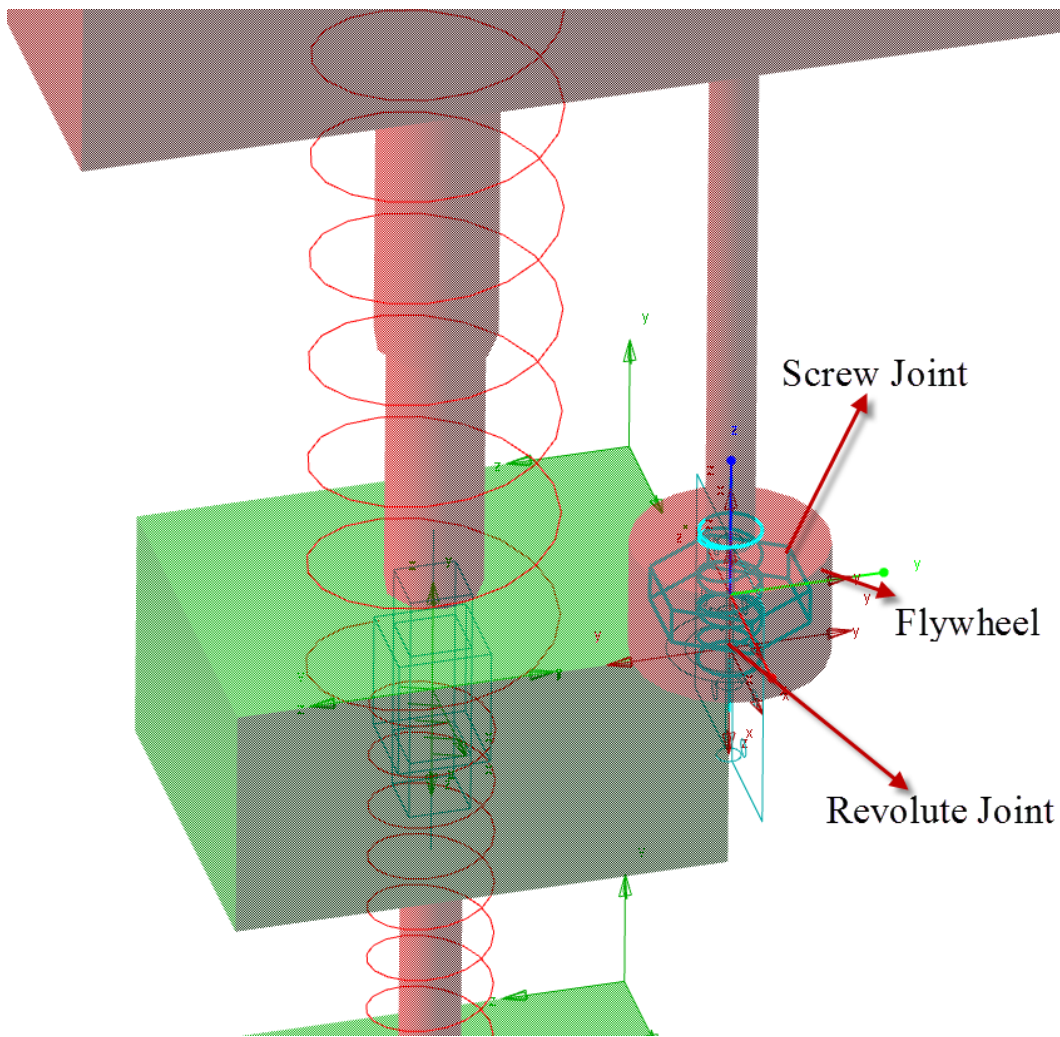


Figure 3.5: Detailed view of the inerter modeled in ADAMS®

The parameters used in ADAMS® inerter model are given in Table 3.1.

Table 3.1: Inerter Parameters used in ADAMS® Inerter Model

Parameter	Value
Pitch of the screw-ball joint	500
$I_{flywheel}$	$2e+6 \text{ kg} \cdot \text{mm}^2$
$m_{flywheel}$	1kg
$d_{flywheel}$	80mm

Overview of the three suspension systems are shown in Figure 3.6.

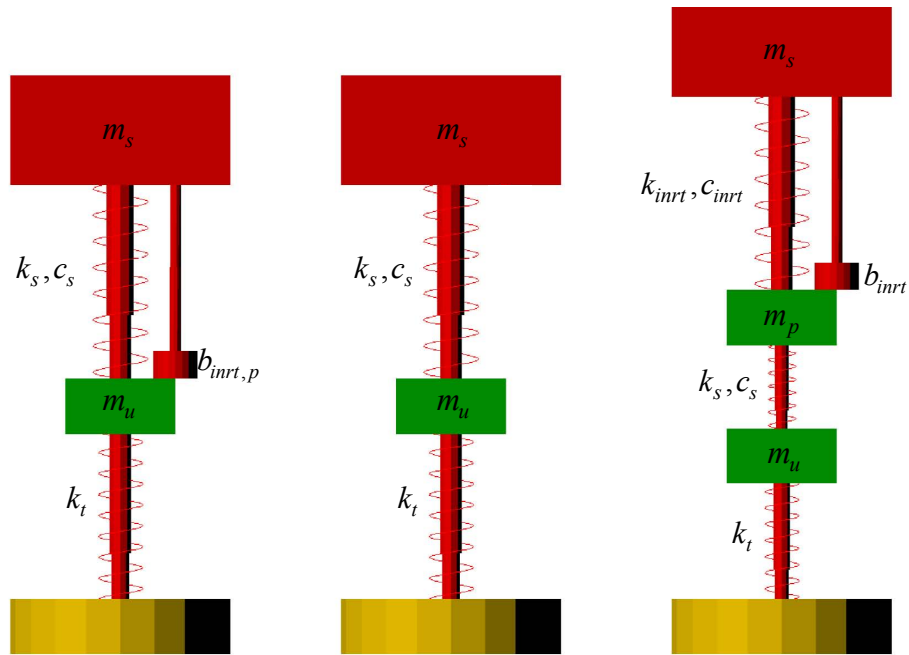


Figure 3.6: Suspension systems modeled in ADAMS®/View

Frequency responses of the systems are shown in Figure 3.7.

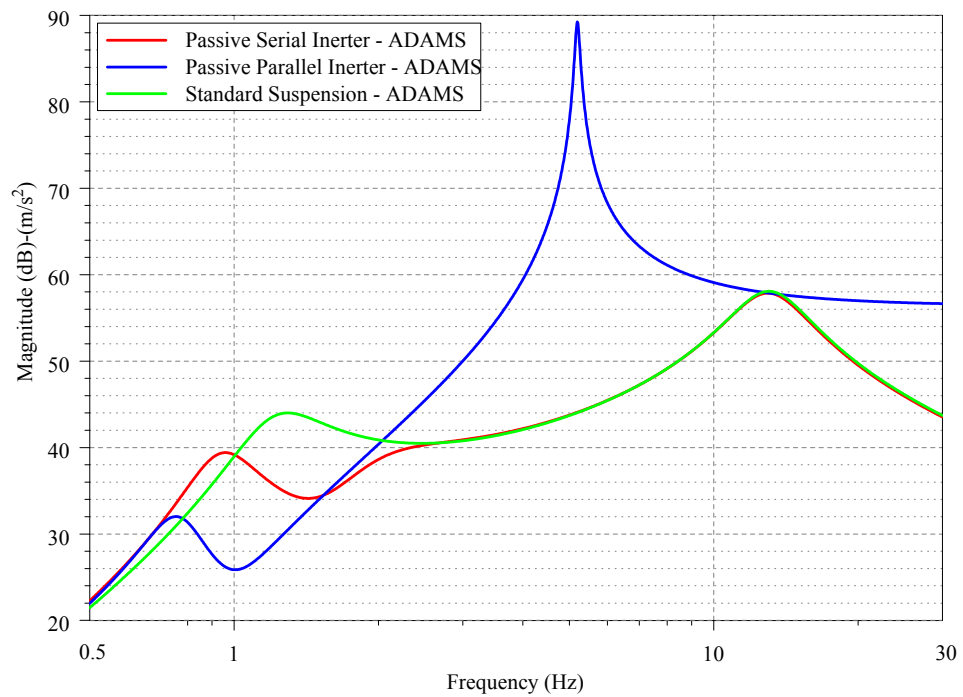


Figure 3.7: Frequency response of the sprung mass accelerations obtained by ADAMS®/Vibration

Finally, ADAMS® results can be used to cross-check the validity of the mathematical models

of the passive systems. In Figure 3.8, both mathematical model results and ADAMS results are shown.

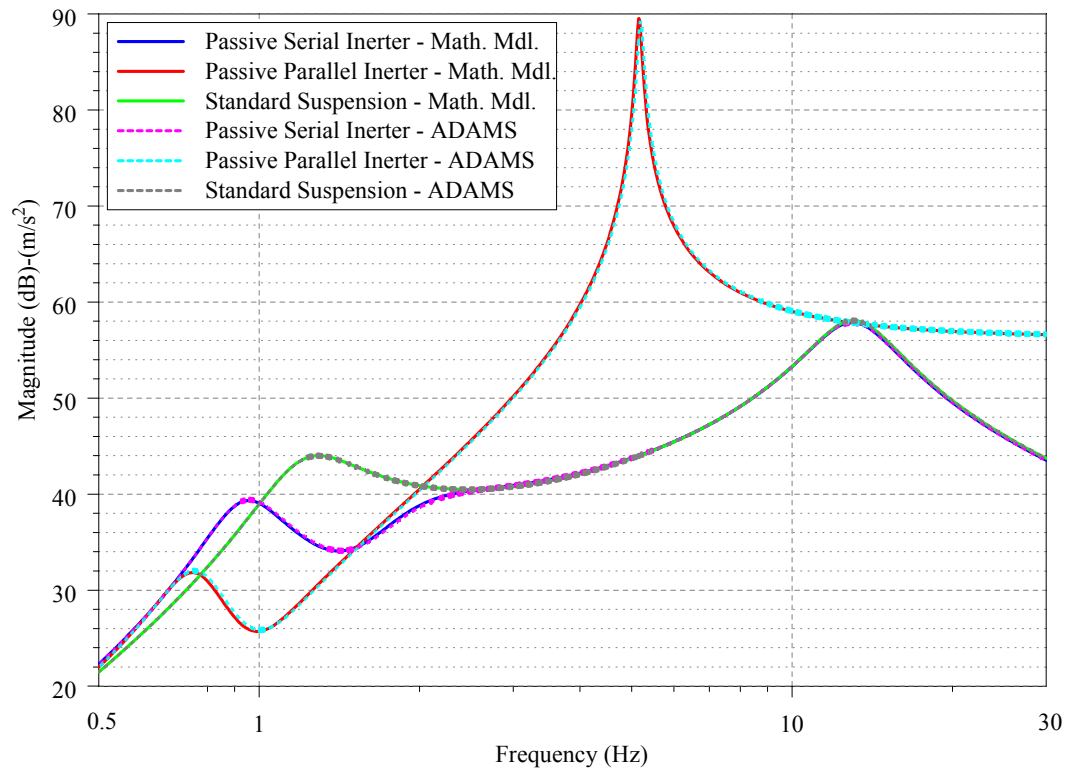


Figure 3.8: Superposed frequency responses of sprung mass acceleration

CHAPTER 4

RANDOM ROAD PROFILE MODELING

4.1 ISO-8608 Road Profiles

As a road profile excitation, sine waves and step functions were used for evaluating the performance of the vehicle dynamics. However, those deterministic inputs only provide a limited conditions for evaluation of performance and far away from the actual road conditions. Since the vehicles are exposed to random road profiles more than deterministic road profiles, using randomly generated profiles will be more appropriate. The road profiles can be represented by PSD functions in the frequency domain. It is the most common way to characterize the road roughness. For that purpose, ISO-8608 random road profiles [16] are generated according to the PSD values given in Table 4.1.

Table 4.1: Road Roughness Classification

Road Class	Geometric Mean of Degree of Roughness $\Phi(\Omega_0) (10^{-6}m^2/rad/m)$
A (very good)	4
B (good)	16
C (average)	64
D (poor)	256
E (very poor)	1024
F	4096
G	16384
H	65536

The PSD of the road profile can be represented by equation 4.1. Generally, road classes from A to E are considered as excitation of the quarter car model for on-road studies. Beyond E class, non-linearities of the suspension elements will also play a role in the suspension performance.

$$\Phi(\Omega) = \Phi(\Omega_0) \left(\frac{\Omega}{\Omega_0} \right)^{-\omega} \quad (4.1)$$

where

Ω = Spatial frequency (rad/m),

$\Phi(\Omega_0)$ = value of the psd at $\Omega_0=1$ rad/m (reference value),
 ω =waviness value (in [16], $\omega=2$ is the suggested value).

Shaping filter method given in [3] is used for generating the ISO-8608 random road profiles. The road profile that vehicle with velocity of V experiences can be generated by using a first order linear filter. The filter is represented by a differential equation shown in equation 4.2.

$$\dot{z}_r(t) = -\alpha z_r(t) + \omega(t) \quad (4.2)$$

$\omega(t)$ is a white noise input with a PSD provided in equation 4.3.

$$\Psi_\omega = \frac{2\alpha V \sigma^2}{\pi} \quad (4.3)$$

where

α =road roughness parameter (rad/m),

σ^2 = variance of road roughness (m²),

V = vehicle speed (m/s).

The PSD of a randomly generated road profile is defined by equation 4.4.

$$\Psi(\omega) = \frac{2\alpha V \sigma^2}{\omega^2 + \alpha^2 V^2}. \quad (4.4)$$

Generated ISO-8608 road profile PSD lines are represented by Figure 4.1.

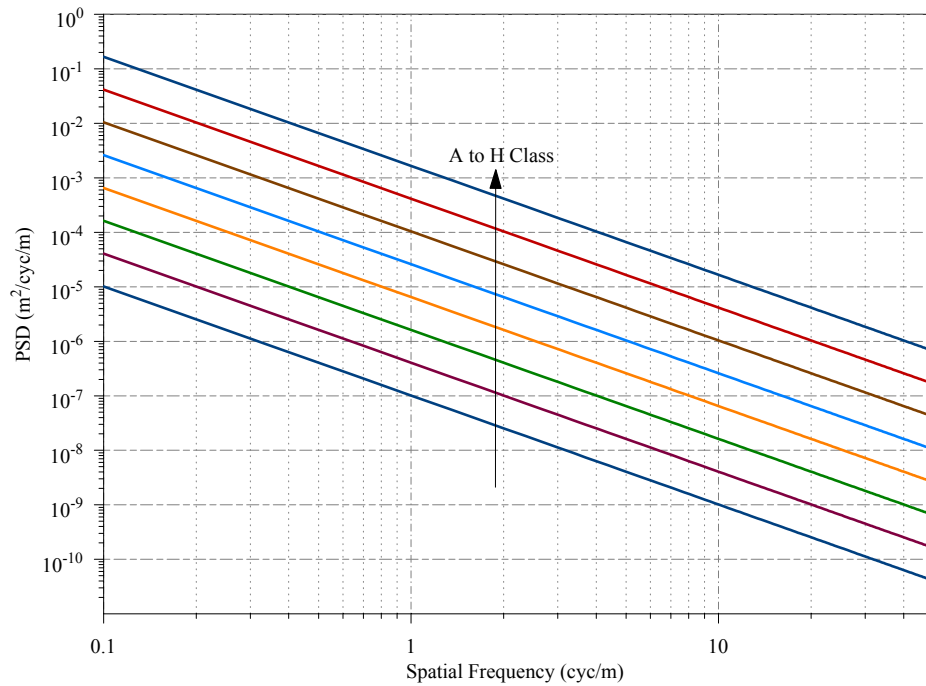


Figure 4.1: ISO-8608 PSD Lines

σ^2 namely the variance of the road is expressed by equation 4.5.

$$\sigma^2 = \frac{1}{2\pi} \int_0^\infty \Phi(\omega) d\Omega = \frac{\Phi(\Omega_0)}{2\pi} \left(\frac{2}{\Omega_1} - \frac{1}{\Omega_N} \right). \quad (4.5)$$

By equating equation 4.4 and equation 4.5 at the reference spatial frequency $\Omega_0=1$ rad/m, is found as 0.1 rad/m. While generating the road surfaces for $V=30$, $V=60$ and $V=90$ kph vehicle speeds, the parameters given in Table 4.2 are chosen.

Table 4.2: Road Generation Parameters

Parameter	Value
Ω_1	0.01π
Ω_N	6π
N	150
ω	2
t_{final}	200s
dt	$0.25 \times \frac{\Omega_N V}{2\pi}$

Figure 4.2 and 4.3 belong to a road profile of class B with $V=30$ kph.

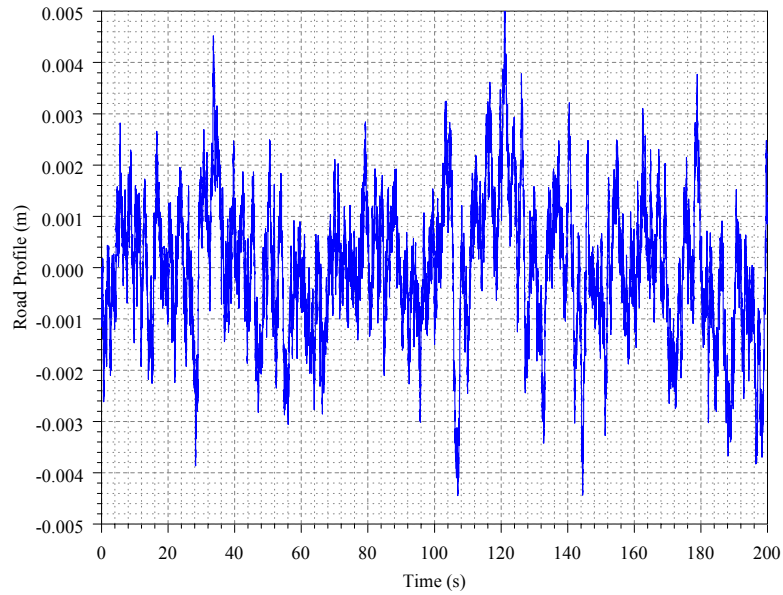


Figure 4.2: Generated B-class ISO-8608 road profile for $V=30$ kph

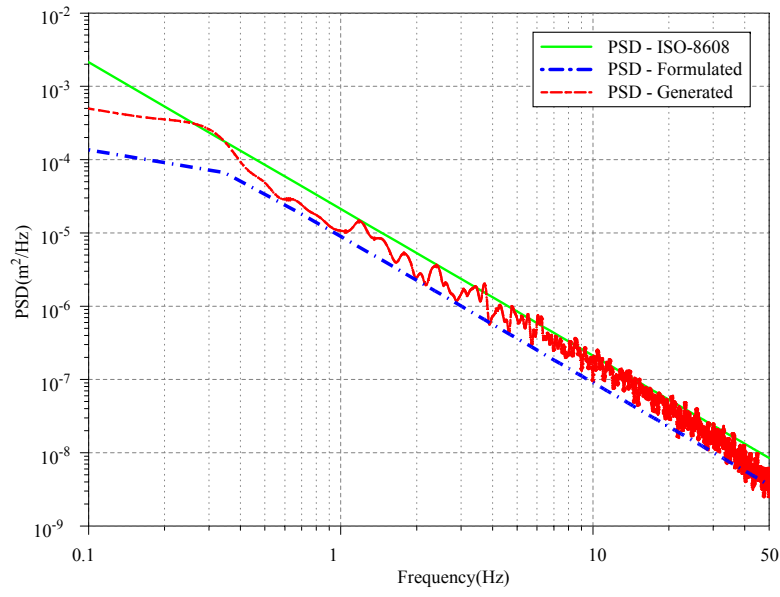


Figure 4.3: PSD lines of B-class ISO-8608 road profile for $V=30$ kph

Figure 4.4 and 4.5 belong to a road profile of class B with $V=60$ kph.

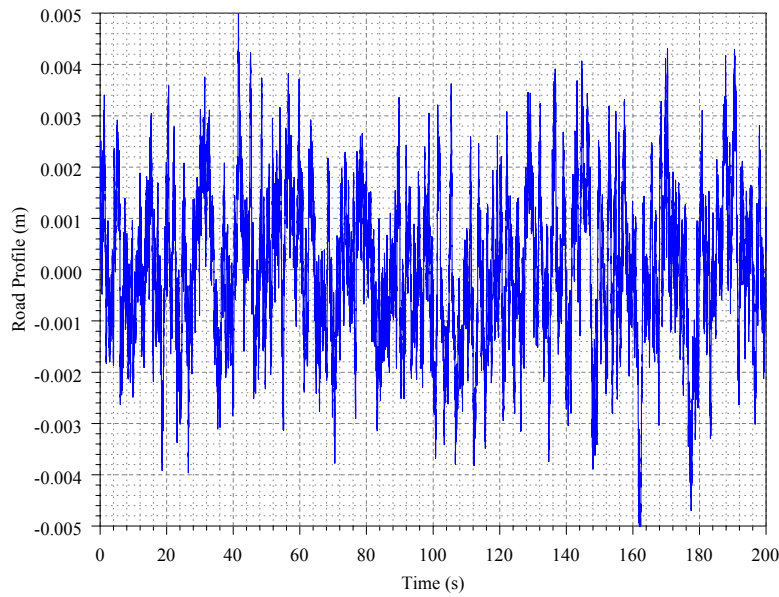


Figure 4.4: Generated B-class ISO-8608 road profile for $V=60$ kph

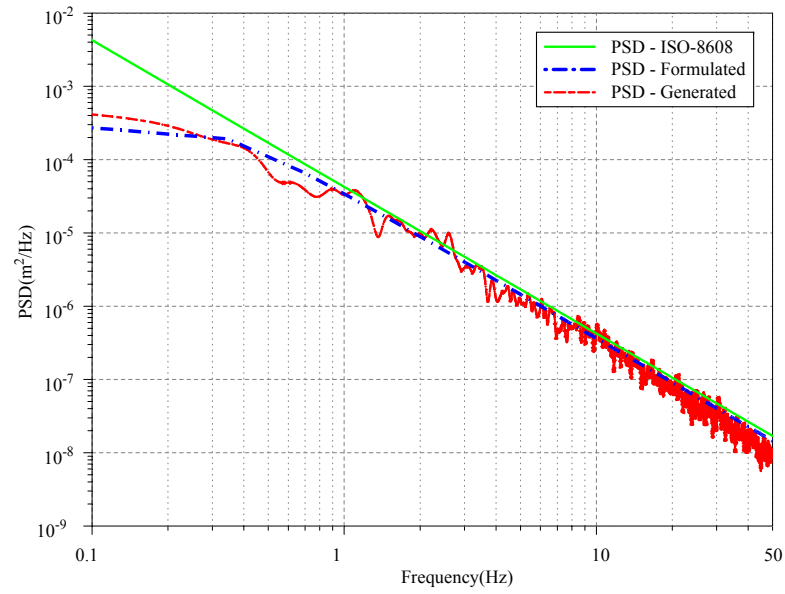


Figure 4.5: PSD lines of B-class ISO-8608 road profile for $V=60$ kph

Figure 4.6 and 4.7 belong to a road profile of class B with $V=90$ kph.

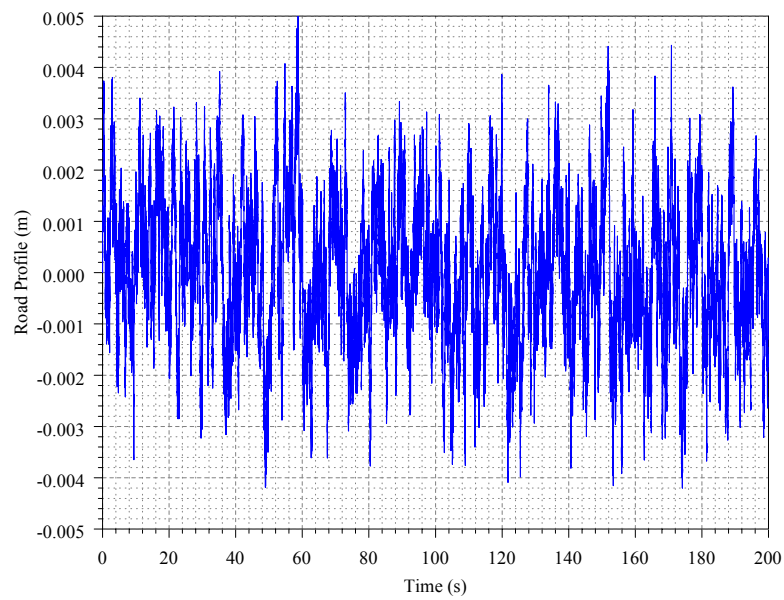


Figure 4.6: Generated B-class ISO-8608 road profile for $V=90$ kph

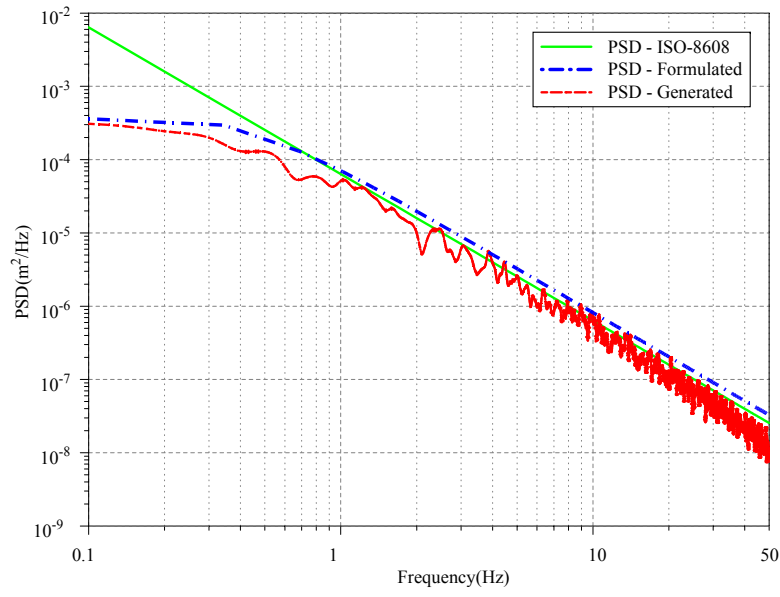


Figure 4.7: PSD lines of B-class ISO-8608 road profile for $V=90$ kph

Time domain simulations, optimizations, evaluations of ride comfort and road holding quality of the optimized suspension system are done by using the randomly generated road profiles.

CHAPTER 5

OPTIMIZATION

5.1 Introduction

Optimization process involves in selecting the cost functions to penalize the desired system properties. Due to the effect of the cost functions on optimization process, they must be chosen carefully. In order to evaluate the ride comfort, sprung mass acceleration in both time domain and frequency domain is investigated. On the other hand, tire deflection is investigated in time domain for a specific road to determine the road holding performance of the vehicle. In this chapter, cost functions given in equation (5.1) are used for optimization process.

$$\begin{aligned} J_1 &= \sqrt{\sum_{t=t_1}^{t_2} \left| \frac{\ddot{z}_3(t)^2}{N} \right|} \\ J_2 &= \sqrt{\sum_{\omega=\omega_1}^{\omega_2} \left| \frac{S_y(\omega) H(\omega) G_{sma}(\omega)^2}{N} \right|} \\ J_3 &= \sqrt{\sum_{t=t_1}^{t_2} \left| \frac{(z_1(t) - z_0(t))^2}{N} \right|} \\ J_4 &= \sqrt{\sum_{t=t_1}^{t_2} \left| \frac{(z_3(t) - z_1(t))^2}{N} \right|} \end{aligned} \tag{5.1}$$

where,

- J_1 : RMS of Sprung Mass Acceleration ($t_1=0$ s, $t_2=200$ s),
- J_2 : The area under the PSD of Sprung Mass Acceleration ($\omega_1=0.1$ Hz, $\omega_2=30$ Hz),
- J_3 : RMS of Tire Deflection ($t_1=0$ s, $t_2=200$ s),
- J_4 : Suspension Deflection ($t_1=0$ s, $t_2=200$ s),
- $S_y(\omega)$: PSD of a chosen road profile,
- $H(\omega)$: Frequency weighting transfer function given in [16],

- N : Number of samples.

In previous chapters, the geometry of the suspension with serial inerter was explained with the reason behind the idea. However, suspension deflection is still be penalized with J_4 for further improvement. Optimizations are done by utilizing the Genetic Algorithm available in MATLAB software. The optimization problem consists of 4 objective functions. At this point, the problem can be regarded as multi-objective optimization. However, multi-objective optimization with genetic algorithm provides equally optimal points called Pareto optimal set, which needs another selection process. In order to avoid that selection process, 4 objective functions are combined in one scalar objective function and single-objective optimization algorithm is applied. This method is called scalarization. In equation 5.2, converted single objective function is given.

$$J_{single} = \rho_1 J_1 + \rho_2 J_2 + \rho_3 J_3 + \rho_4 J_4. \quad (5.2)$$

In order to achieve stable optimization results, all of the objectives are normalized and multiplied with weighting factors [17]. Since the normalized values are used, there will be no different order of magnitudes and weighting factors will be effective during the optimization process. For all the cases, minimum and maximum values of each objective function are calculated before the optimization process without regard to other objective functions. The points corresponding to those values are called utopia points. Normally, with the combined objective function, they cannot be achieved. That is, simultaneous minimization of all the objective functions is not possible with one design point. Then, during the optimization process, the normalization procedure can be applied by using the equation (5.3).

$$f_i^{norm} = \frac{f_i(x) - f_i^0}{f_i^{max} - f_i^0} \quad (5.3)$$

where,

i : 1,2, ... , k (k is the number of objective functions),

f_i^0 : optimum value of the i th objective function,

f_i^{max} : maximum value of the i th objective function.

5.2 Optimization with ISO Roads

Before the optimization process, in order to understand the effects of the inerter on the ride comfort and road holding, trade-off curves for different road types and vehicle speeds are plotted. To compare suspension systems on a standard basis, standard suspension is regarded as a reference model, and normalization method is used. The cost function of the standard system for a specific case is assumed to be 1. Values for passive serial inerter greater than 1 mean that the performance is superior.

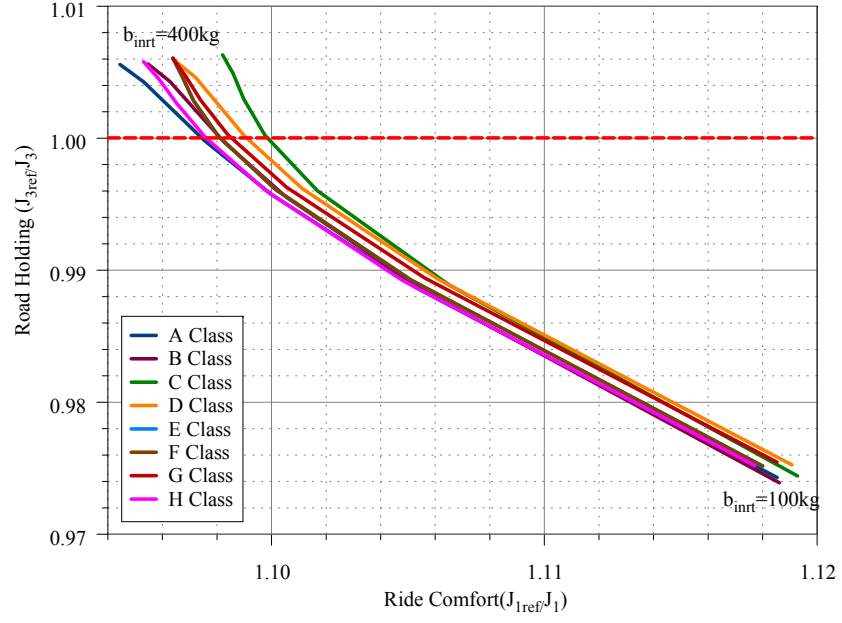


Figure 5.1: J_3 vs. J_1 with different inertance values at $V=30\text{kph}$ (Passive serial inerter, $k_{inrt} = 35000\text{N/m}$, $c_{inrt} = 2000\text{Ns/m}$, $k_s = 15000\text{N/m}$, $c_s = 900\text{Ns/m}$)

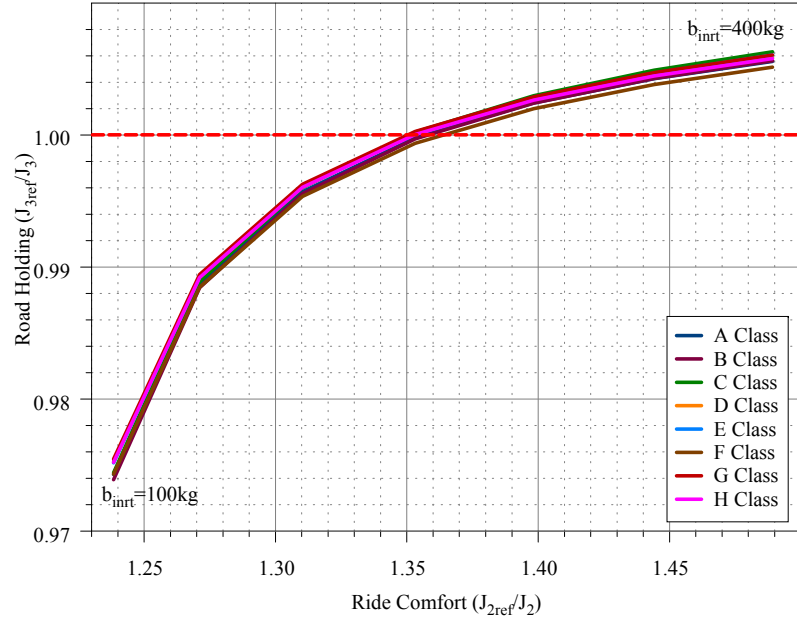


Figure 5.2: J_3 vs. J_2 with different inertance values at $V=30\text{kph}$ (Passive serial inerter, $k_{inrt} = 35000\text{N/m}$, $c_{inrt} = 2000\text{Ns/m}$, $k_s = 15000\text{N/m}$, $c_s = 900\text{Ns/m}$)

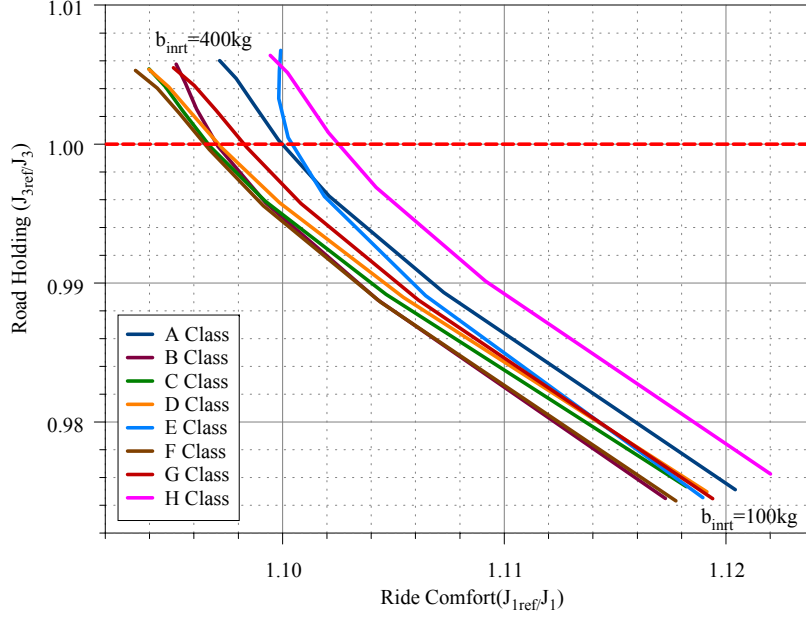


Figure 5.3: J_3 vs. J_1 with different inertance values at $V=60\text{kph}$ (Passive serial inerter, $k_{inrt} = 35000\text{N/m}$, $c_{inrt} = 2000\text{Ns/m}$, $k_s = 15000\text{N/m}$, $c_s = 900\text{Ns/m}$)

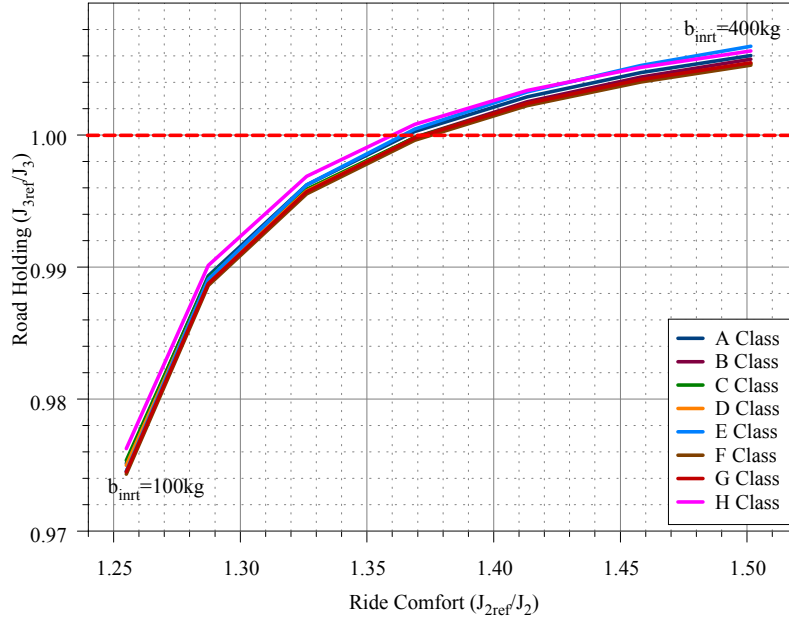


Figure 5.4: J_3 vs. J_2 with different inertance values at $V=60\text{kph}$ (Passive serial inerter, $k_{inrt} = 35000\text{N/m}$, $c_{inrt} = 2000\text{Ns/m}$, $k_s = 15000\text{N/m}$, $c_s = 900\text{Ns/m}$)

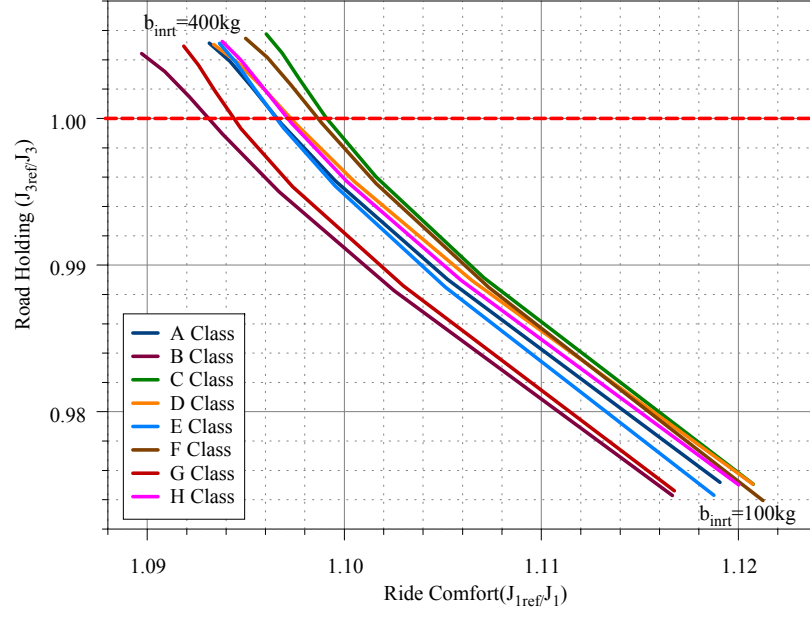


Figure 5.5: J_3 vs. J_1 with different inertance values at $V=90\text{kph}$ (Passive serial inerter, $k_{inrt} = 35000\text{N/m}$, $c_{inrt} = 2000\text{Ns/m}$, $k_s = 15000\text{N/m}$, $c_s = 900\text{Ns/m}$)

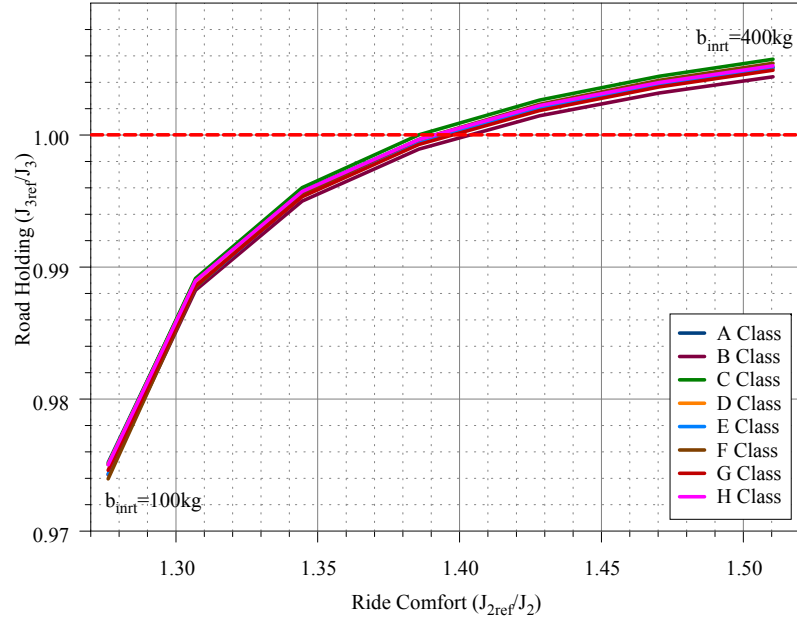


Figure 5.6: J_3 vs. J_2 with different inertance values at $V=90\text{kph}$ (Passive serial inerter, $k_{inrt} = 35000\text{N/m}$, $c_{inrt} = 2000\text{Ns/m}$, $k_s = 15000\text{N/m}$, $c_s = 900\text{Ns/m}$)

5.3 Semi-Active Suspension comparison with Passive Suspensions

In terms of road holding and ride comfort, the semi-active suspension locus are nothing but the isolated points. These points are plotted with passive suspensions' curves.

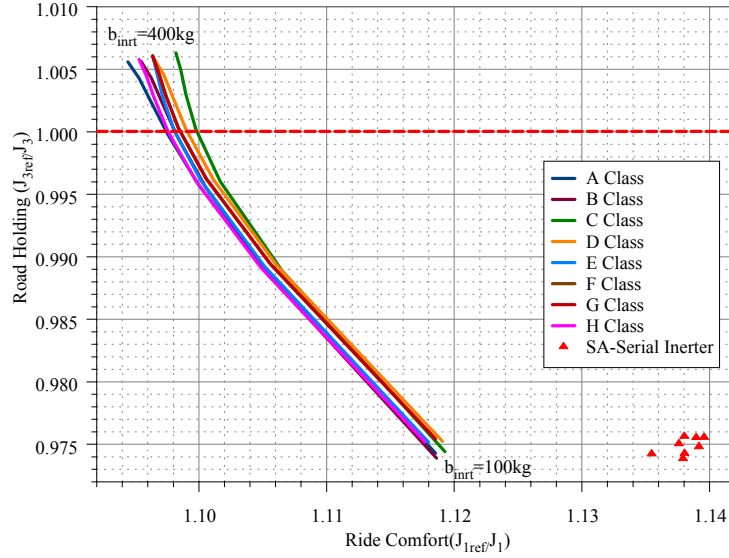


Figure 5.7: J_3 vs J_1 with different inertance values at $V=30\text{kph}$ (Passive serial inerter and semi-active serial inerter, $k_{inrt} = 35000\text{N/m}$, $c_{inrt} = 2000\text{Ns/m}$, $k_s = 15000\text{N/m}$, $c_s = 900\text{Ns/m}$)

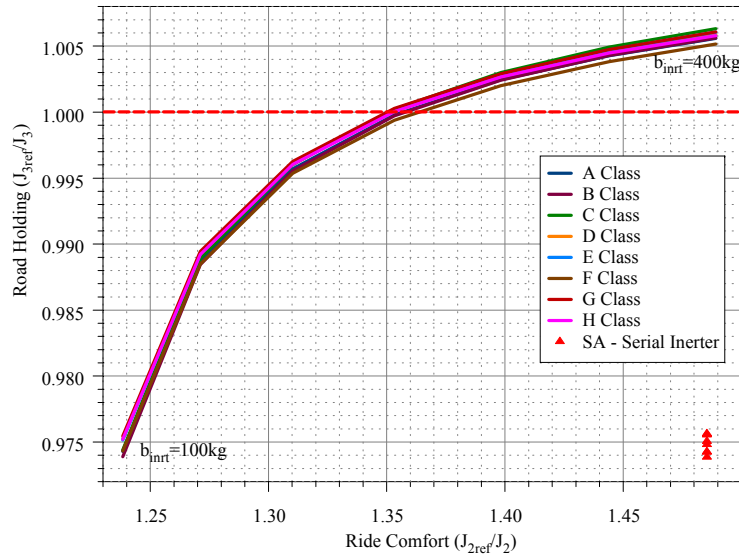


Figure 5.8: J_3 vs J_2 with different inertance values at $V=30\text{kph}$ (Passive serial inerter and semi-active serial inerter, $k_{inrt} = 35000\text{N/m}$, $c_{inrt} = 2000\text{Ns/m}$, $k_s = 15000\text{N/m}$, $c_s = 900\text{Ns/m}$)

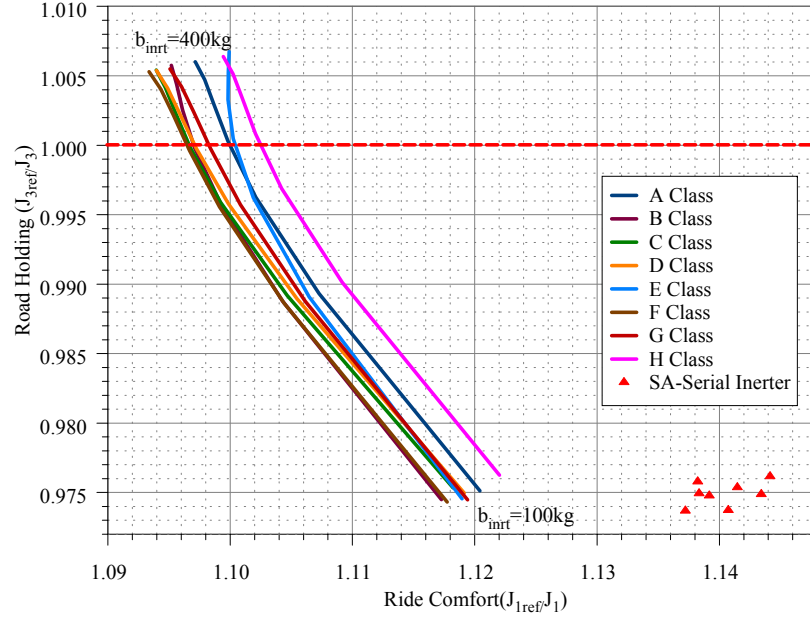


Figure 5.9: J_3 vs J_1 with different inertance values at $V=60\text{kph}$ (Passive serial inerter and semi-active serial inerter, $k_{inrt} = 35000\text{N/m}$, $c_{inrt} = 2000\text{Ns/m}$, $k_s = 15000\text{N/m}$, $c_s = 900\text{Ns/m}$)

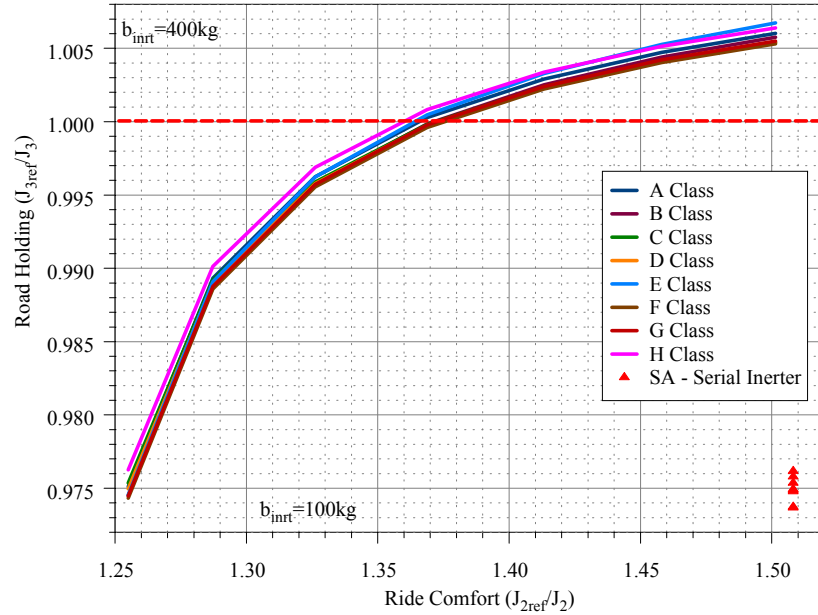


Figure 5.10: J_3 vs J_2 with different inertance values at $V=60\text{kph}$ (Passive serial inerter and semi-active serial inerter, $k_{inrt} = 35000\text{N/m}$, $c_{inrt} = 2000\text{Ns/m}$, $k_s = 15000\text{N/m}$, $c_s = 900\text{Ns/m}$)

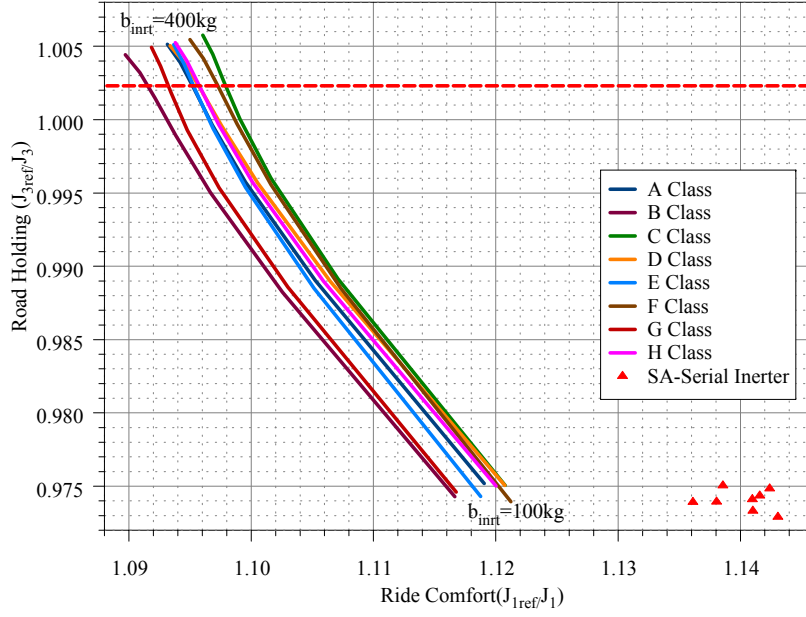


Figure 5.11: J_3 vs J_1 with different inertance values at $V=90\text{kph}$ (Passive serial inerter and semi-active serial inerter, $k_{inrt} = 35000\text{N/m}$, $c_{inrt} = 2000\text{Ns/m}$, $k_s = 15000\text{N/m}$, $c_s = 900\text{Ns/m}$)

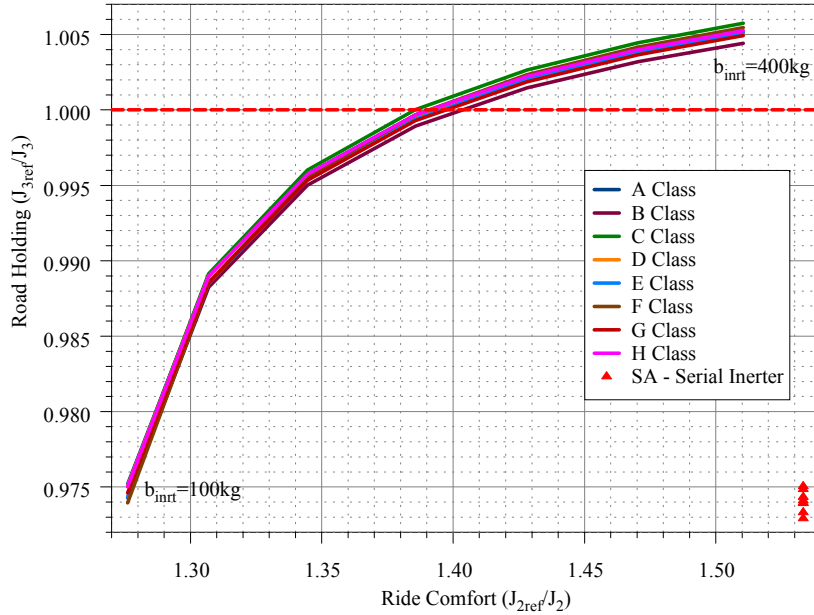


Figure 5.12: J_3 vs J_2 with different inertance values at $V=90\text{kph}$ (Passive serial inerter and semi-active serial inerter, $k_{inrt} = 35000\text{N/m}$, $c_{inrt} = 2000\text{Ns/m}$, $k_s = 15000\text{N/m}$, $c_s = 900\text{Ns/m}$)

5.4 The Effect of Change of Suspension Damping on Inerter Performance

In order to see the effect of suspension damping on the inerter performance, results given in previous section are also recalculated by using 2 different damping values, which are $c_s = 1500\text{Ns/m}$ and $c_s = 1800\text{Ns/m}$. First result set is given for $c_s = 1500\text{Ns/m}$.

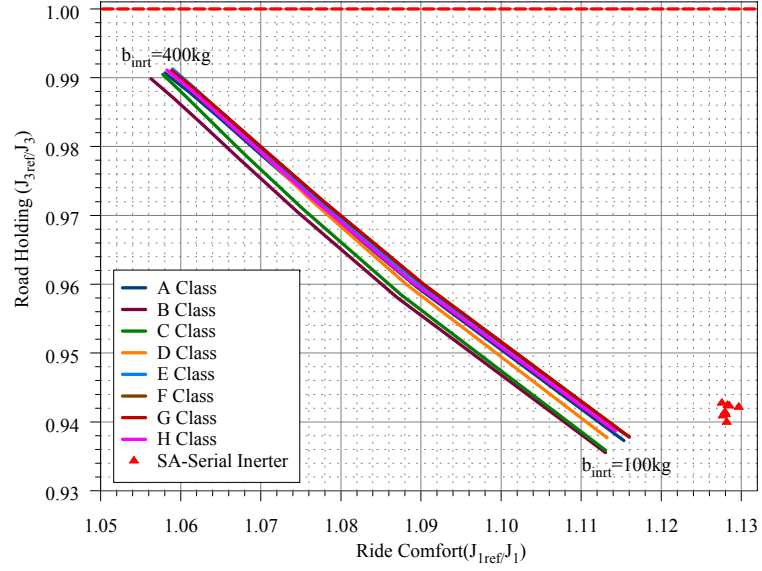


Figure 5.13: J_3 vs J_1 with different inertance values at $V=30\text{kph}$ (Passive serial inerter and semi-active serial inerter, $k_{inrt} = 35000\text{N/m}$, $c_{inrt} = 2000\text{Ns/m}$, $k_s = 15000\text{N/m}$, $c_s = 1500\text{Ns/m}$)

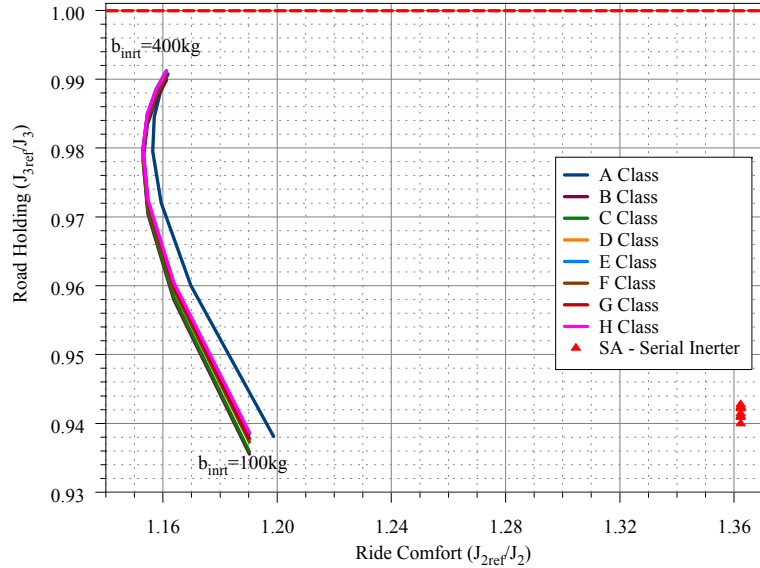


Figure 5.14: J_3 vs J_2 with different inertance values at $V=30\text{kph}$ (Passive serial inerter and semi-active serial inerter, $k_{inrt} = 35000\text{N/m}$, $c_{inrt} = 2000\text{Ns/m}$, $k_s = 15000\text{N/m}$, $c_s = 1500\text{Ns/m}$)

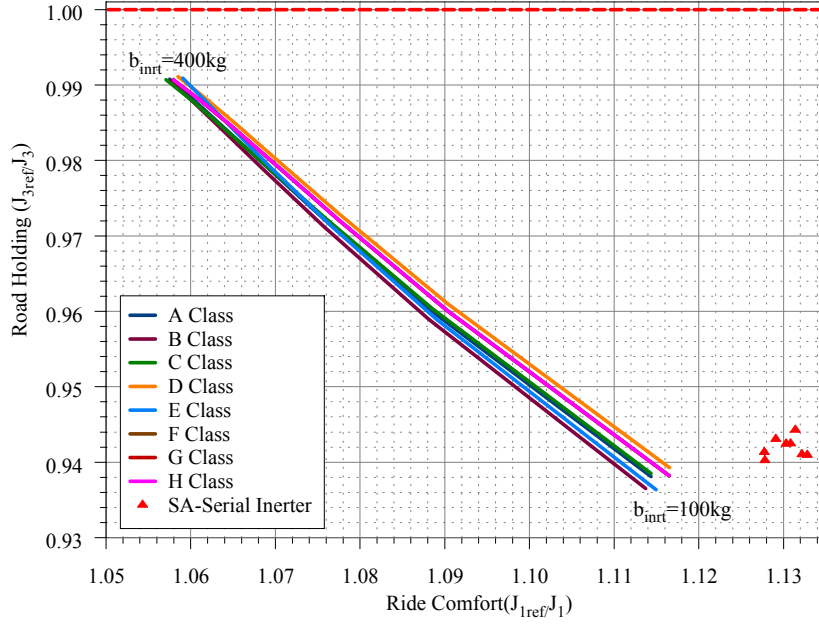


Figure 5.15: J_3 vs J_1 with different inertance values at $V=60\text{kph}$ (Passive serial inerter and semi-active serial inerter, $k_{inrt} = 35000\text{N/m}$, $c_{inrt} = 2000\text{Ns/m}$, $k_s = 15000\text{N/m}$, $c_s = 1500\text{Ns/m}$)

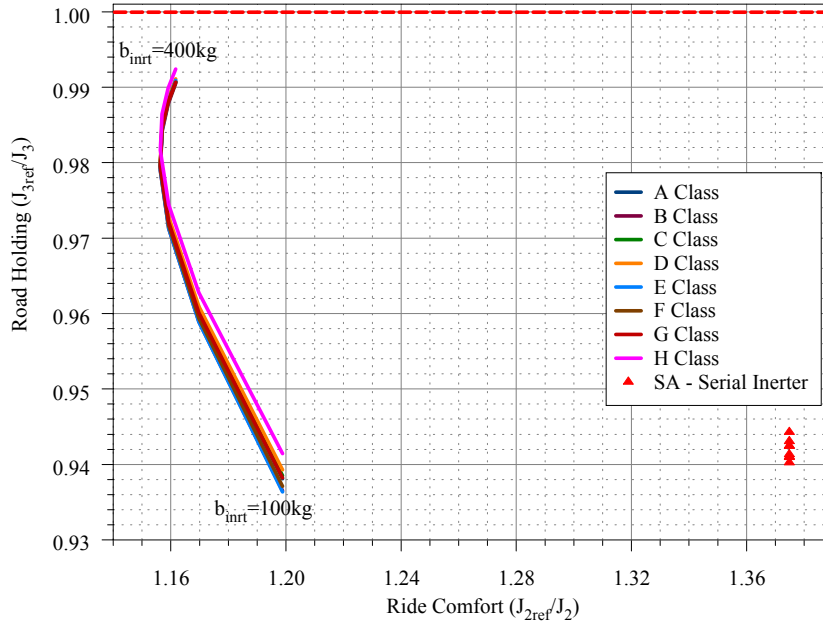


Figure 5.16: J_3 vs J_2 with different inertance values at $V=60\text{kph}$ (Passive serial inerter and semi-active serial inerter, $k_{inrt} = 35000\text{N/m}$, $c_{inrt} = 2000\text{Ns/m}$, $k_s = 15000\text{N/m}$, $c_s = 1500\text{Ns/m}$)

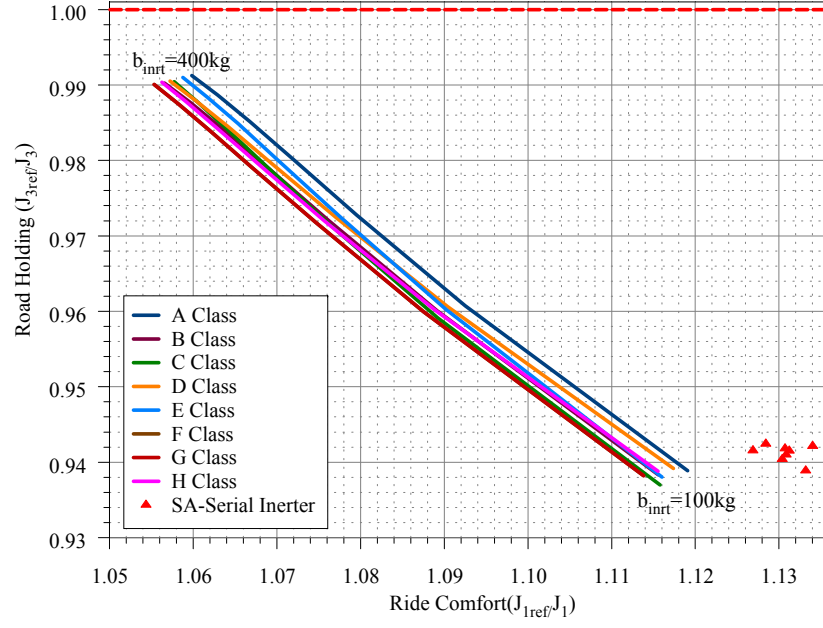


Figure 5.17: J_3 vs J_1 with different inertance values at $V=90\text{kph}$ (Passive serial inerter and semi-active serial inerter, $k_{inrt} = 35000\text{N/m}$, $c_{inrt} = 2000\text{Ns/m}$, $k_s = 15000\text{N/m}$, $c_s = 1500\text{Ns/m}$)

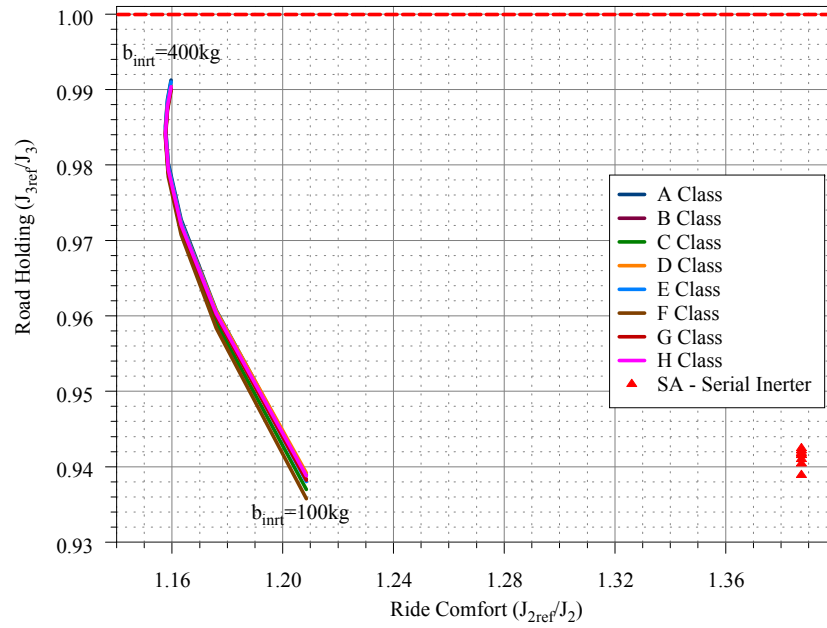


Figure 5.18: J_3 vs J_2 with different inertance values at $V=90\text{kph}$ (Passive serial inerter and semi-active serial inerter, $k_{inrt} = 35000\text{N/m}$, $c_{inrt} = 2000\text{Ns/m}$, $k_s = 15000\text{N/m}$, $c_s = 1500\text{Ns/m}$)

Second and final result set is given for $c_s = 1800\text{Ns/m}$.

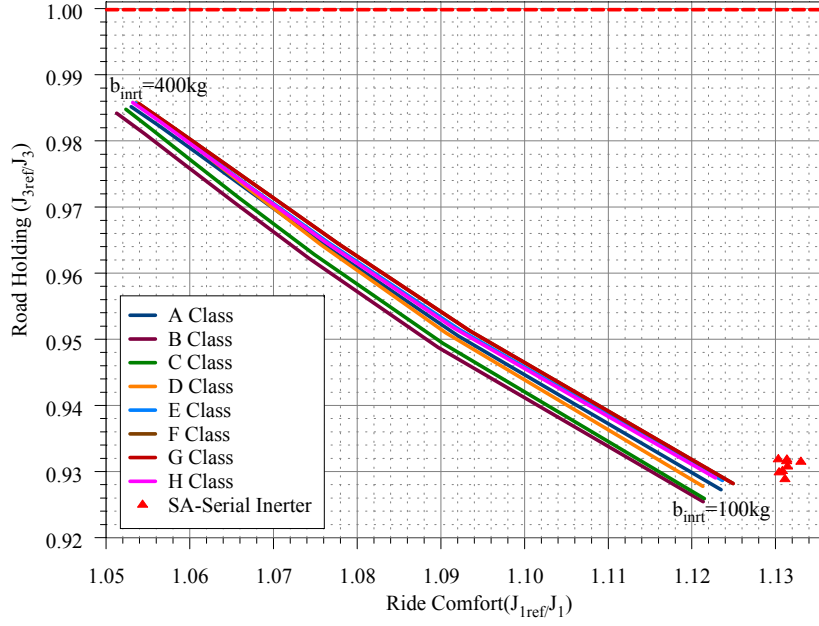


Figure 5.19: J_3 vs J_1 with different inertance values at $V=30\text{kph}$ (Passive serial inerter and semi-active serial inerter, $k_{inrt} = 35000\text{N/m}$, $c_{inrt} = 2000\text{Ns/m}$, $k_s = 15000\text{N/m}$, $c_s = 1800\text{Ns/m}$)

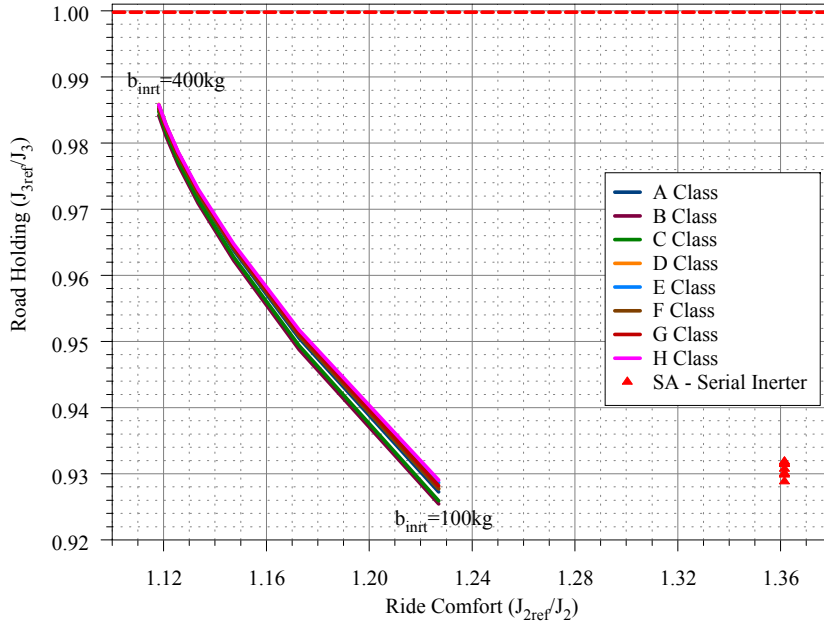


Figure 5.20: J_3 vs J_2 with different inertance values at $V=30\text{kph}$ (Passive serial inerter and semi-active serial inerter, $k_{inrt} = 35000\text{N/m}$, $c_{inrt} = 2000\text{Ns/m}$, $k_s = 15000\text{N/m}$, $c_s = 1800\text{Ns/m}$)

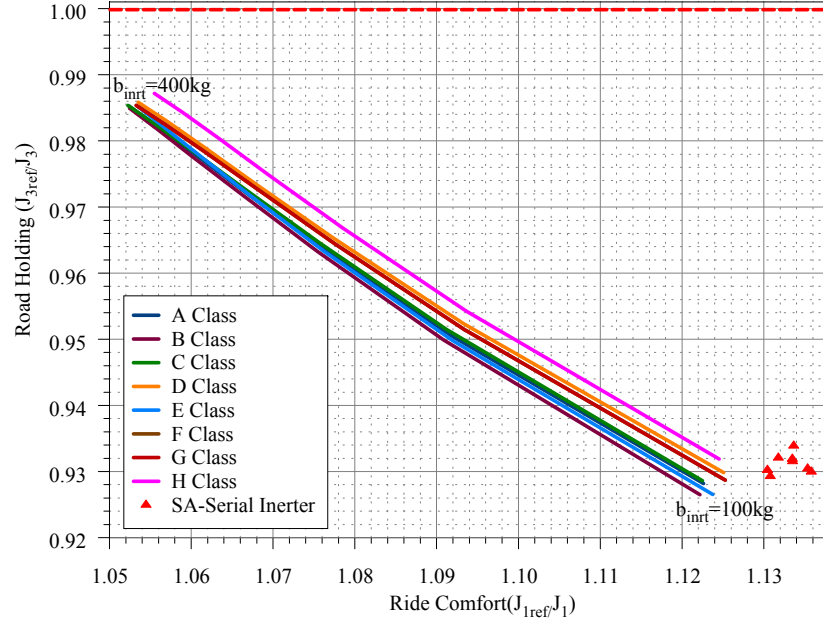


Figure 5.21: J_3 vs J_1 with different inertance values at $V=60\text{kph}$ (Passive serial inerter and semi-active serial inerter, $k_{inrt} = 35000\text{N/m}$, $c_{inrt} = 2000\text{Ns/m}$, $k_s = 15000\text{N/m}$, $c_s = 1800\text{Ns/m}$)

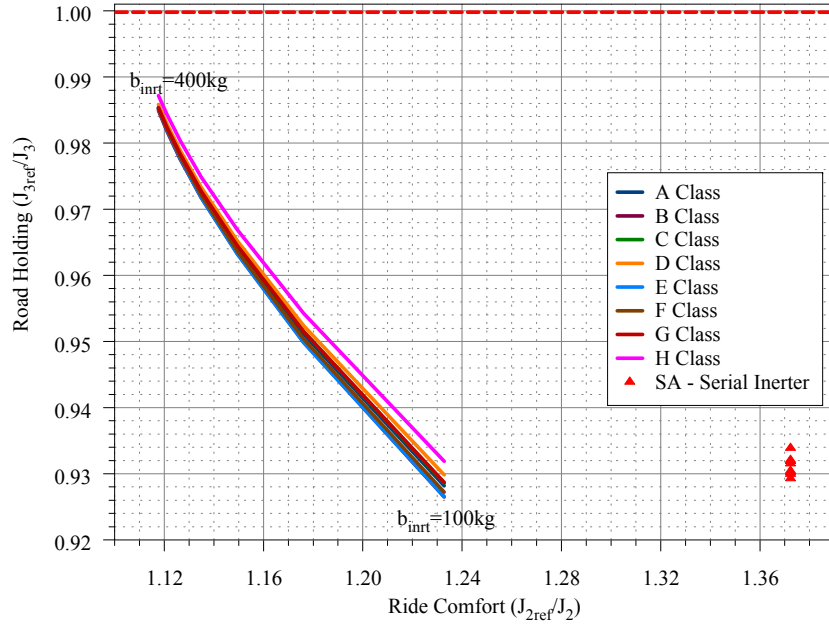


Figure 5.22: J_3 vs J_2 with different inertance values at $V=60\text{kph}$ (Passive serial inerter and semi-active serial inerter, $k_{inrt} = 35000\text{N/m}$, $c_{inrt} = 2000\text{Ns/m}$, $k_s = 15000\text{N/m}$, $c_s = 1800\text{Ns/m}$)

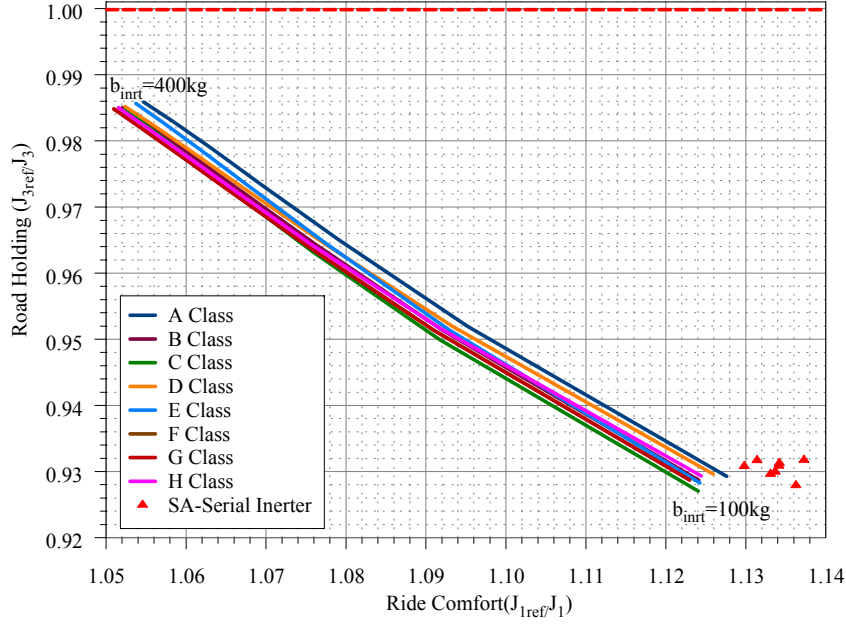


Figure 5.23: J_3 vs J_1 with different inertance values at $V=90\text{kph}$ (Passive serial inerter and semi-active serial inerter, $k_{inrt} = 35000\text{N/m}$, $c_{inrt} = 2000\text{Ns/m}$, $k_s = 15000\text{N/m}$, $c_s = 1800\text{Ns/m}$)

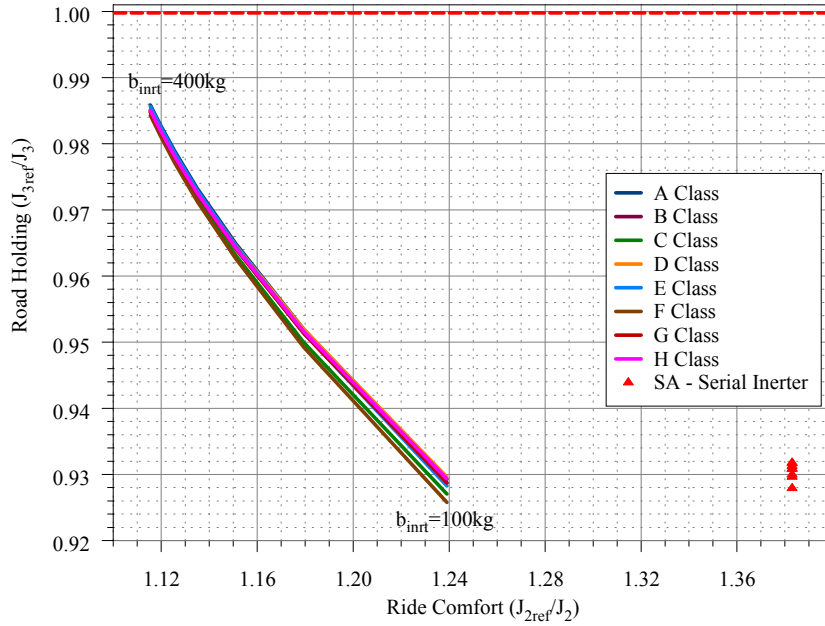


Figure 5.24: J_3 vs J_2 with different inertance values at $V=90\text{kph}$ (Passive serial inerter and semi-active serial inerter, $k_{inrt} = 35000\text{N/m}$, $c_{inrt} = 2000\text{Ns/m}$, $k_s = 15000\text{N/m}$, $c_s = 1800\text{Ns/m}$)

When three cases given above are considered, inerter will work most effectively in a sus-

pension system with lower damping coefficient. In other words, if the inerter is applied to a suspension system with low damping coefficient, both ride comfort and road holding performance are increased with the increasing inertance constant.

From the $J_3 - J_1$ and $J_3 - J_2$ curves given above, general effect of the inerter on the vehicle behavior can be summarized as in Figure 5.28. In addition to those results, the effect of inertance on the working space of the suspension is shown in the following J_4 - Inertance versus b_{inrt} figures.

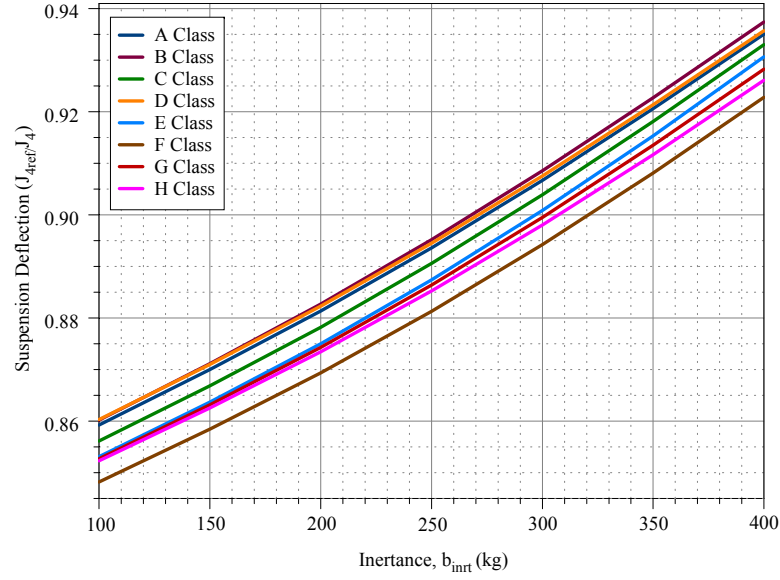


Figure 5.25: J_4 vs. inertance, b_{inrt} at $V=30\text{kph}$ (Passive serial inerter, $k_{inrt} = 35000\text{N/m}$, $c_{inrt} = 2000\text{Ns/m}$)

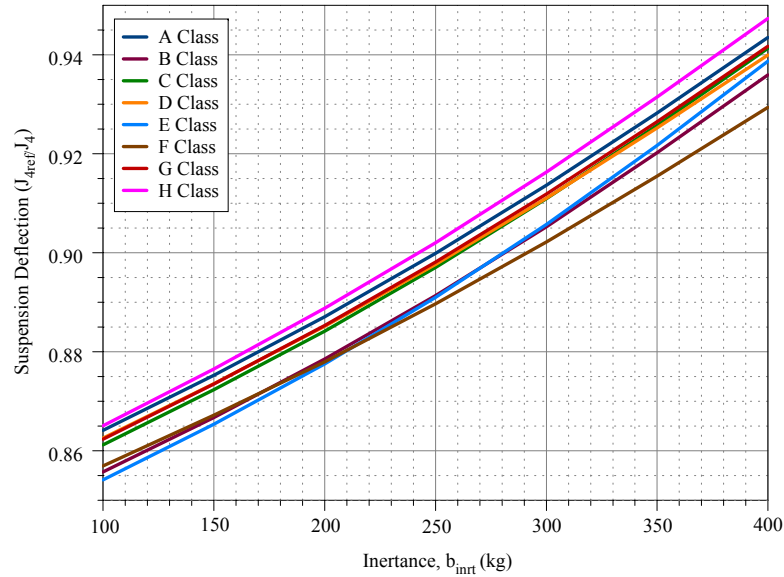


Figure 5.26: J_4 vs. inertance, b_{inrt} at $V=60\text{kph}$ (Passive serial inerter, $k_{inrt} = 35000\text{N/m}$, $c_{inrt} = 2000\text{Ns/m}$)

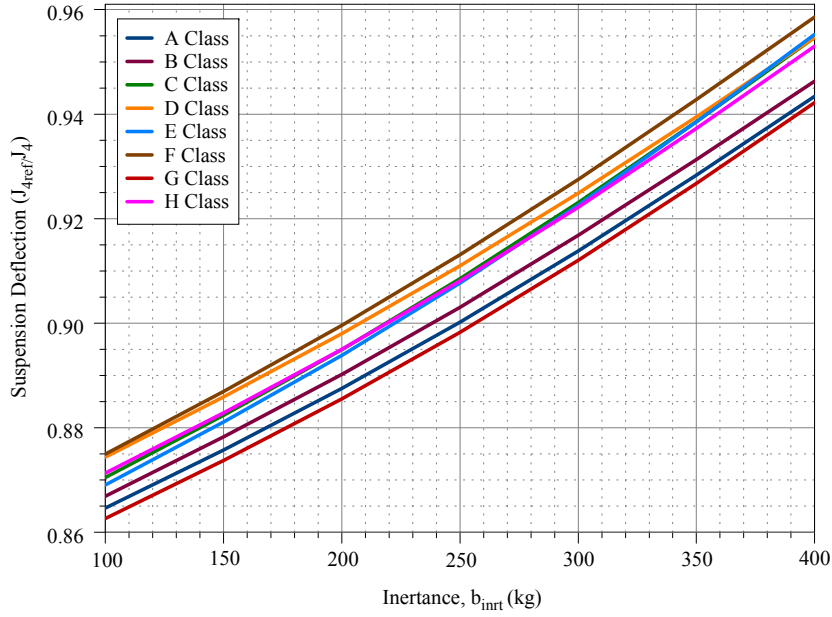


Figure 5.27: J_4 vs. inertance, b_{inrt} at $V=90\text{kph}$ (Passive serial inerter, $k_{inrt} = 35000\text{N/m}$, $c_{inrt} = 2000\text{Ns/m}$)

It can be seen that the increased inertance leads to decreased suspension deflection.

In Figure 5.28, trade-off between road holding and ride comfort for passive serial inerter is given. The curves are only for the generalized results and do not reflect any quantitative result.

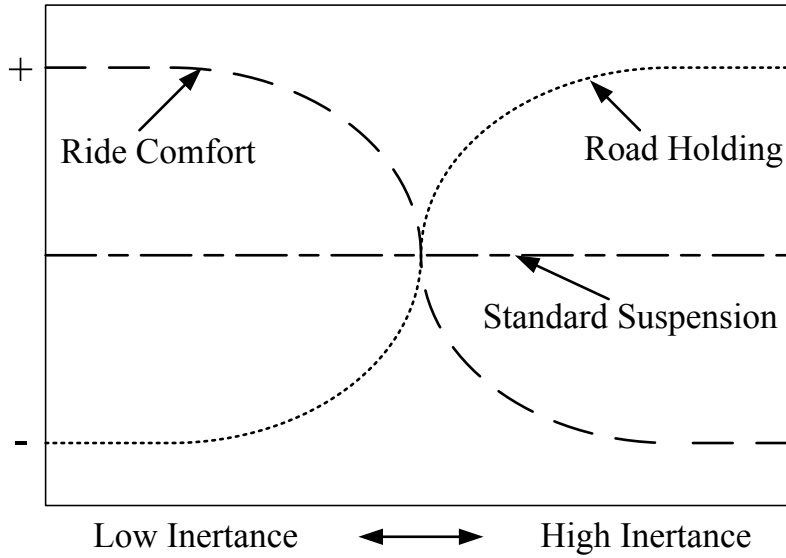


Figure 5.28: Inertance trade-off curves for suspension with inerter

Weighting parameters are chosen such that they penalize J_1 and J_3 more than the remaining

2 objectives in order to improve the time domain performance of ride comfort and handling of the vehicle. Therefore, ρ_1 and ρ_3 values are selected to be higher than the others.

The optimization parameters kept constant and weighting parameters are given in Table 5.1.

Table 5.1: Parameters Used in Optimization

Parameter	Value
k_s	15000
c_s	900
ρ_1	1.2
ρ_2	0.4
ρ_3	2.6
ρ_4	0.5

Design space of the suspension is another vital concept. For a design problem, it is a combination of all feasible designs. Therefore, feasible design space selection is important for the optimization process. Boundaries are chosen in a physically applicable manner. The design space of the parameters to be optimized is given in Table 5.2. The limits are also selected according to the values available in previous studies available in the literature.

Table 5.2: Lower and Upper Bounds of Parameters to be Optimized

Parameter	Limits
k_{inrt}	35000 N/m - 70000 N/m
c_{inrt}	200 - 2000 N.s/m
b_{inrt}	100 kg - 400 kg

Before proceeding into optimization process, the effect of inerter stiffness (k_{inrt}) are depicted in the following figures as 3D surfaces.

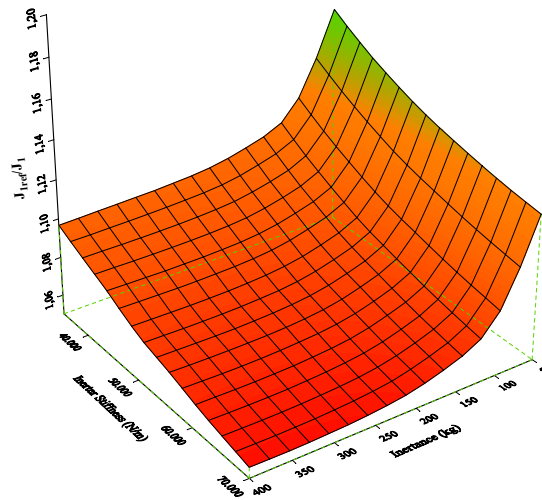


Figure 5.29: J_1 at $V=60\text{kph}$, A class road

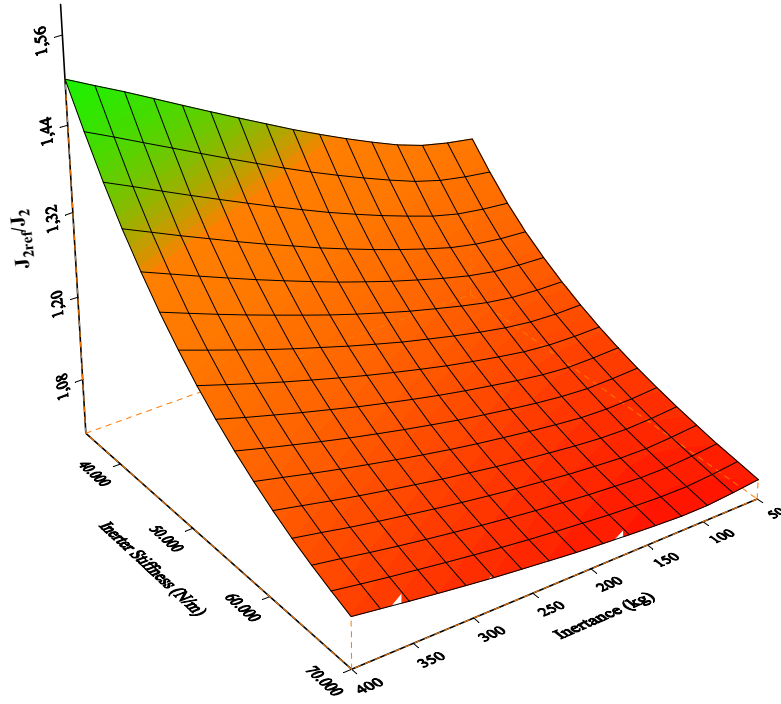


Figure 5.30: J_2 at $V=60\text{kph}$, A class road

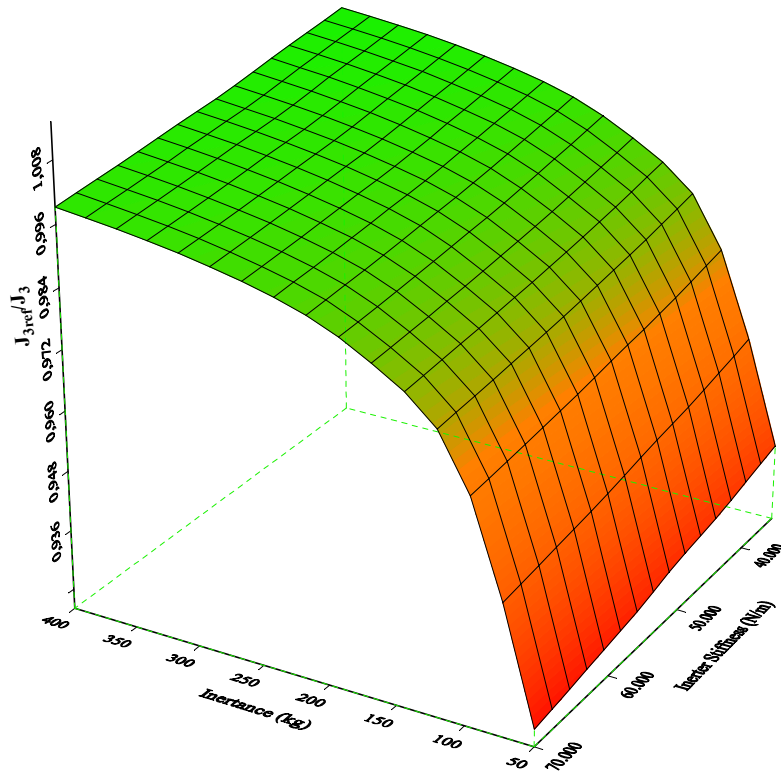


Figure 5.31: J_3 at $V=60\text{kph}$, A class road

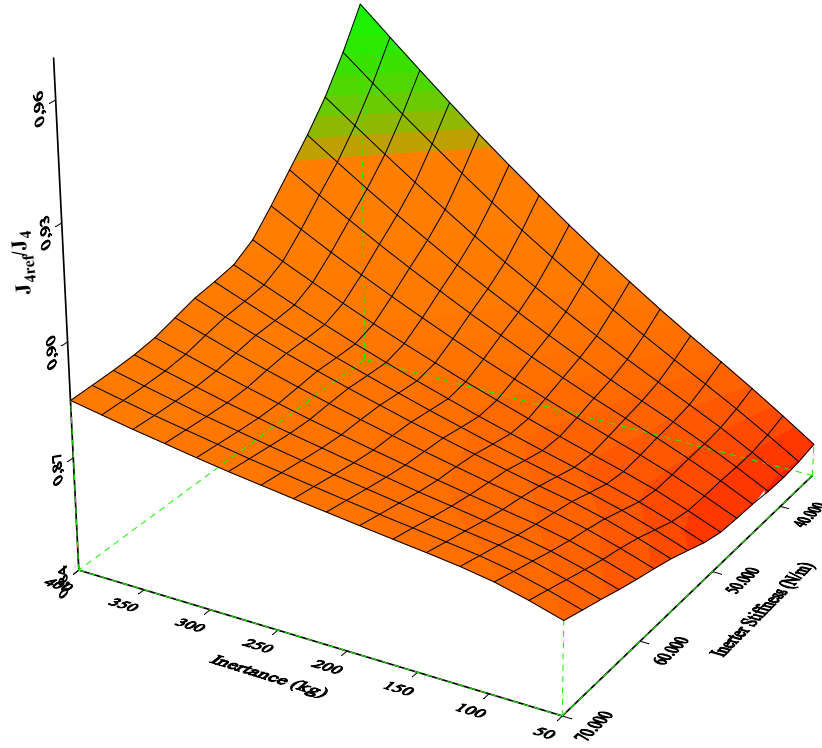


Figure 5.32: J_4 at $V=60\text{kph}$, A class road

The flowchart of the optimization process is shown in Figure 5.33.

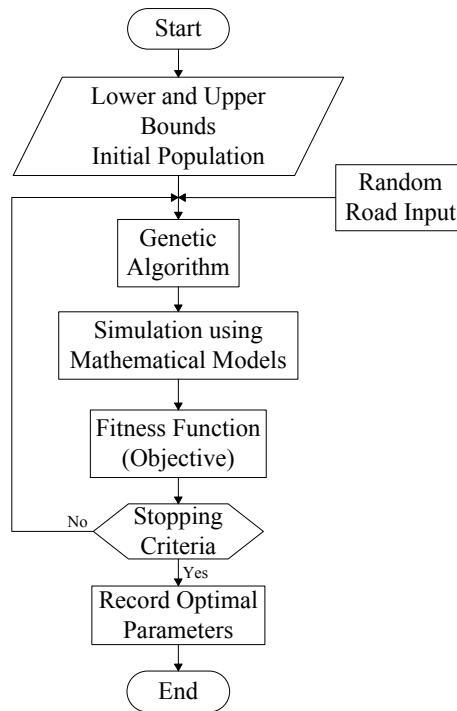


Figure 5.33: Optimization algorithm flowchart

Parameters chosen as a result of the optimization process are given in Table 5.3. These parameters are used in ISO-2631 ride comfort evaluation method, half-car model ISO-8608 road profile simulations and standard hump profile simulations. Other vehicle parameters that are kept constant are given in Table 5.4.

Table 5.3: Optimized Parameters

Parameter	Value
k_{inrt}	35000N/m
c_{inrt}	2000N.s/m
b_{inrt}	400kg

Table 5.4: Constant Vehicle Parameters

Parameter	Value
m_s	240kg
m_p	3kg
m_u	30kg
k_s	15000N/m
c_s	900N.s/m
k_t	190000N/m

Figure 5.34, 5.35 and 5.36 show the reduction in individual objective functions J_1 , J_2 and J_3 relative to standard suspension, and Figure 5.37 shows the reduction in overall objective function $\rho_1 J_1 + \rho_2 J_2 + \rho_3 J_3 + \rho_4 J_4$.

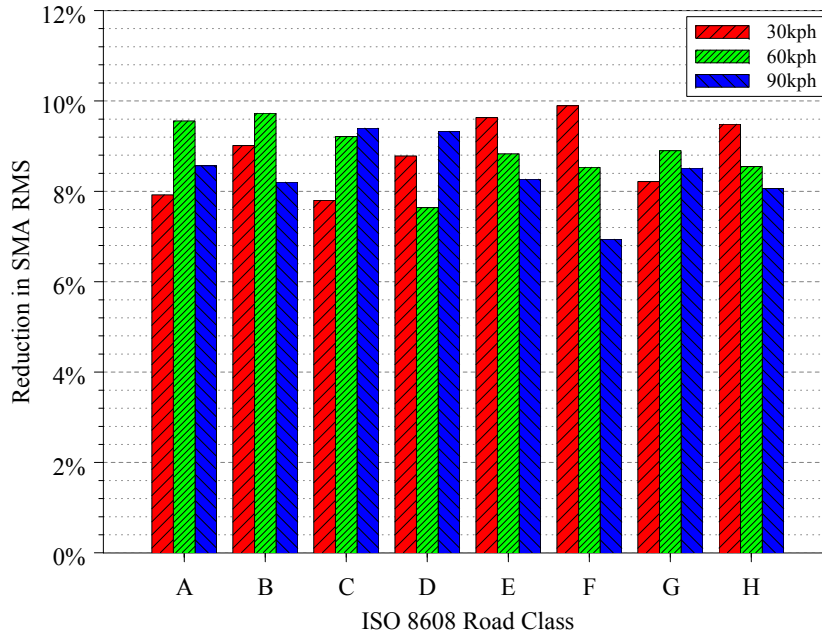


Figure 5.34: Reduction in sprung mass acceleration RMS (J_1)

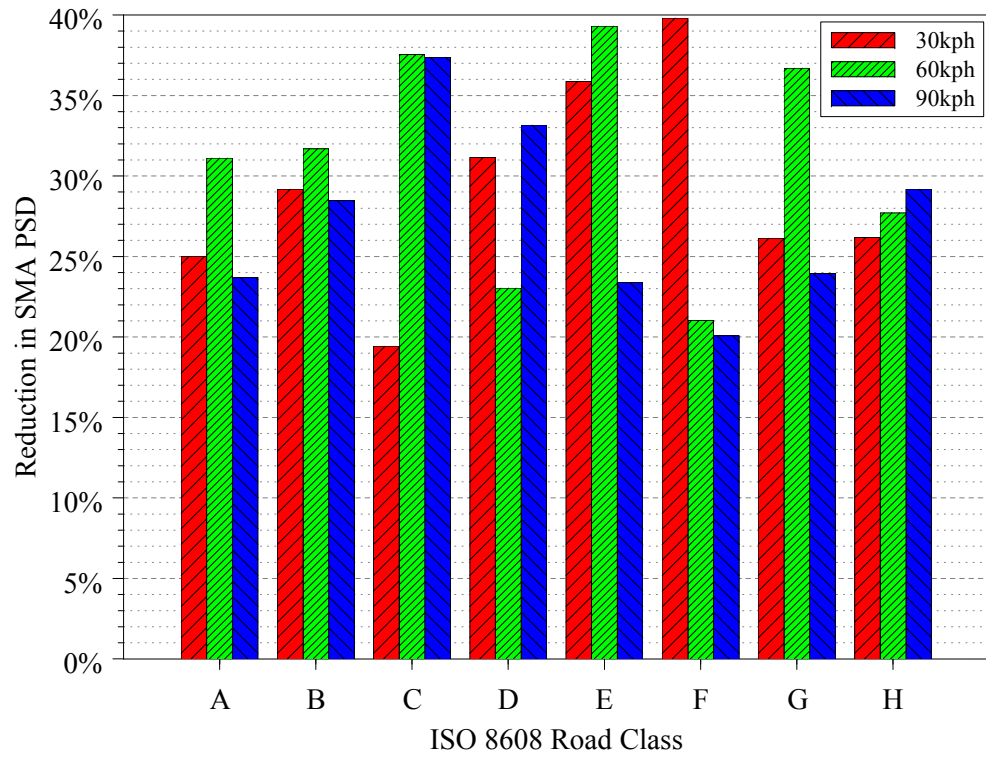


Figure 5.35: Reduction in sprung mass acceleration PSD (J_2)

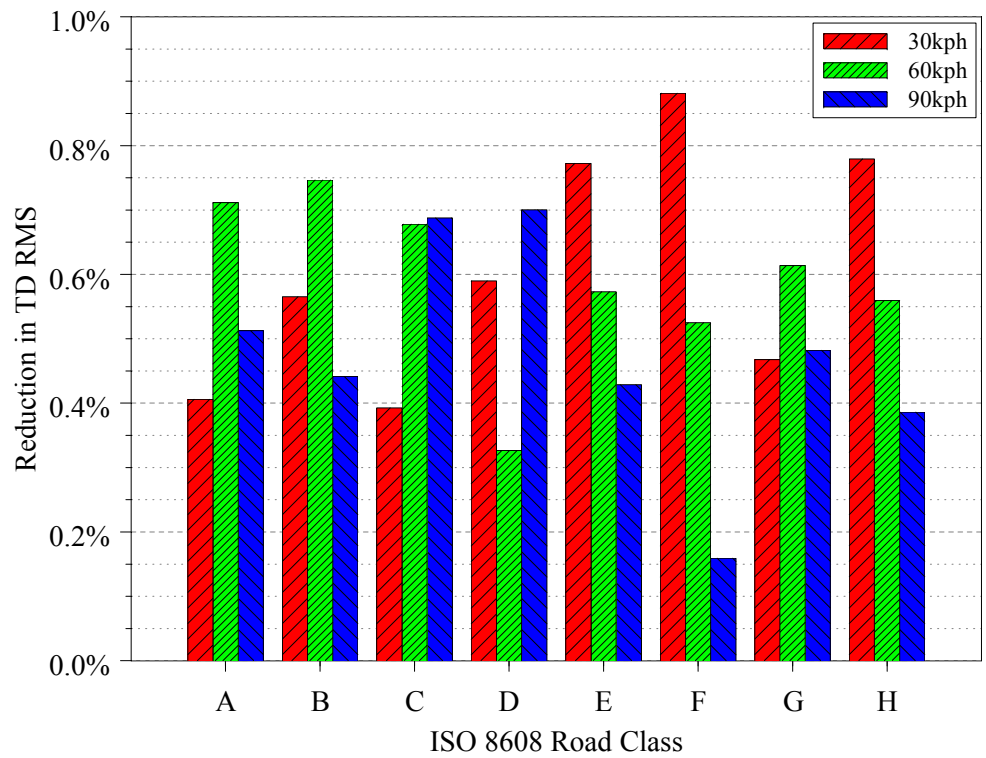


Figure 5.36: Reduction in tire deflection RMS (J_3)

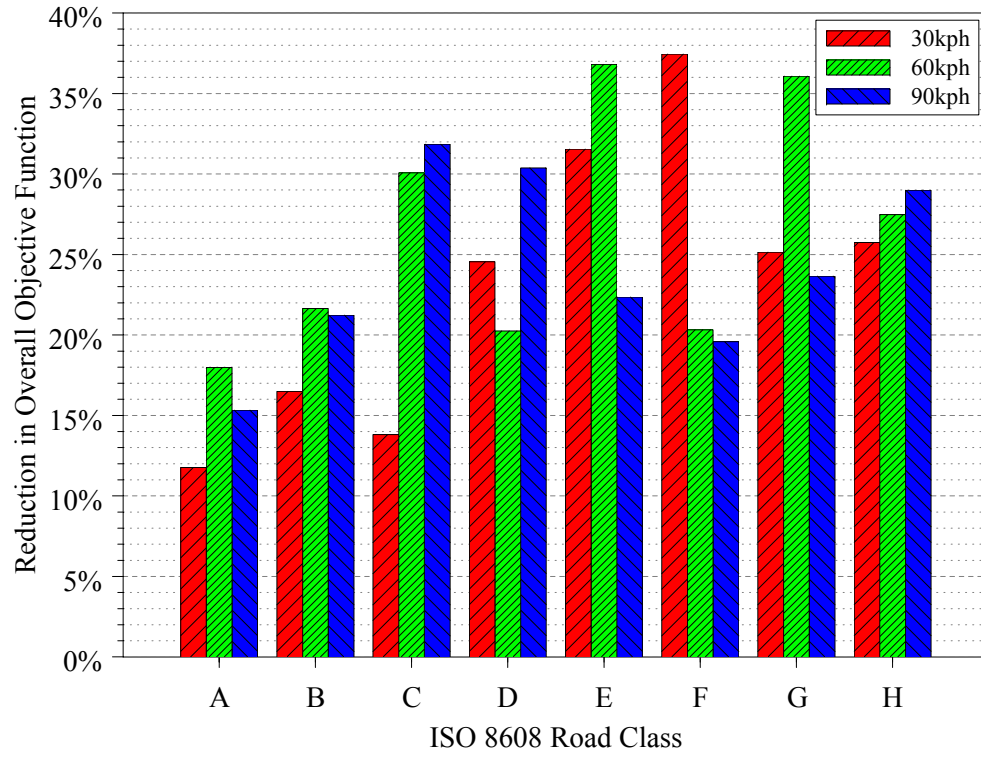


Figure 5.37: Reduction in overall cost function $\rho_1 J_1 + \rho_2 J_2 + \rho_3 J_3 + \rho_4 J_4$

CHAPTER 6

RIDE COMFORT EVALUATION

Considering the results given in Chapter 5 and the quarter-car models given in Chapter 2, the following time-domain measurements are considered for evaluation of performance and determination of the characteristics of the suspension system:

- the vertical acceleration of the sprung mass(body) to evaluate the ride comfort,
- the tire deflection to evaluate the road-holding.

In addition to time-domain performance evaluation, frequency-domain performance is also investigated with ISO-2631 frequency weighted PSD of the sprung mass acceleration to evaluate the ride comfort. Even the suspension deflection limits can be included in the analysis. In this thesis, the performance issue is not be dealt with. The reason is that nonlinear suspension behavior is significant in suspension limits. However, it was included in Chapter 5 to penalize the deflection of the suspension regardless of the remaining analysis.

6.1 ISO-2631 Comfort Frequency Weightings

According to [18], response of the body to wave phenomena can be modeled by using a frequency weighting that is a frequency response function. It is also stated that the vibration at 5 Hz than at 100 Hz creates 10 times more sensitivity to seated human body. Therefore, at 100 Hz, measurements are reduced by 10 times compared to the vibrations at 5 Hz, in order to keep the subjective sensation parity between the two frequencies. The frequency weightings given in [11] preserve the continuum of weightings and are prepared for frequency range of perception of humans. They are applied to time-domain measurements of acceleration of the vehicle body and attenuate the mechanical characteristics of the vibrating frames. Although, it is argued that there are some problems with frequency weightings, currently no alternative method for the evaluation of vibrations is available and has proved to be better than the frequency weighting method.

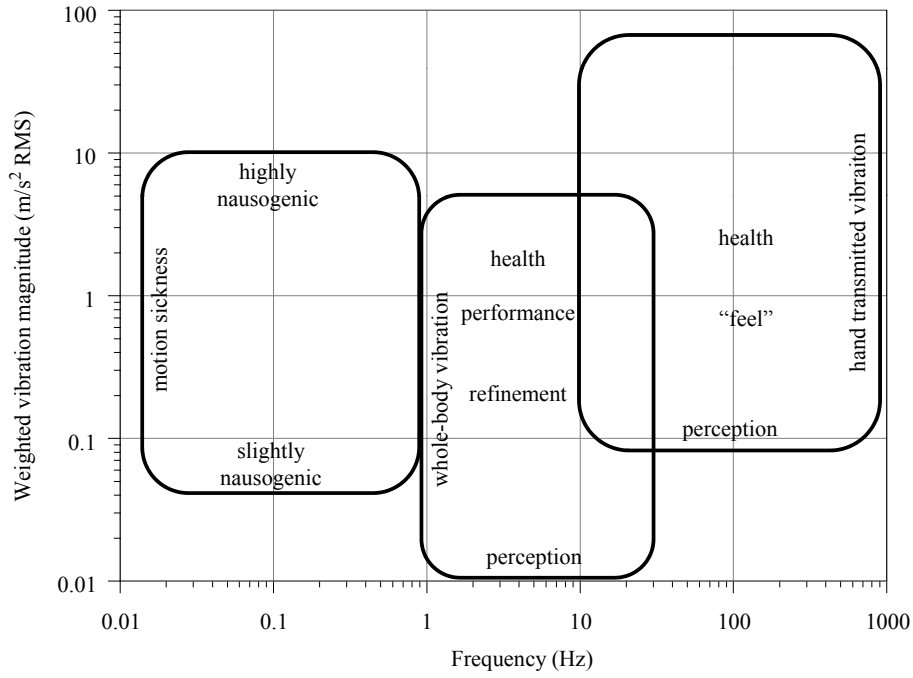


Figure 6.1: Typical frequency ranges and magnitudes of interest for the study of motion sickness, whole-body vibration, and hand-transmitted vibration

Table 6.1: ISO 2631 Frequency Weightings for Vertical Vibrations[11]

Frequency (Hz)	Weight	Frequency (Hz)	Weight
0.1	0.0321	2	0.531
0.125	0.0486	2.5	0.631
0.16	0.079	3.15	0.804
0.2	0.121	4	0.967
0.25	0.182	5	1.039
0.315	0.263	6.3	1.054
0.4	0.352	8	1.036
0.5	0.418	10	0.988
0.63	0.459	12.5	0.902
0.8	0.477	16	0.768
1	0.482	20	0.636
1.25	0.484	25	0.513
1.6	0.494	31.5	0.405

In order to evaluate the ride comfort using the ISO-2631 criteria, the method given in [11] is

used.

$$a(t_0) = \sqrt{\frac{1}{\tau} \int_{t_0-\tau}^{t_0} a_\omega(t)^2 dt} \quad (6.1)$$

where

$a_\omega(t)$: instantaneous frequency weighted acceleration,

τ : the integration time for running average,

t : time,

t_0 : time of observation(instantaneous time).

When calculating the weighted rms value in time domain, $a_\omega(t)$, filter given in equation 6.6 is used. The transfer function of the filter can be expressed as a production of 4 different functions. The first one is the high pass filter.

$$|H_h(\omega)| = \left| \frac{\omega^2}{\omega^2 + \sqrt{2}\omega_1\omega + \omega_1^2} \right| \quad (6.2)$$

where

$$\omega_1 = 2\pi f_1,$$

f_1 =corner frequency.

The second one is the low pass filter.

$$|H_l(\omega)| = \left| \frac{\omega_2^2}{\omega_2^2 + \sqrt{2}\omega_2\omega + \omega^2} \right| \quad (6.3)$$

where

$$\omega_2 = 2\pi f_2,$$

f_2 =corner frequency.

The third one is the acceleration-velocity transition which creates proportionality to acceleration at lower frequencies and proportionality to velocity at higher frequencies.

$$|H_t(\omega)| = \left| \frac{1 + \frac{\omega}{\omega_3}}{1 + \frac{\omega}{Q_4\omega_4} + \left(\frac{\omega}{\omega_4}\right)^2} \right| \quad (6.4)$$

where

$$\omega_3 = 2\pi f_3,$$

$$\omega_4 = 2\pi f_4.$$

The last one is the upward step which creates proportionality to jerk.

$$|H_s(\omega)| = \left| \frac{1 + \left(\frac{\omega}{Q_5\omega_5}\right) + \left(\frac{\omega}{\omega_5}\right)^2}{1 + \left(\frac{\omega}{Q_6\omega_6}\right) + \left(\frac{\omega}{\omega_6}\right)^2} \left(\frac{\omega_5}{\omega_6}\right)^2 \right| \quad (6.5)$$

where

$$\omega_5 = 2\pi f_5,$$

$$\omega_6 = 2\pi f_6.$$

The effect of the transfer functions is explained such that $|H_h(\omega)||H_l(\omega)|$ product is the band-limited pass filter and $|H_t(\omega)||H_s(\omega)|$ actual weighting transfer function.

$$|H(\omega)| = |H_h(\omega)| |H_l(\omega)| |H_t(\omega)| |H_s(\omega)|. \quad (6.6)$$

Figure 6.2 shows the magnitude of the overall weighting transfer function given in equation 6.6.

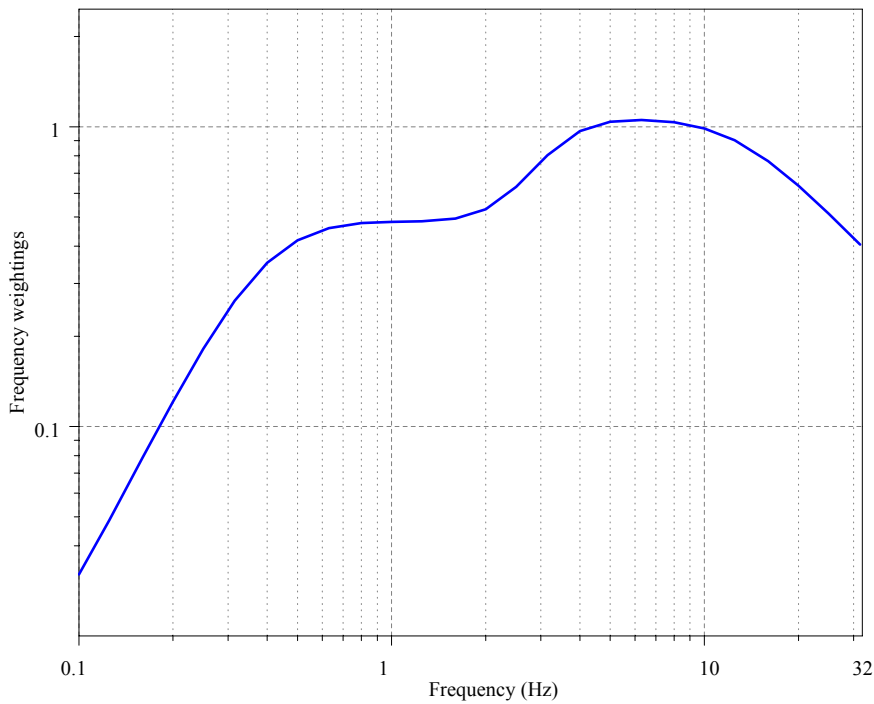


Figure 6.2: Frequency weightings for vertical vibrations

Power spectral density is the most common technique for analyzing the frequency content of signals for human vibration applications as it is ideally suited to the analysis of random signal types. It generates a measure of the energy contained within a frequency band. PSD splits up the original signal into shorter segments and calculates the FFT for each section. The length of each individual segment is selected such that the FFT generates an appropriate frequency resolution. For example, if a frequency resolution of 0.25 Hz is required, each segment must last 4 s. Usually, the segments overlap and are “windowed” to ensure data integrity. The unit of a PSD for an acceleration signal is $(m/s^2)^2/Hz$. By using the frequency weighting curve shown in Figure 6.2, PSDs of sprung mass accelerations for $V=30$ kph on B class road are shown in Figure 6.3, 6.4 and 6.5.

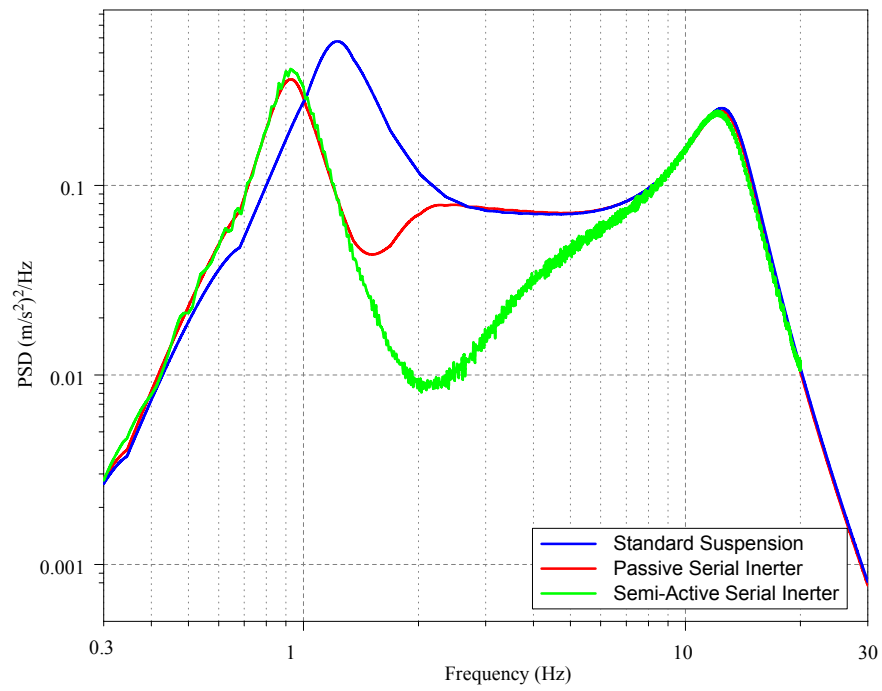


Figure 6.3: Weighted PSDs of sprung mass acceleration for $V=30\text{kph}$ on B class road

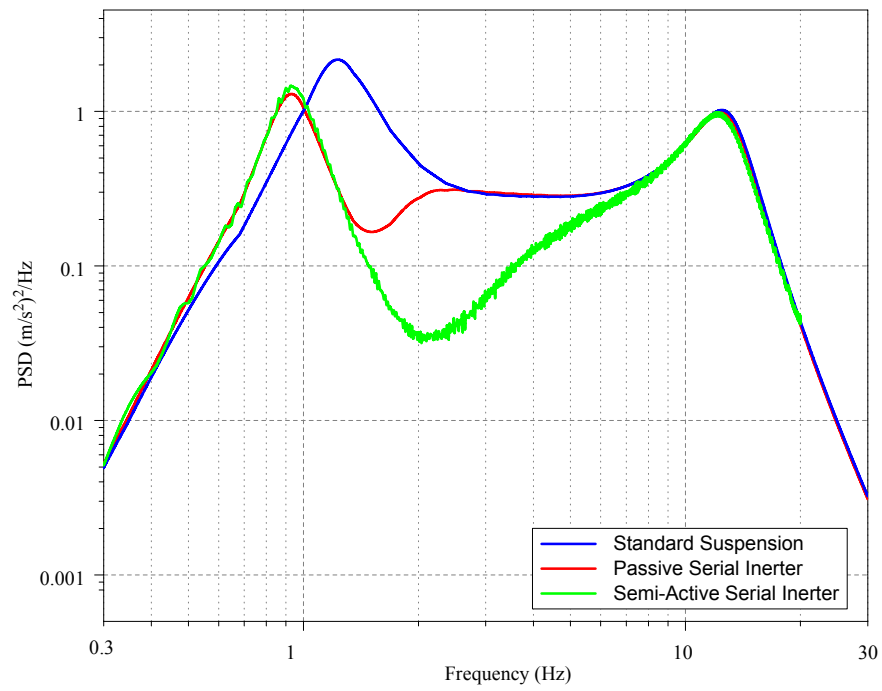


Figure 6.4: Weighted PSDs of sprung mass acceleration for $V=60\text{kph}$ on B class road

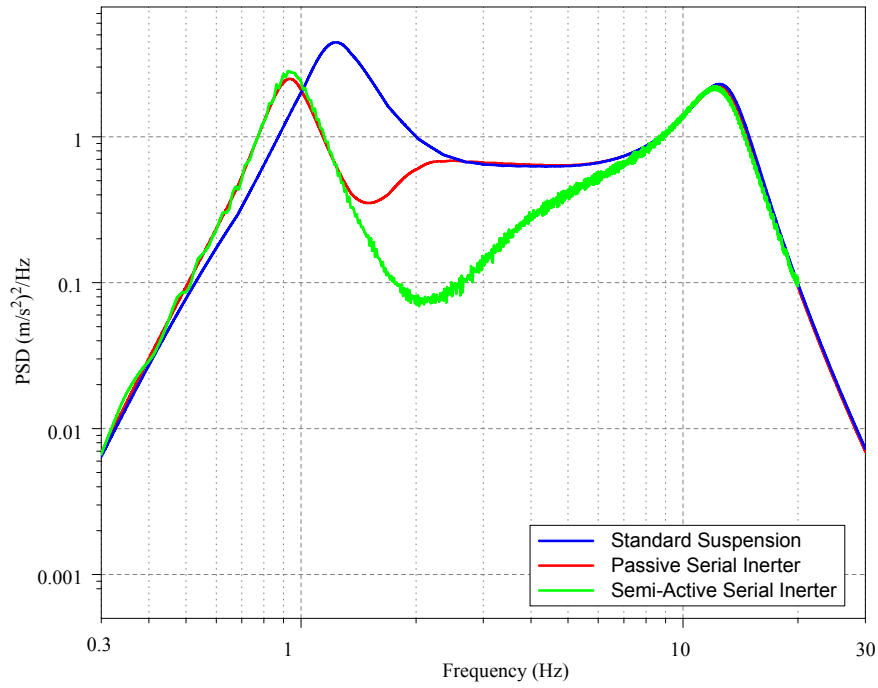


Figure 6.5: Weighted PSDs of sprung mass acceleration for $V=90\text{kph}$ on B class road

In Figure 6.6, 6.7 and 6.8, the weighted acceleration RMS values calculated by using the running rms method are shown. The degree of the discomfort values are listed in Table 6.2 and provide an insight for perception of comfort to those exposed a whole-body vibration. Weighted acceleration RMS values can be evaluated by using those values.

Table 6.2: ISO 2631 Comfort Ratings [3]

RMS Acceleration (m/s^2)	Scale of Discomfort
<0.315	Not uncomfortable
0.315-0.63	A little uncomfortable
0.5-1	Fairly uncomfortable
0.8-1.6	Uncomfortable
1.25-2.5	Very uncomfortable
>2	Extremely uncomfortable

The weighted sprung mass acceleration RMS of 3 suspension systems are shown in Figure 6.6, 6.7 and 6.8.

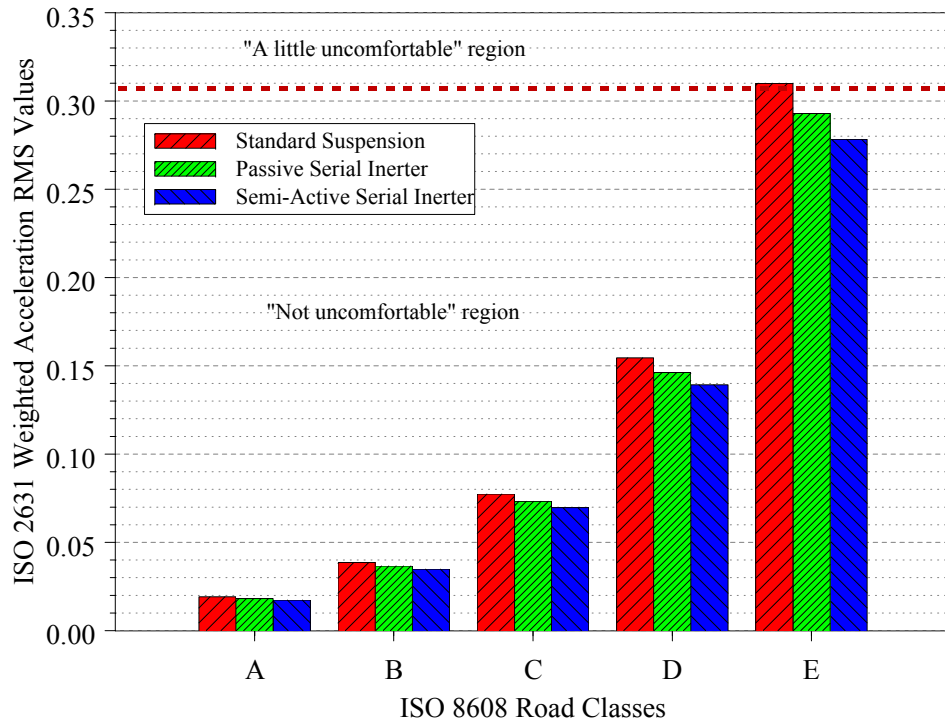


Figure 6.6: Weighted sprung mass acceleration RMS values for $V=30\text{kph}$

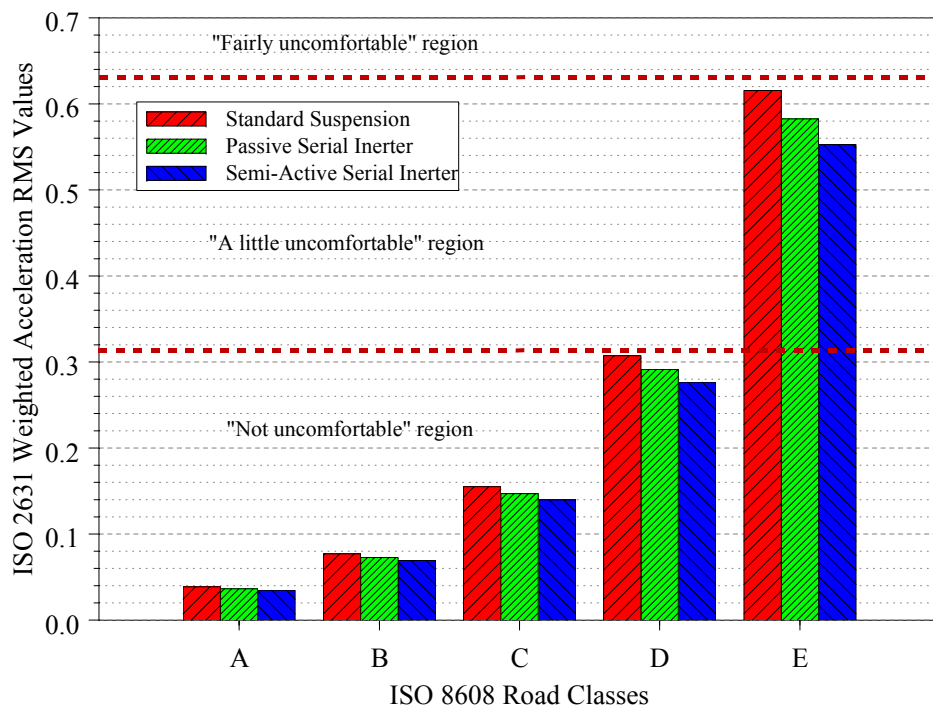


Figure 6.7: Weighted sprung mass acceleration RMS values for $V=60\text{kph}$

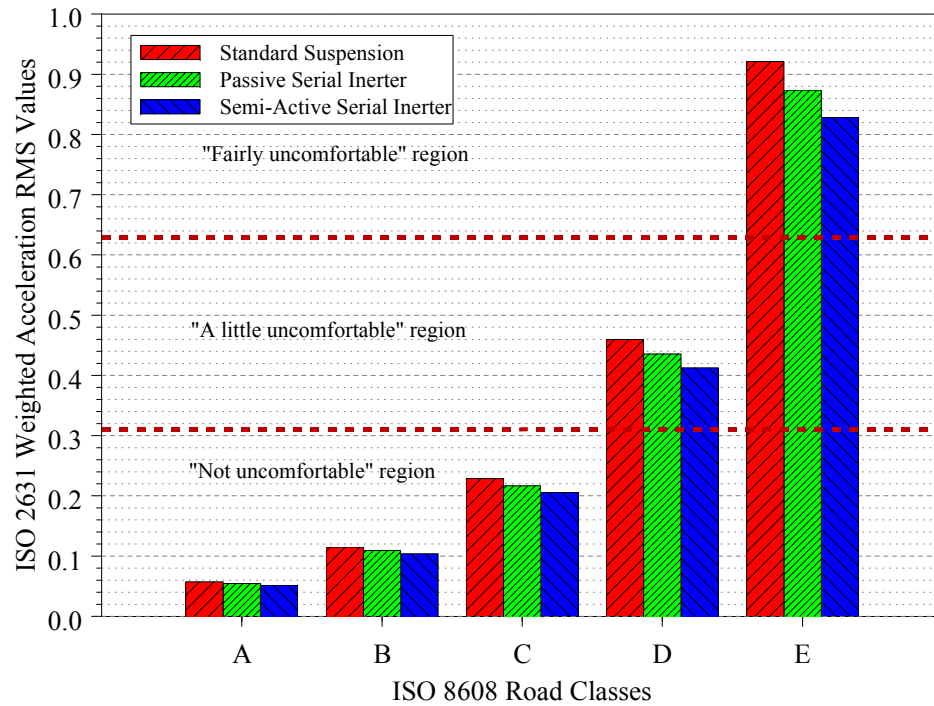


Figure 6.8: Weighted sprung mass acceleration RMS values for $V=90\text{kph}$

The percentage reduction in weighted sprung mass acceleration RMS of suspension systems with inerter are shown in Figure 6.9, 6.10 and 6.11.

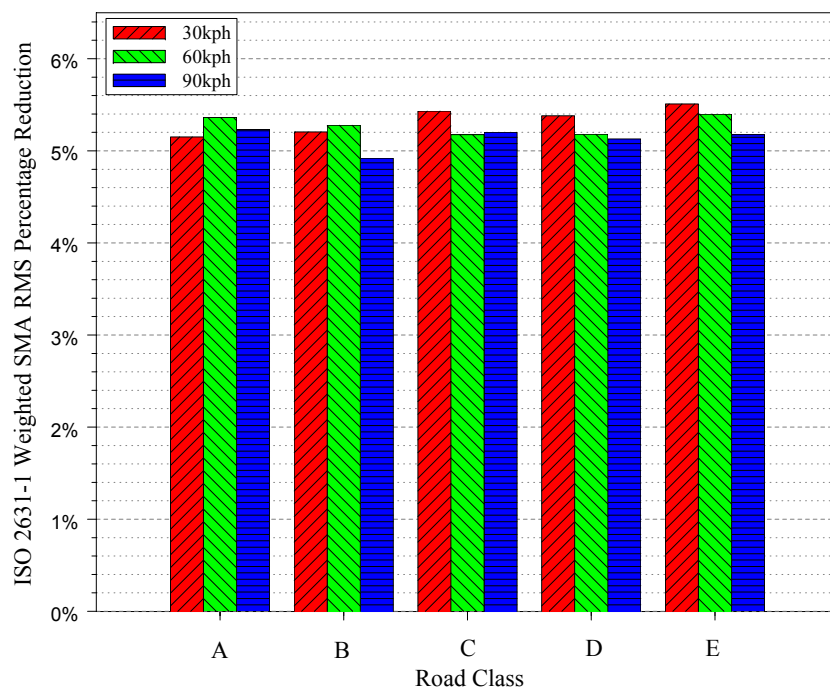


Figure 6.9: Percentage reduction in passive serial inerter SMA RMS with respect to standard suspension

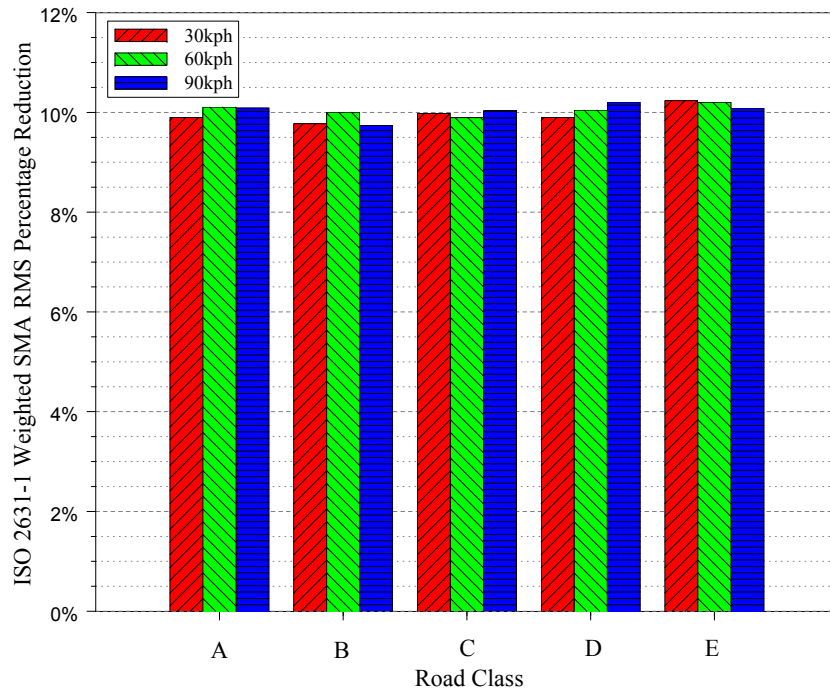


Figure 6.10: Percentage reduction in semi-active serial inerter SMA RMS with respect to standard suspension

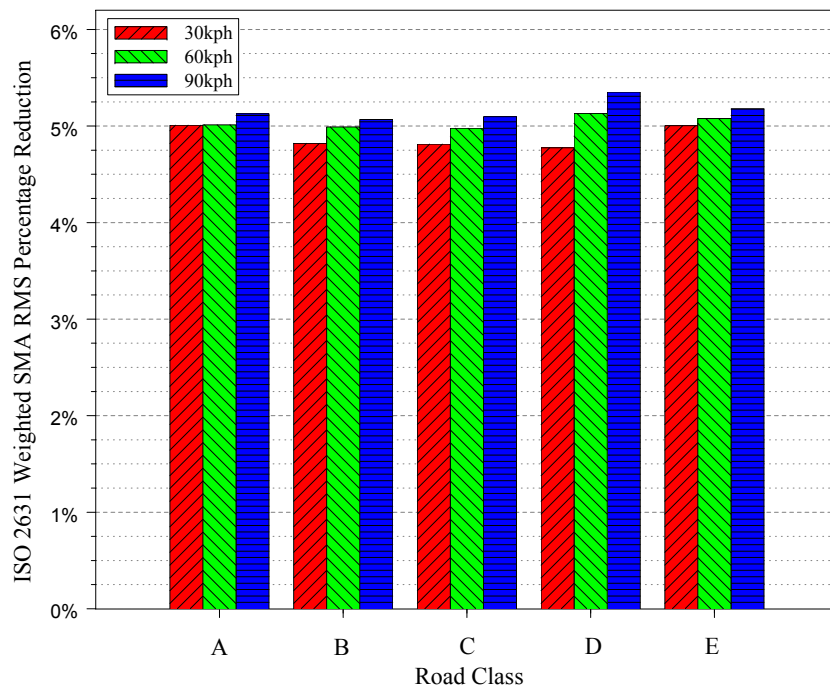


Figure 6.11: Percentage reduction in semi-active serial inerter SMA RMS with respect to passive serial inerter

CHAPTER 7

SIMULATIONS

Half-car models are utilized in time domain simulations. The purpose of the simulations is that showing the transient and steady-state characteristics of the suspension, as well as, the performance of the suspension with passive and semi-active inerter. The parameters given in Table 7.1 is used in half-car models.

Table 7.1: Parameters Used in Half-Car Models

Parameter	Value
m_s	480kg
$m_{p,f}$	3kg
$m_{p,r}$	3kg
$m_{u,f}$	30kg
$m_{u,r}$	30kg
k_f	15000N/m
k_r	15000N/m
c_f	900N.s/m
c_r	900N.s/m
k_t	190000N/m
$k_{inrt,f}$	35000N/m
$k_{inrt,r}$	35000N/m
$c_{inrt,f}$	2000N.s/m
$c_{inrt,r}$	2000N.s/m
$b_{inrt,f}$	400kg
$b_{inrt,r}$	400kg

7.1 ISO-8608 Road Simulations

The effect of the inerter on the sprung mass acceleration can be seen in time domain in the following simulations. For 3 different suspension systems, simulation results using ISO-8608 road profiles are shown in the following figures.

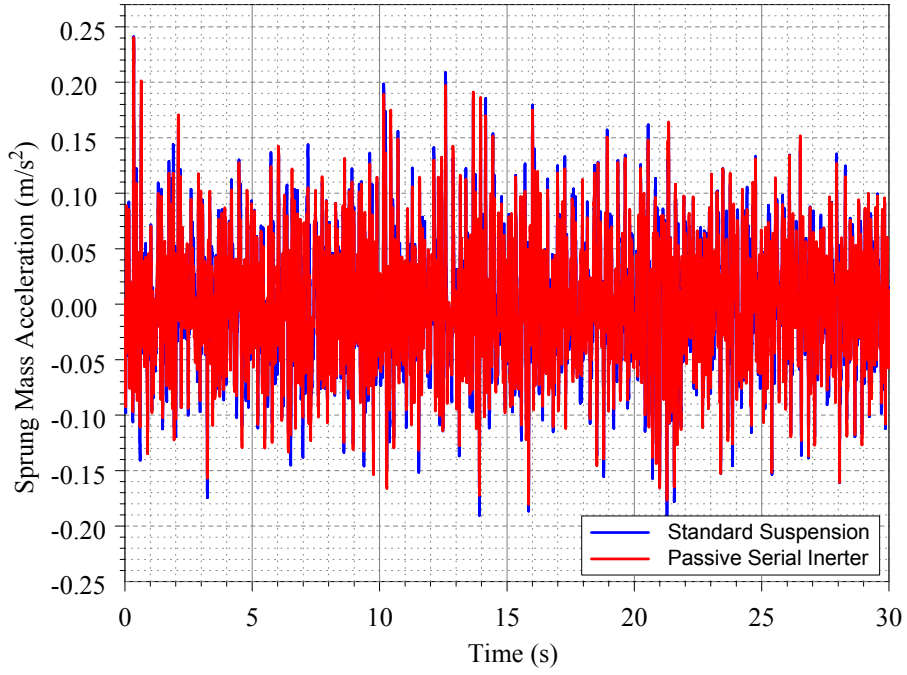


Figure 7.1: Simulation for standard suspension and passive serial inerter at $V=30\text{kph}$, B-class road

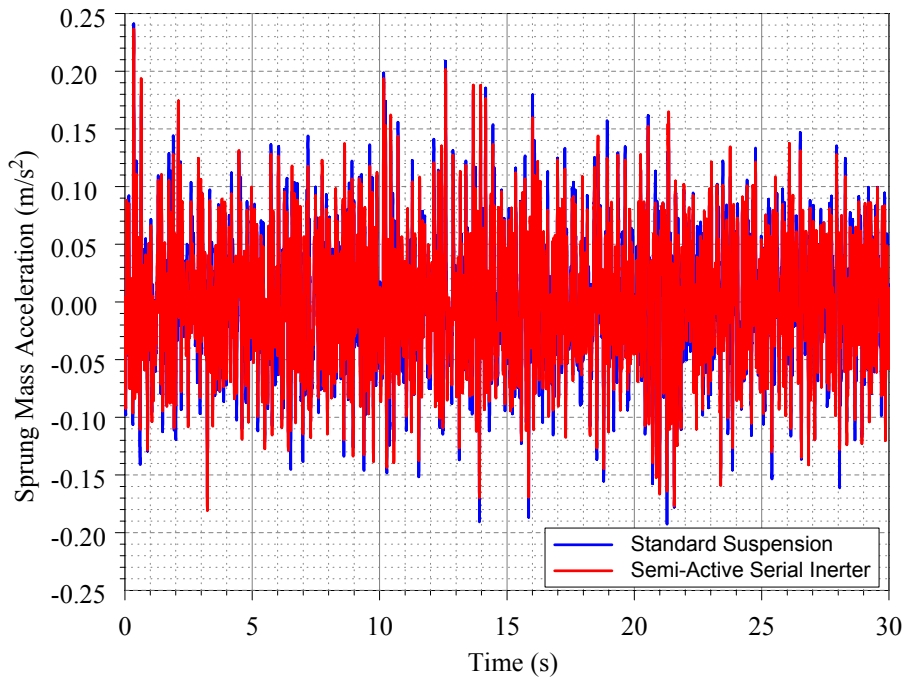


Figure 7.2: Simulation for standard suspension and semi-active serial inerter at $V=30\text{kph}$, B-class road

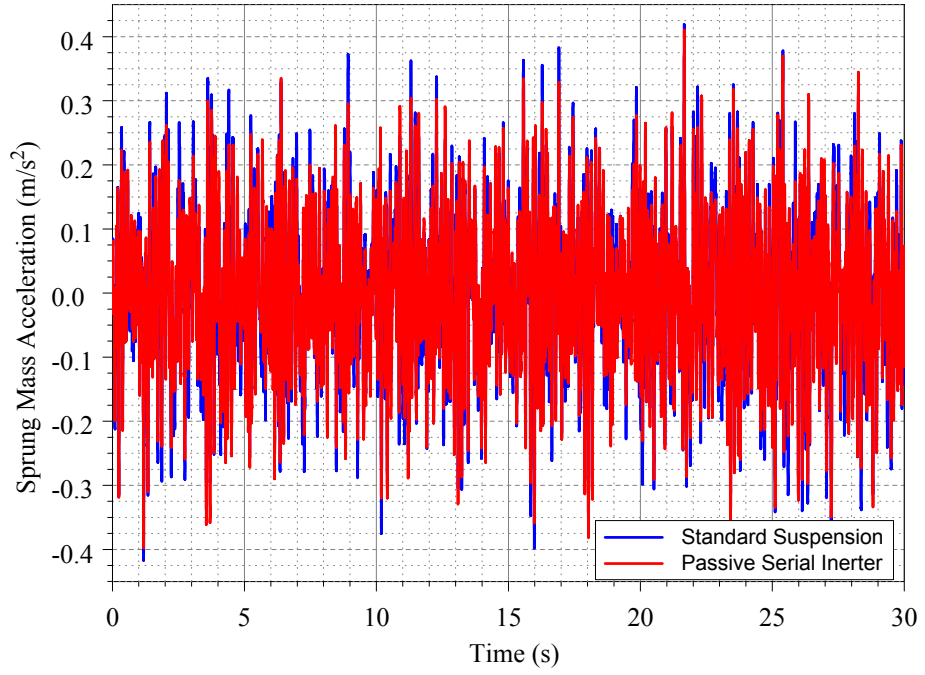


Figure 7.3: Simulation for standard suspension and passive serial inerter at $V=60\text{kph}$, B-class road

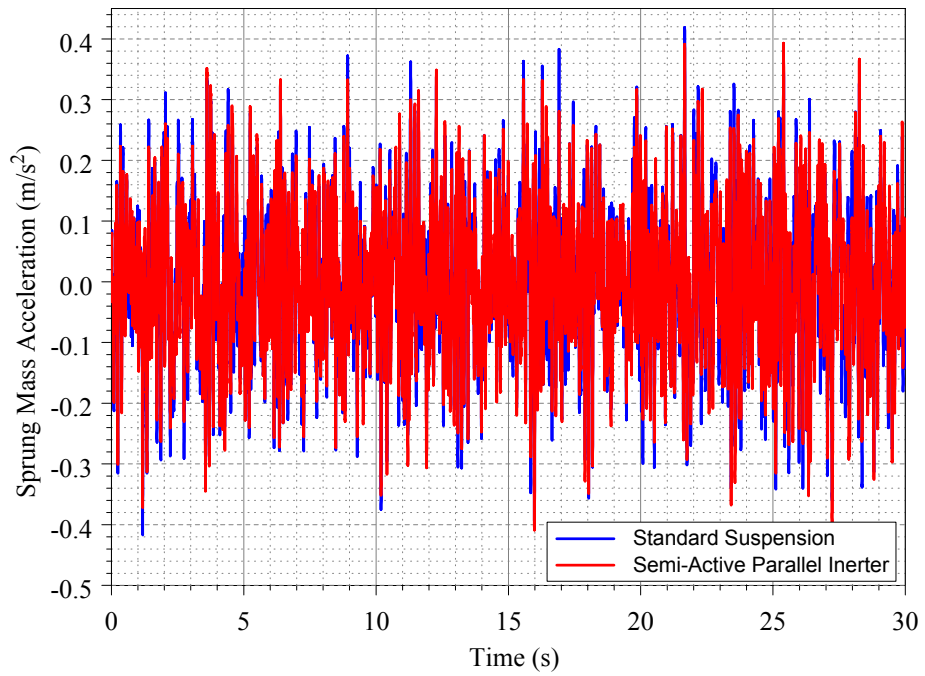


Figure 7.4: Simulation for standard suspension and semi-active serial inerter at $V=60\text{kph}$, B-class road

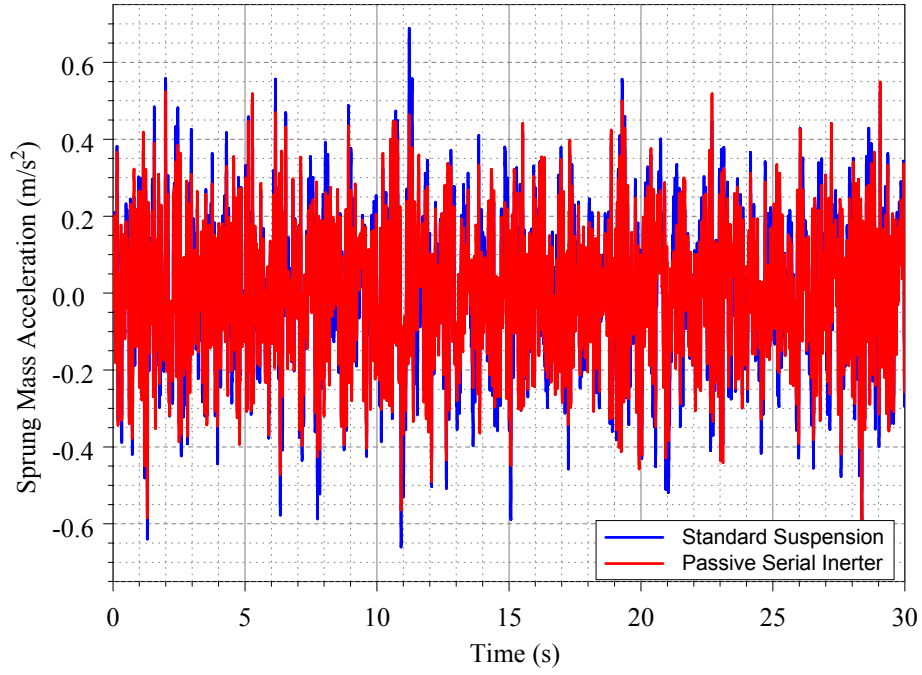


Figure 7.5: Simulation for standard suspension and passive serial inerter at $V=90\text{kph}$, B-class road

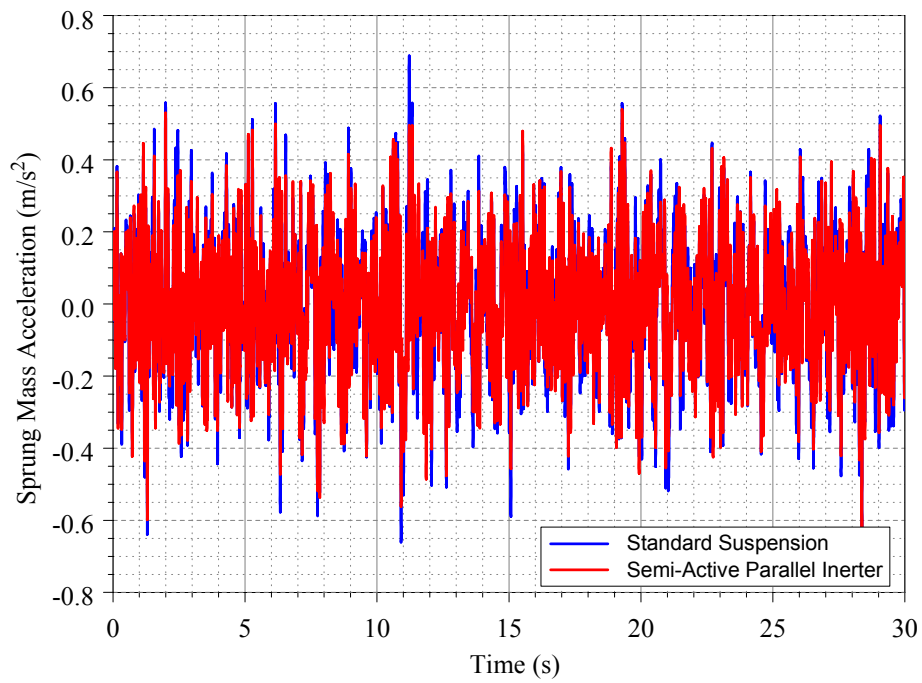


Figure 7.6: Simulation for standard suspension and semi-active serial inerter at $V=90\text{kph}$, B-class road

The reduction in the sprung mass acceleration can be seen clearly in time domain simulations and those results are expected when SMA RMS values given in chapter 5 are considered.

In order to show the physical behavior of the passive serial inerter during the operation, force applied by the inerter on the sprung mass acceleration and the total force applied on the sprung mass are shown in Figure and .

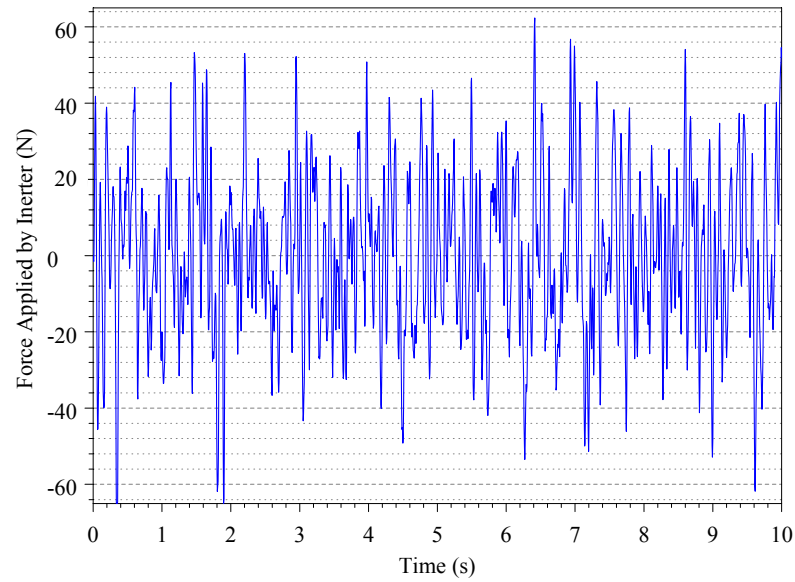


Figure 7.7: Force applied by inerter on the sprung mass at $V=30\text{kph}$, B-class road (passive serial inerter)

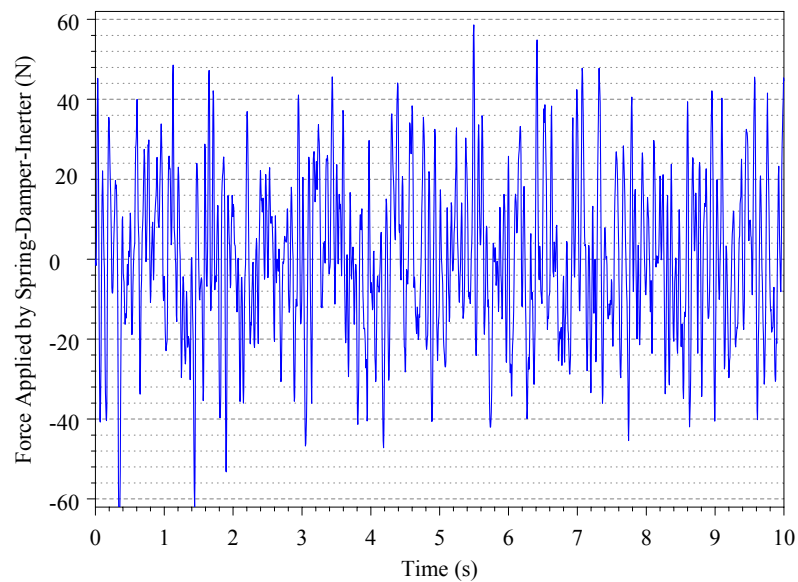


Figure 7.8: Force applied by spring-damper-inerter on the sprung mass at $V=30\text{kph}$, B-class road (passive serial inerter)

Furthermore, in order to show the physical behavior of the semi-active serial inerter during the operation, force applied by the inerter on the sprung mass acceleration and the total force applied on the sprung mass and variation of the inertance are shown in Figure , and .

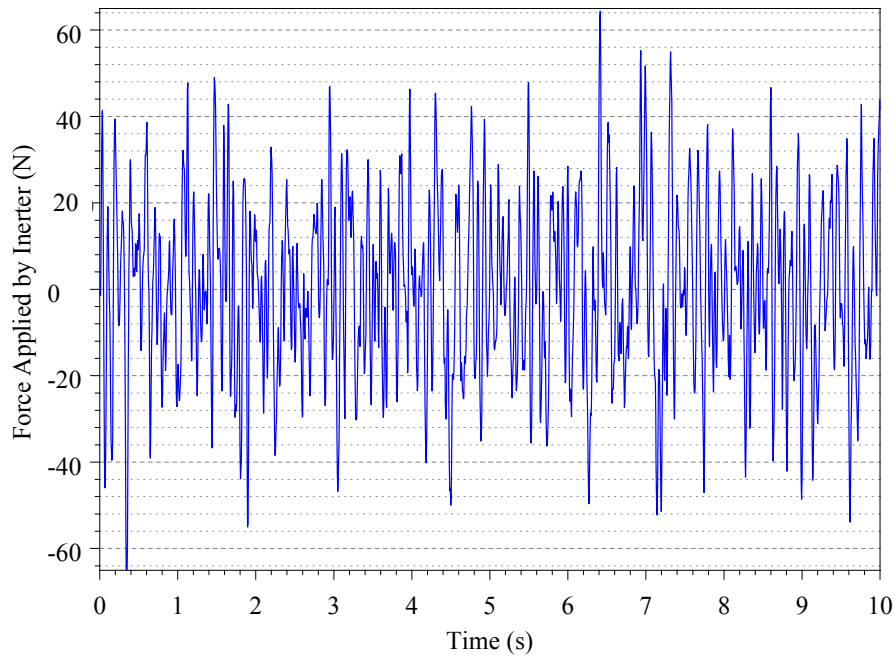


Figure 7.9: Force applied by inerter on the sprung mass at $V=30\text{kph}$, B-class road (semi-active serial inerter)

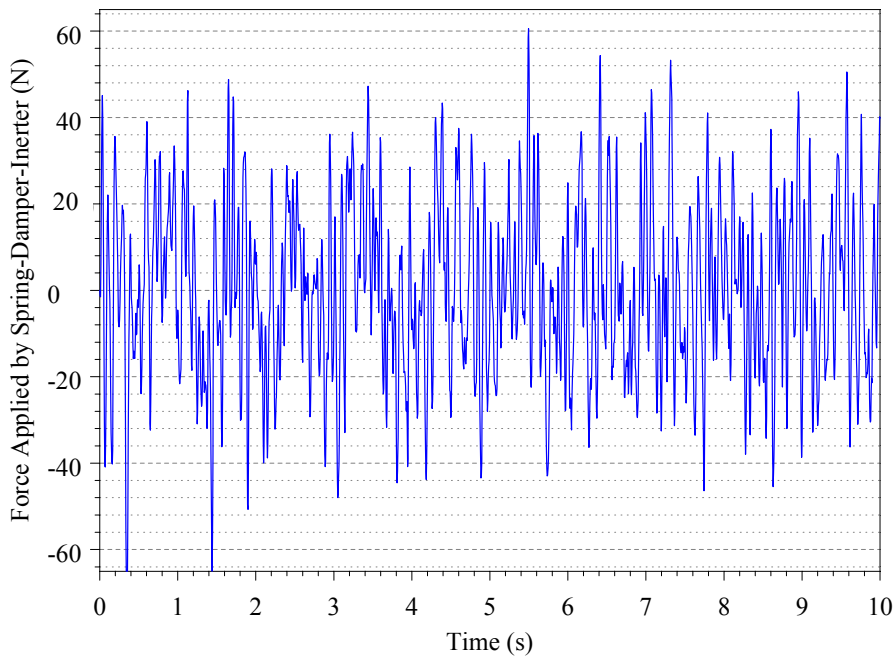


Figure 7.10: Force applied by spring-damper-inerter on the sprung mass at $V=30\text{kph}$, B-class road (semi-active serial inerter)

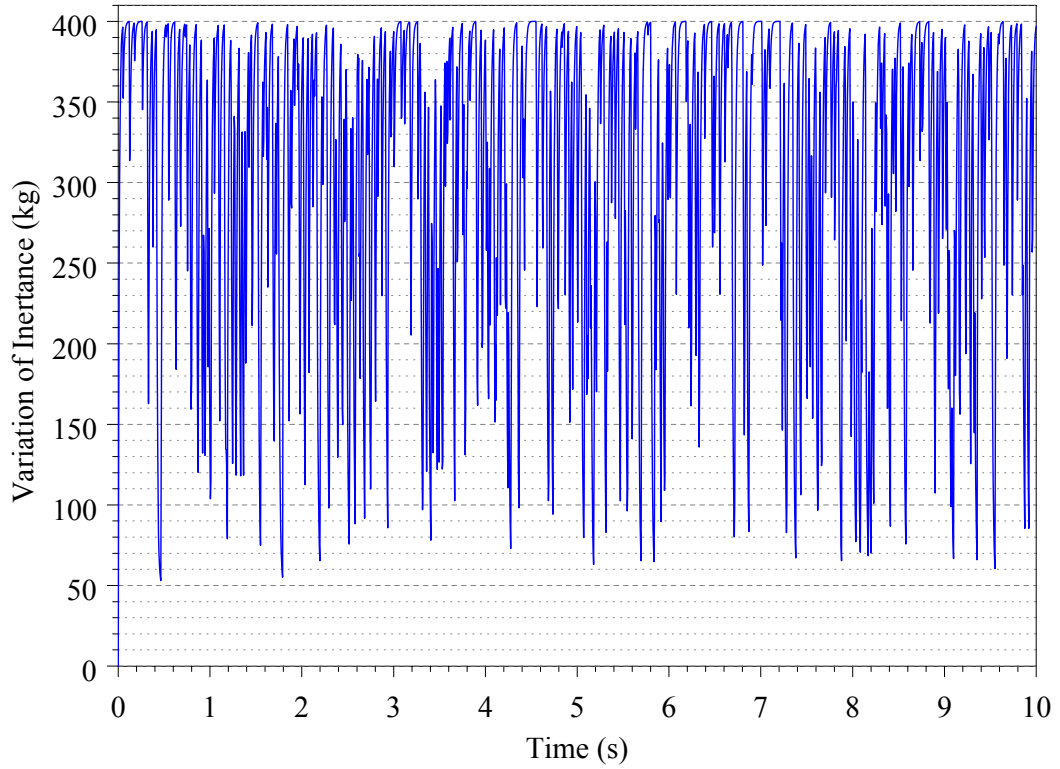


Figure 7.11: Force applied by spring-damper-inerter on the sprung mass at $V=30\text{kph}$, B-class road (semi-active serial inerter)

7.2 Hump Simulations

Hump simulations are done by using the pitch oriented half-car models given in previous chapters. In order to see the effect of passive and semi-active inerter, 2 different types of hump are used. These hump profiles are standard circular hump profile and standard trapezoidal hump profile.

7.2.1 Standard Circular Hump

The standard dimensions of a standard circular hump given in [19] are 7.5mm-10mm height and 3.6m-3.8m width.

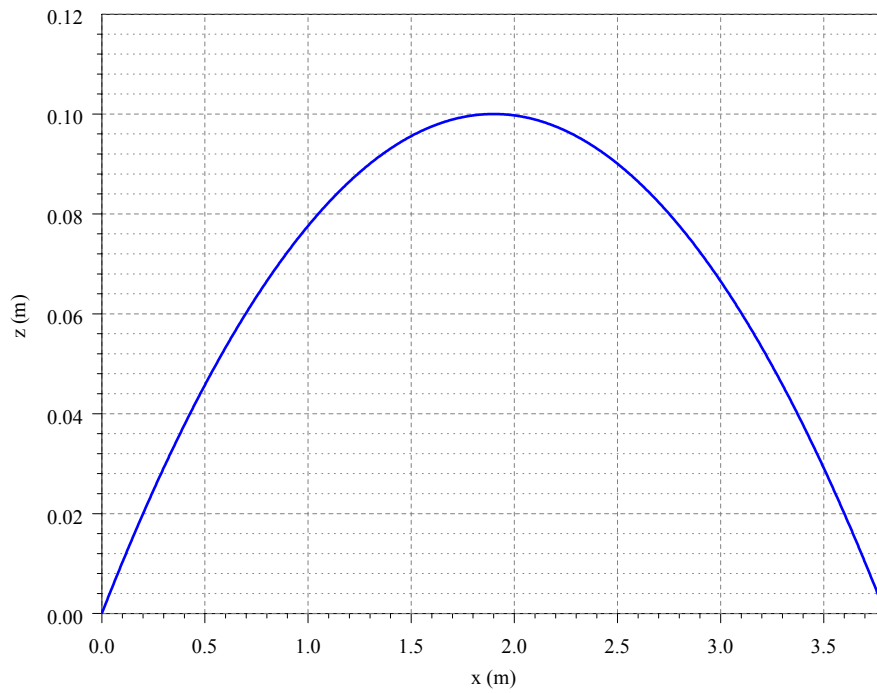


Figure 7.12: Standard circular hump profile

After the simulations, maximum peak sprung mass accelerations versus vehicle speed in the range of 25-45kph for 4 different suspension systems are given in Figure 7.13.

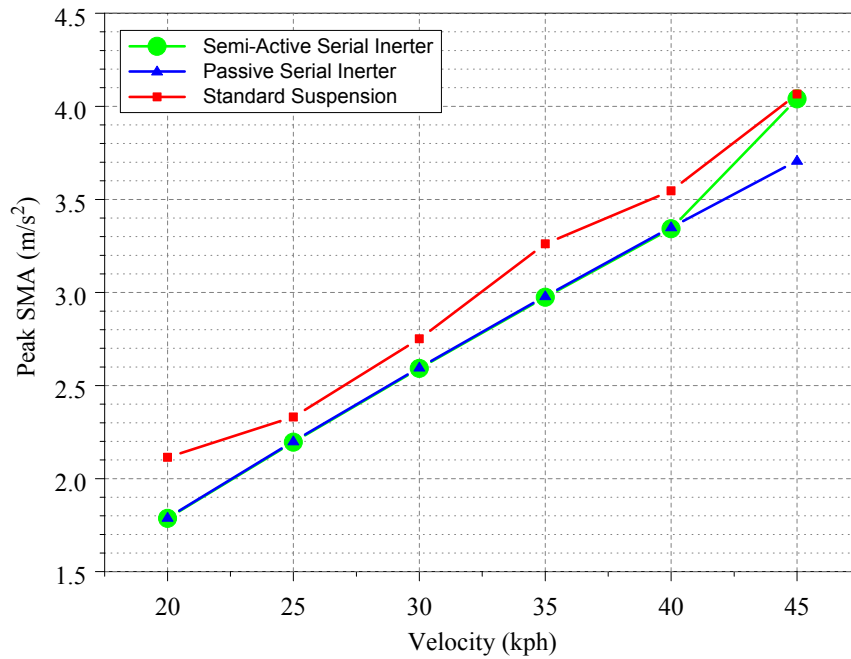


Figure 7.13: Peak sprung mass acceleration for different vehicle speeds

The inerter effect on the peak SMA is said to be positive. Therefore, peak SMA values are smaller in all vehicle speeds.

Before presenting the simulation results, vehicle passing over standard circular hump is illustrated in Figure 7.14 for visual purposes using the vehicle parameters given in Table 7.1.

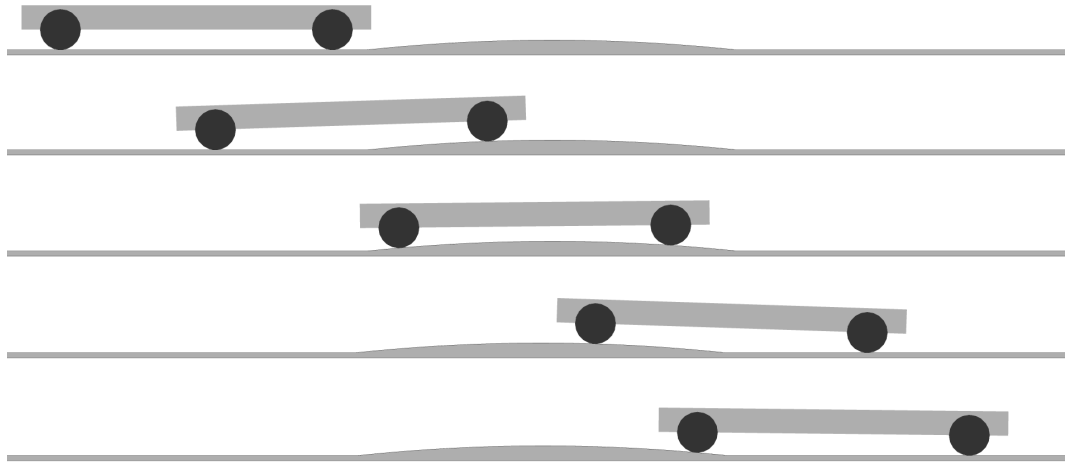


Figure 7.14: Vehicle passing over standard circular hump

Simulation results for standard circular hump are given in the following figures.

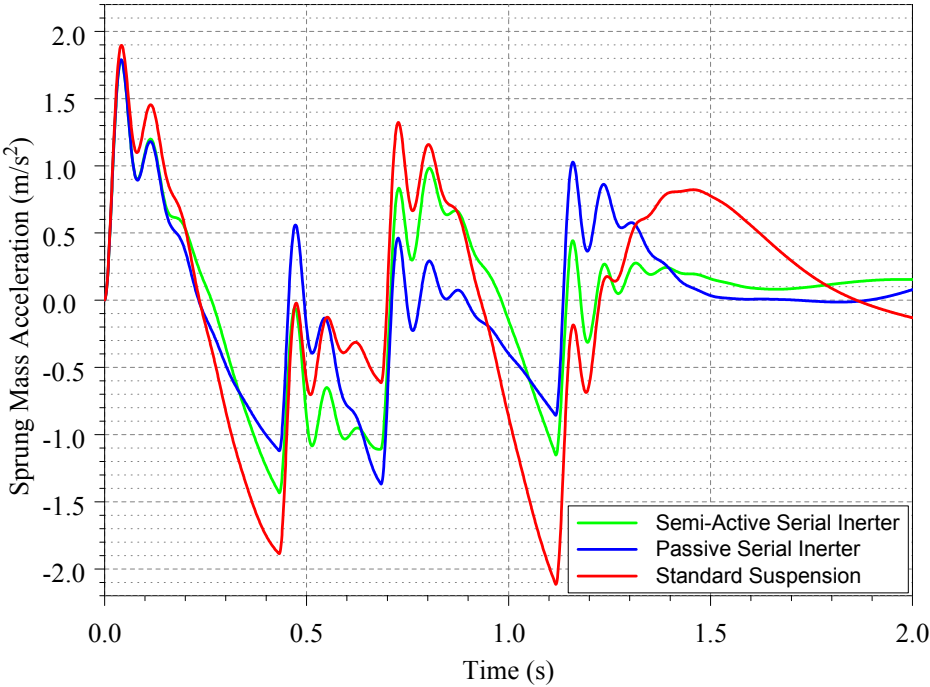


Figure 7.15: Standard circular hump simulation for $V=20\text{kph}$

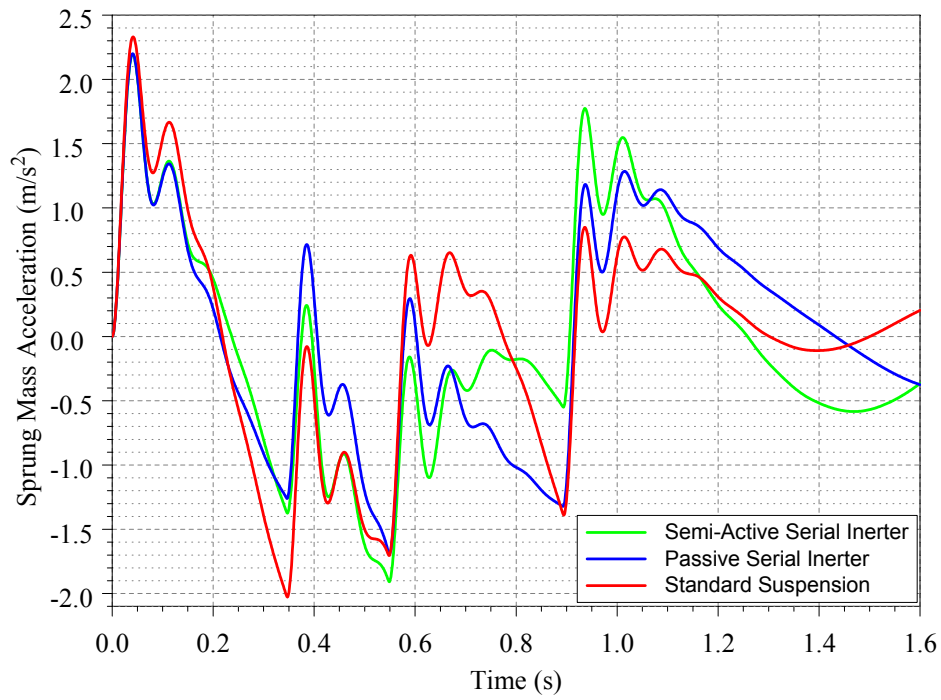


Figure 7.16: Standard circular hump simulation for $V=25\text{kph}$

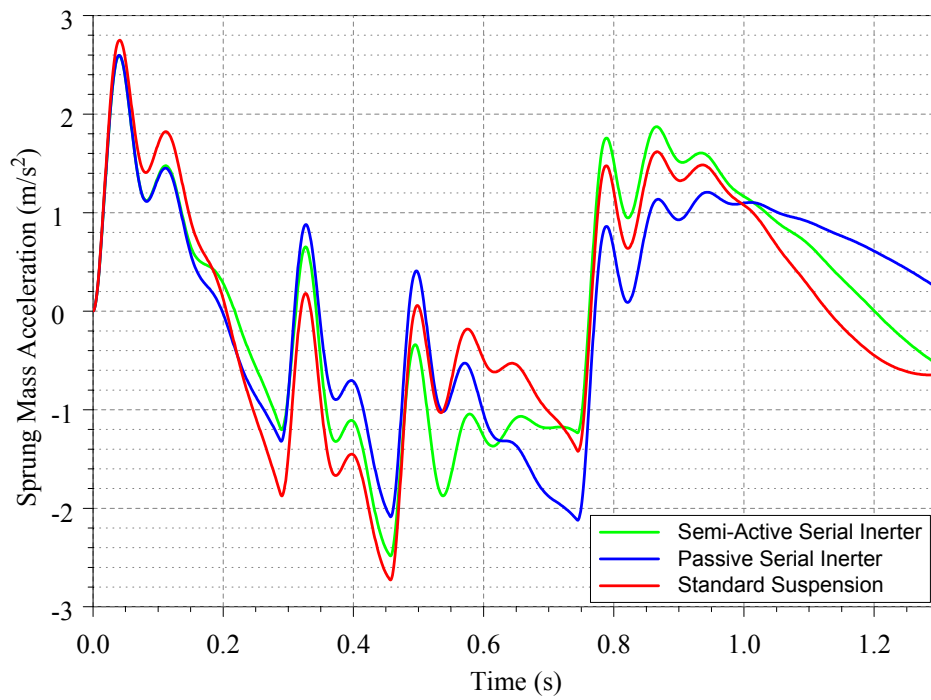


Figure 7.17: Standard circular hump simulation for $V=30\text{kph}$

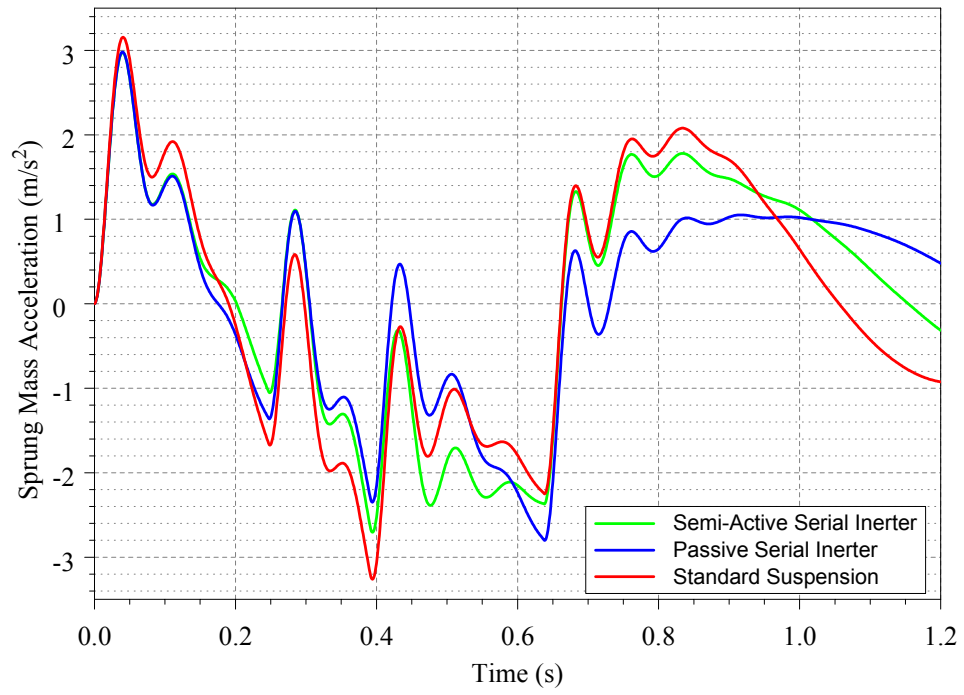


Figure 7.18: Standard circular hump simulation for $V=35\text{kph}$

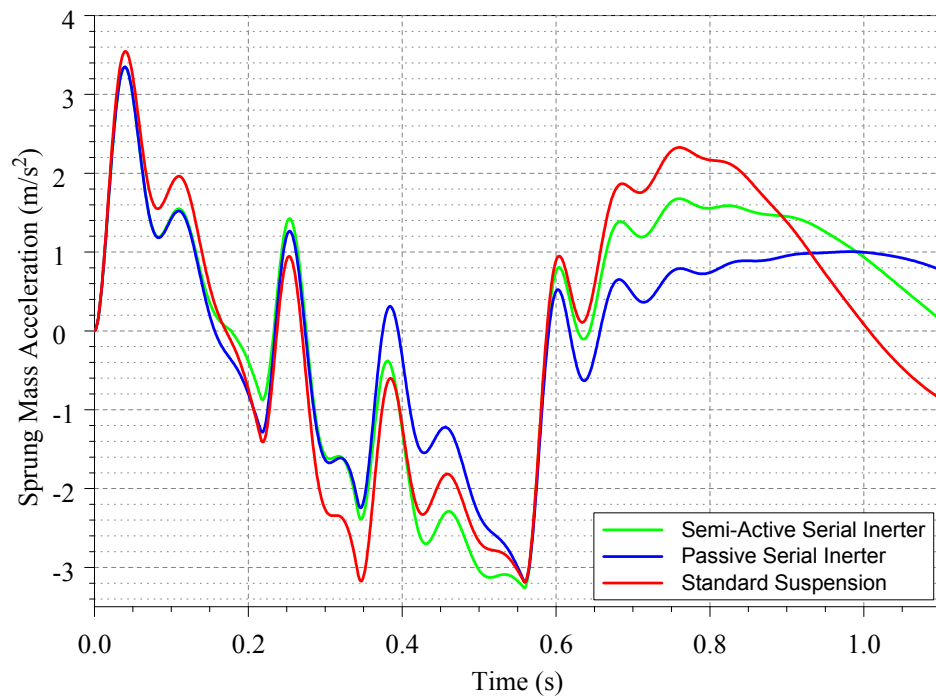


Figure 7.19: Standard circular hump simulation for $V=40\text{kph}$

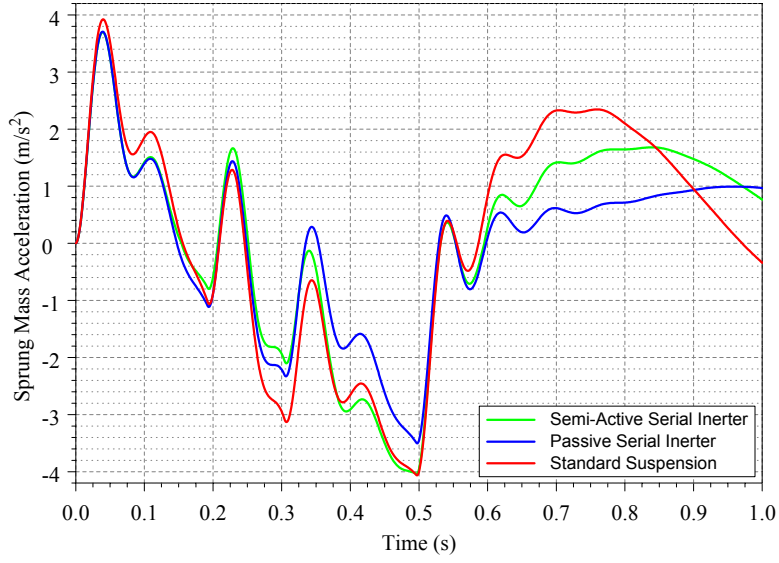


Figure 7.20: Standard circular hump simulation for $V=45\text{kph}$

For relatively low velocities, time domain characteristics are better than the standard suspension with both passive and semi-active serial inerter. To sum up, inerter is advantageous for standard circular hump profiles.

7.2.2 Standard Trapezoidal Hump

The standard dimensions of a standard trapezoidal hump given in [20] are 10mm height and 6m width.

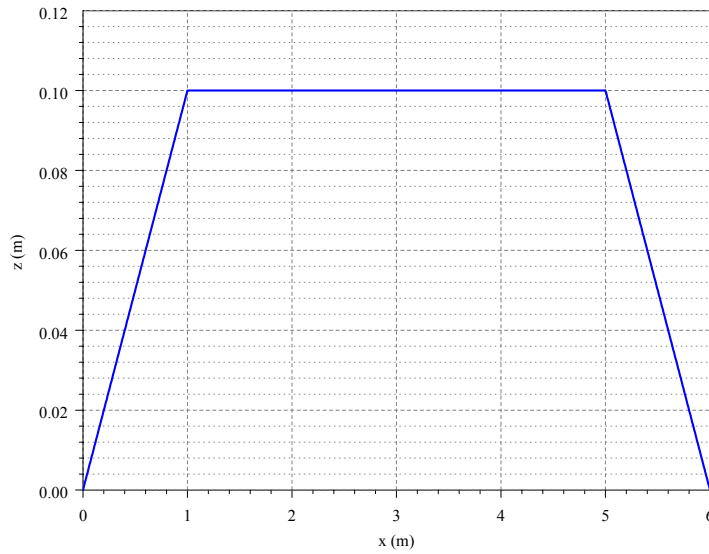


Figure 7.21: Standard trapezoidal hump profile

After the simulations, maximum peak sprung mass accelerations versus vehicle speed in the range of 25-45kph for 4 different suspension systems are given in Figure 7.22.

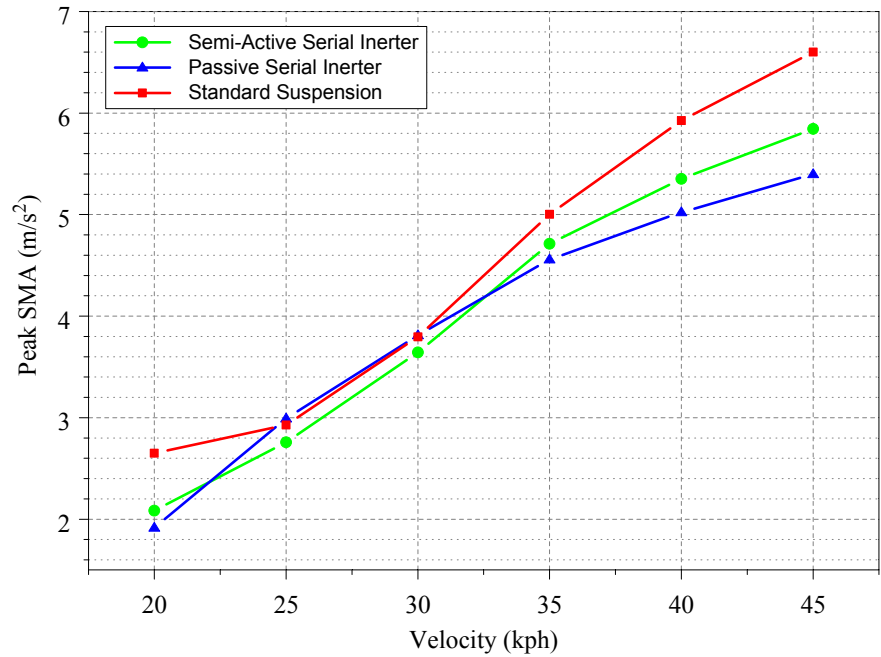


Figure 7.22: Peak sprung mass acceleration for different vehicle speeds

The inerter effect on the peak SMA is also positive for standard trapezoidal hump profile. As a results, peak SMA values are smaller in all vehicle speeds. Vehicle passing over standard trapezoidal hump is illustrated in Figure 7.23 using the vehicle parameters given in Table 7.1.

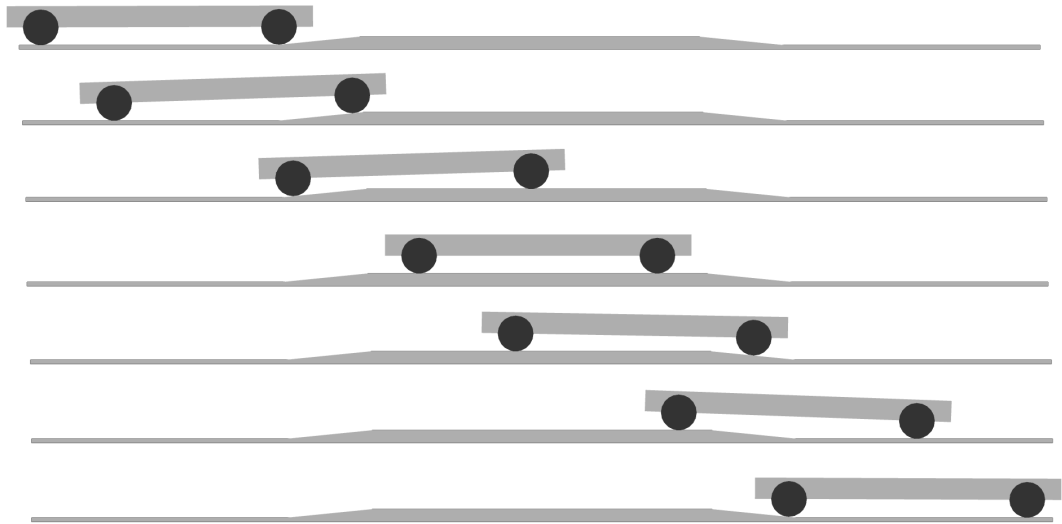


Figure 7.23: Vehicle passing over standard trapezoidal hump

Simulation results for standard trapezoidal bump are given in the following figures.

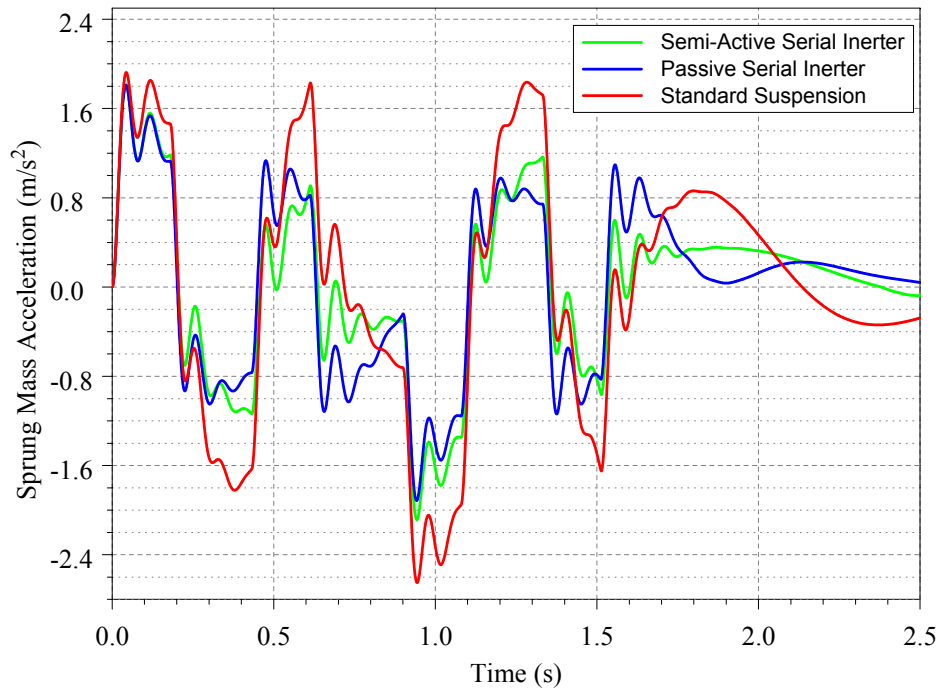


Figure 7.24: Standard trapezoidal hump simulation for $V=20\text{kph}$

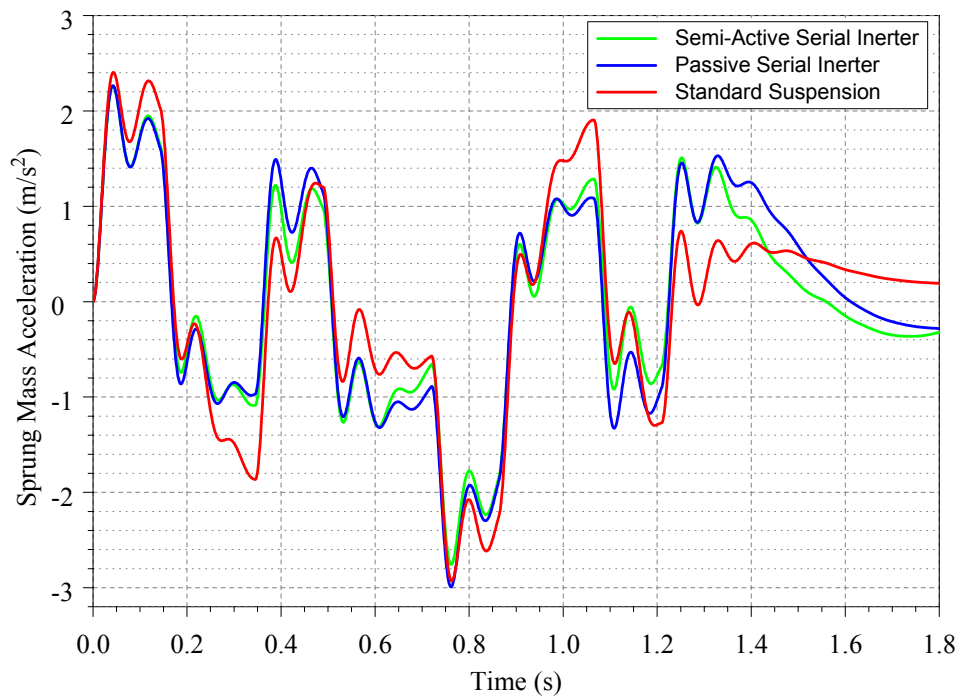


Figure 7.25: Standard trapezoidal hump simulation for $V=25\text{kph}$

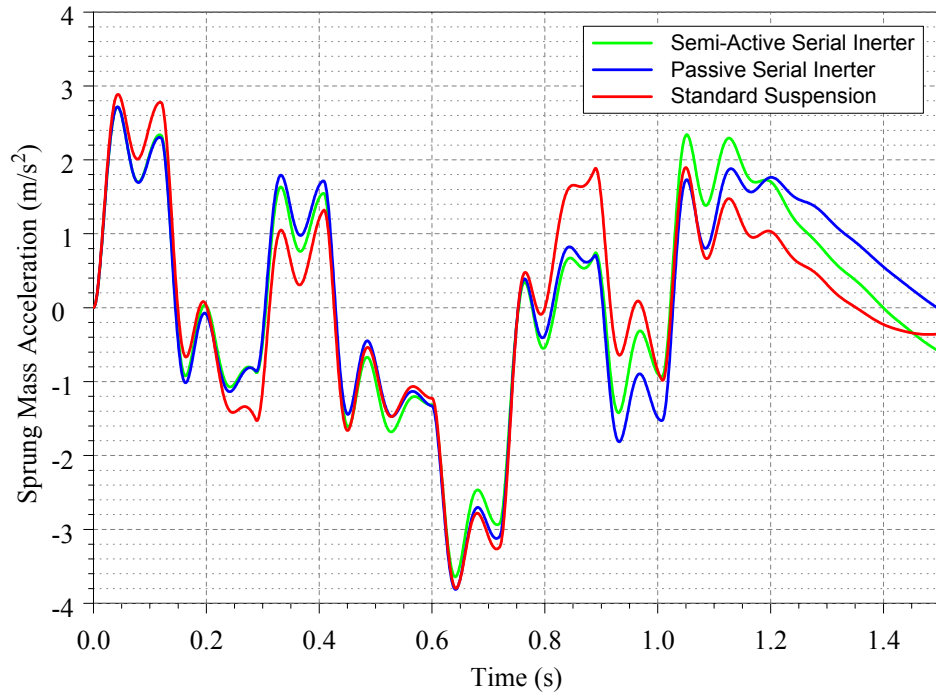


Figure 7.26: Standard trapezoidal hump simulation for $V=30\text{kph}$

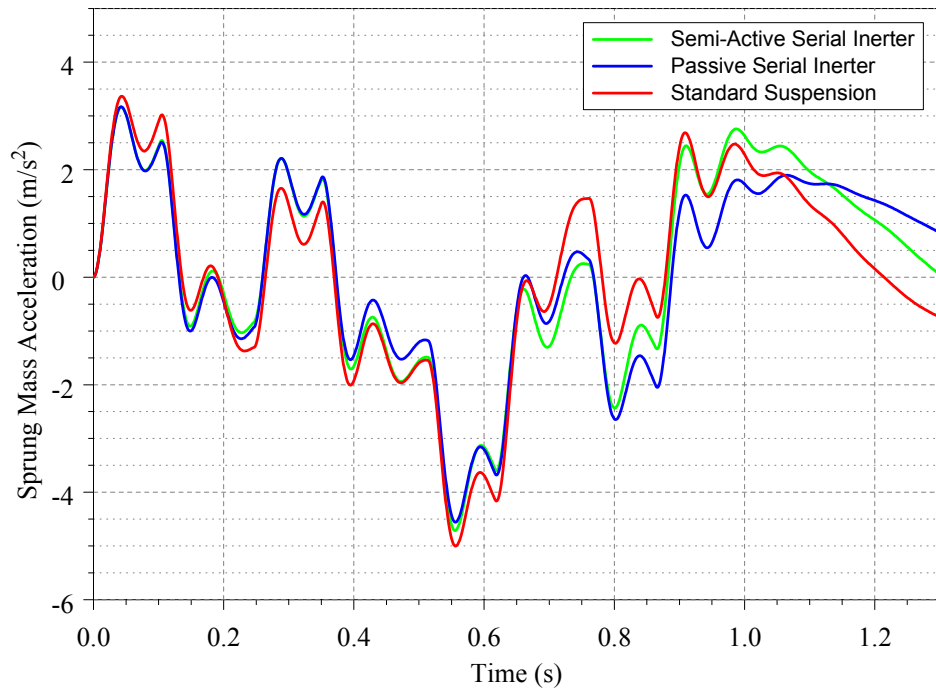


Figure 7.27: Standard trapezoidal hump simulation for $V=35\text{kph}$

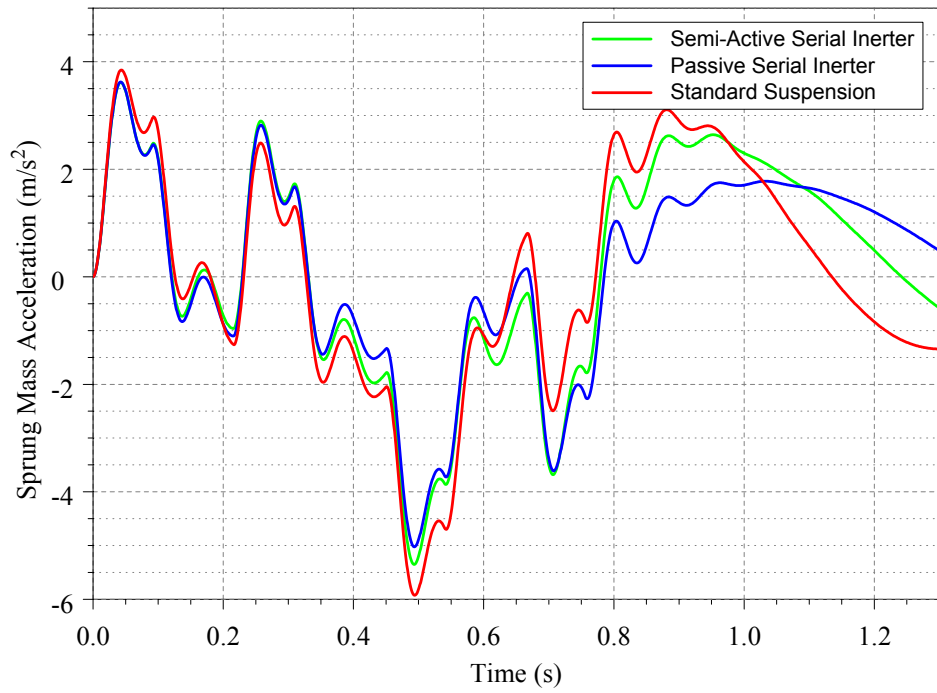


Figure 7.28: Standard trapezoidal hump simulation for $V=40\text{kph}$

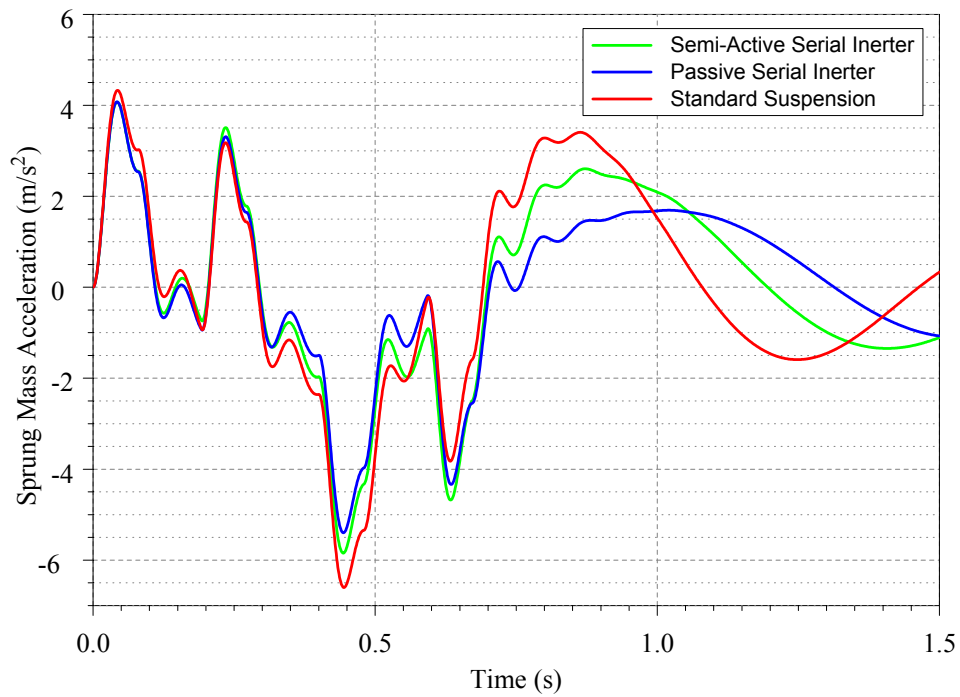


Figure 7.29: Standard trapezoidal hump simulation for $V=45\text{kph}$

The situation is almost same for the standard circular hump profile. In this case, for rela-

tively low velocities, time domain characteristics are better than the standard suspension with both passive and semi-active serial inerter. In short, inerter is also advantageous for standard trapezoidal hump profiles.

CHAPTER 8

CONCLUSION AND FUTURE WORK

8.1 Conclusion

In this thesis, passive and semi-active serial inerter are implemented on quarter-car and half-car models and their effect on ride comfort and road holding is investigated by using ISO criteria and ISO road profiles. In conclusion, the following comments can be made:

- Since the force applied to a mass by an inerter is directly proportional with acceleration difference between two terminals, it is implemented on the sprung mass rather than the sprung mass. It creates an effect which reduces the acceleration of the sprung mass.
- Considering the passive parallel inerter, it can be concluded that high inertance constant causes a reduction in sprung mass acceleration. However, it increases the magnitude of the wheel-hop motion while decreasing its natural frequency. In other words, with parallel passive inerter, comfortable suspension system with reduced road holding abilities will be designed. Therefore, parallel passive inerter studies are not included.
- Considering the passive serial inerter, it can be stated that the second spring-damper elements parallel to inerter element cause a relaxation in the system in terms of ride comfort. However, the need for a vertical space will be too much with softer springs. Inerter element decreases the need for the vertical space while keeping the ride comfort superior to standard suspension system. It is shown that around 5 percent reduction is obtained by passive serial inerter configuration compared to standard suspension while keeping road holding performance as high as possible and vertical space requirement lower than the initial system.
- Semi-active inerter concept is introduced and applied successfully to the serial inerter arrangement. Semi-active serial inerter configuration provides 10 percent reduction in sprung mass acceleration compared to passive serial inerter and 15 percent reduction in sprung mass acceleration compared to standard suspension. Since the energy requirement for a semi-active system is significantly lower than the active system, the only drawback of this system will be its complex structure consisting of MR fluids, controllers, algorithms, etc.

- Both passive and semi-active inerter configurations are also successful at reducing the peak and overall sprung mass acceleration when the vehicle encounters a standard type of a hump profile.
- Practical implementation of the inerters were made at different configurations, as stated in Chapter 1 - literature review section. Some of those configurations have different physical problems that are ignored by the researchers, even though they were aware of them. The serial inerter configuration proposed in this thesis is a physically realizable system and it does not cause any problem such as damper drift, stiction, etc. The architecture of the passive serial inerter is clearly explained and a remedy to overcome the vertical spacing requirement is suggested in Chapter 2. The only disadvantage of this system is the addition of the another spring - damper couple to the system.
- The reason for the utilization of methods provided by ISO standards is that the more accurate, realistic and acceptable analysis results can be obtained. Road profiles generated by methods suggested by [16] provide a basis for other researchers to compare their results with the ones presented in this thesis.
- The optimization using random road profiles are made for passive serial inerter configuration. The change of inertance parameter is not related with the road class. In other words, one can tune the suspension system easily by using only one inerter parameter obtained as a result of a single optimization process.
- For simplified analysis cases, some suspension parameters are kept constant. However, other parameters can be optimized as well for further fine tuning purposes. This is the advantage of the introduction of a new parameter, inertance, to the system.

8.2 Future Work

The following suggestions can be given in order to improve the study:

- Road holding performance of a suspension system with inerter superior to standard suspension can be modeled and investigated.
- Semi-active inerter and semi-active damper concepts can be implemented to the system at the same time and the effects on the performance can be analyzed.
- Different semi-active control systems can be implemented to the semi-active inerters.
- Different physically realizable inerter configurations can be made and the consequences on the system performance can be investigated.
- Configurations given in this thesis can be applied not only to standard passenger vehicle but also to heavy vehicles.
- Non-linearity of the inerter device can be investigated.

REFERENCES

- [1] R. Rajamani. *Vehicle dynamics and control*. Springer Science+Business Media Inc., 2006.
- [2] M. C. Smith. The inerter concept and its application. In *Society of Instrument and Control Engineers (SICE) Annual Conference*, 1999.
- [3] F. C. Wang, M. F. Hong, and T. C. Lin. Designing and testing a hydraulic inerter. *Proceedings of the Institution of Mechanical Engineers Part C-Journal of Mechanical Engineering Science*, 225(C1):66–72, 2011.
- [4] M. C. Smith and F. C. Wang. Performance benefits in passive vehicle suspensions employing inerters. *Vehicle System Dynamics*, 42(4):235–257, 2004.
- [5] M. C. Smith, Z. Q. Chen, C. Papageorgiou, F. Scheibe, and F. C. Wang. The missing mechanical circuit element. *IEEE Circuits and Systems Magazine*, pages 10–26, 2009.
- [6] F. C. Wang, C. H. Yu, M. L. Chang, and M. Hsu. The performance improvements of train suspension systems with inerters. In *Proceedings of the 45th IEEE Conference on Decision & Control*, 2006.
- [7] G. Richards. More opera than soap. *Engineering & Technology*, 20 June - 10 July 2009:38–41, 2009.
- [8] UC. <http://www.eng.cam.ac.uk/news/stories/2008/mclaren/>, 08 2008.
- [9] M. C. Smith and B. Gartner. Damper and inertial hydraulic device patent wo 2011/095787 a1, August 2011.
- [10] Lotus-Renault. Fluid inerter patent wo 2011/089373 a1, July 2011.
- [11] ISO. Mechanical vibration and shock - evaluation of human exposure to whole-body vibration. Technical Report 2631-1:1997, International Organization for Standardization, 1997.
- [12] M. C. Smith. Force-controlling mechanical device patent wo 2003/005142 a1, February 2002.
- [13] F. C. Wang, C. W. Chen, L. M. K., and M. F. Hong. Performance analyses of building suspension control with inerters. In *Proceedings of the 46th IEEE Conference on Decision and Control*, 2007.
- [14] S. M. Savaresi, C. Poussot-Vassal, C. Spelta, O. Sename, and L. Dugard. *Semi-Active Suspension Control Design for Vehicles*. Elsevier Ltd., 2010.
- [15] E. Guglielmino, T. Sireteanu, C. W. Stammers, G. Ghita, and M. Giuclea. *Improved Vehicle Ride and Road Friendliness*. Springer-Verlag London Limited, 2008.

- [16] ISO. Mechanical vibration - road surface profiles - reporting of measured data. Technical Report 8608, International Organization for Standardization, 1995.
- [17] J. S. Arora. *Introduction to Optimum Design*. Wiley, 2nd edition, 2004.
- [18] N. J. Mansfield. *Human Response to Vibration*. CRC Press LLC, 2005.
- [19] Ts6283, turkish standard.
- [20] <http://www.highways.gov.gh/tcm/rh/th>, July 2013.

APPENDIX A

SIMULINK MODELS OF HALF-CAR MODELS

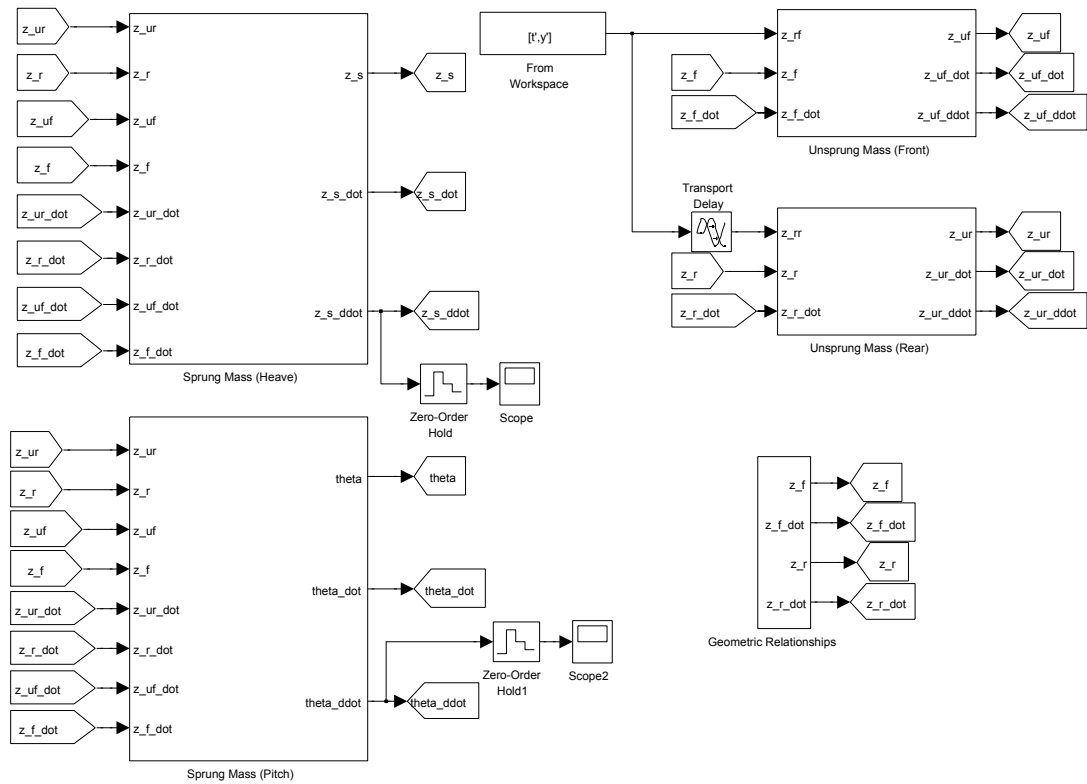


Figure A.1: Overview of half-car model of standard suspension

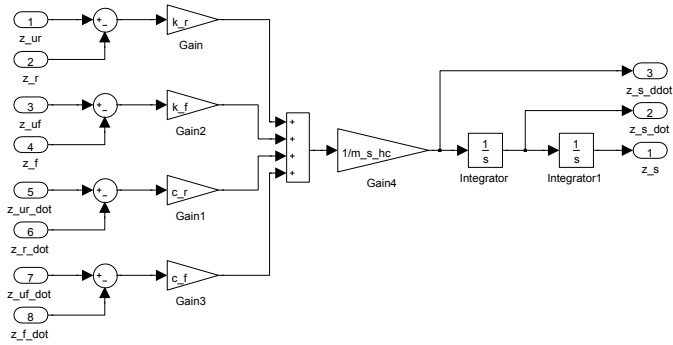


Figure A.2: Heave block of half-car model of standard suspension

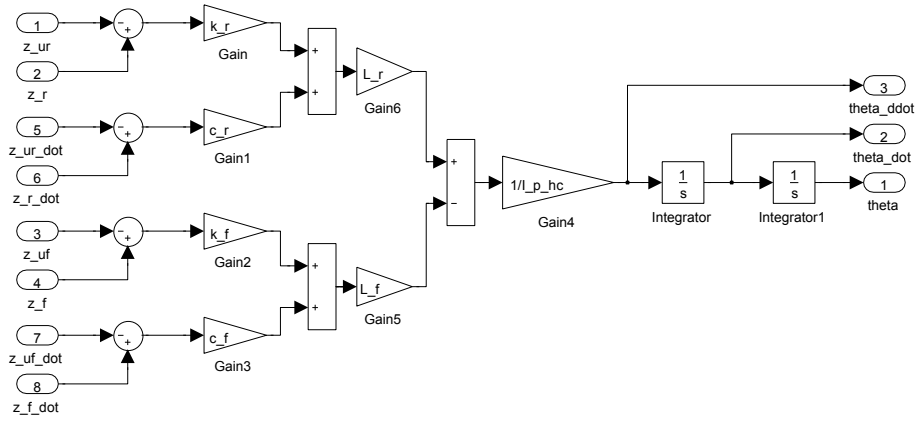


Figure A.3: Pitch block of half-car model of standard suspension

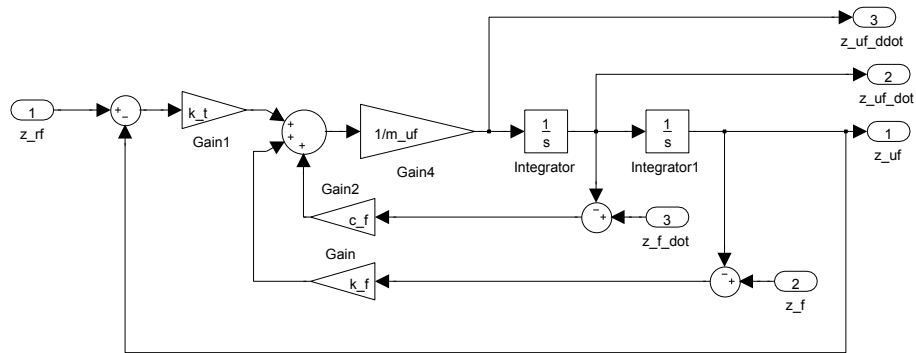


Figure A.4: Front unsprung mass block of half-car model of standard suspension

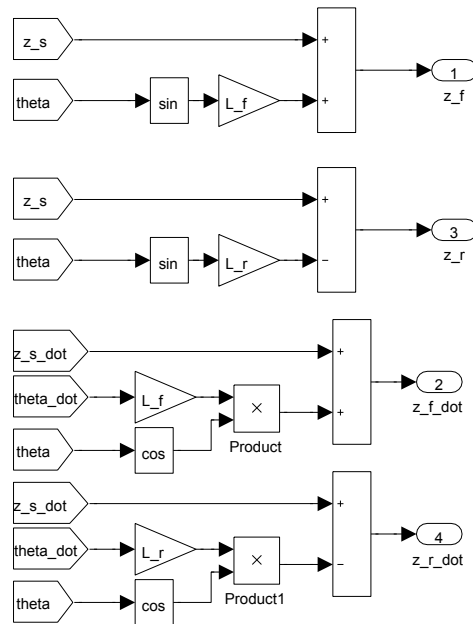


Figure A.5: Geometric relations block of half-car model of standard suspension

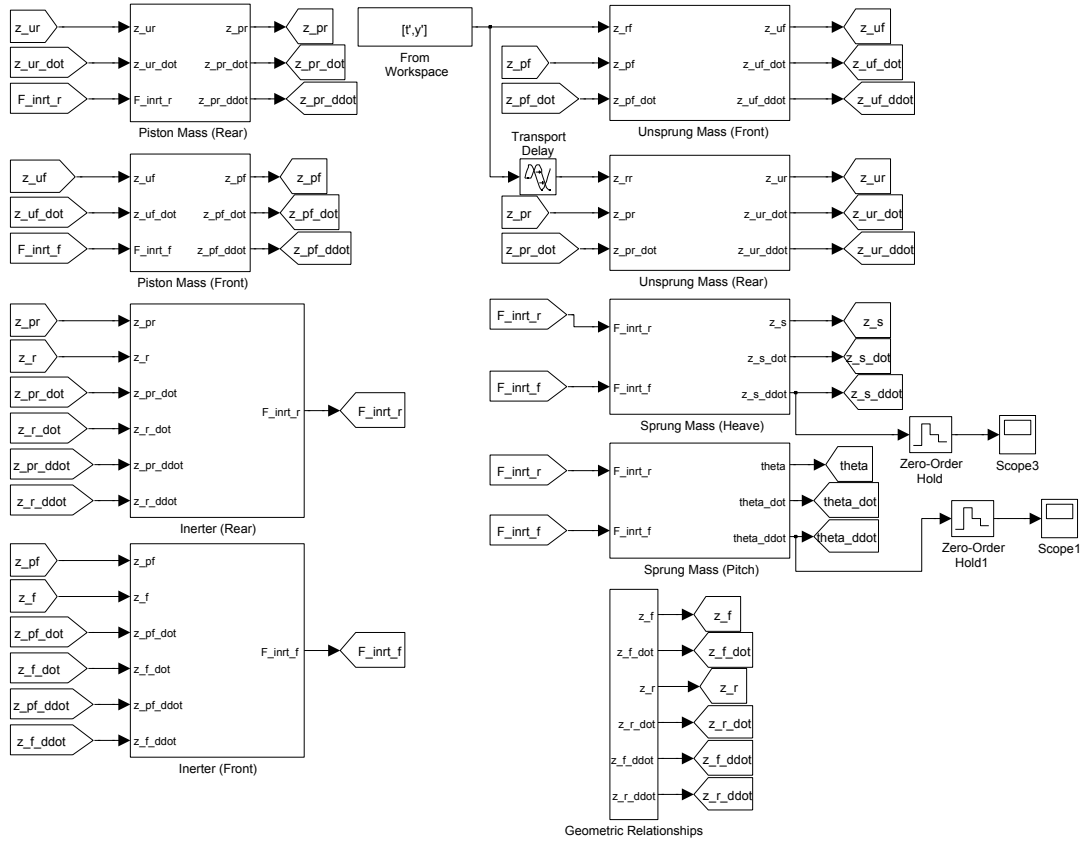


Figure A.6: Overview of half-car model of semi-active serial inerter

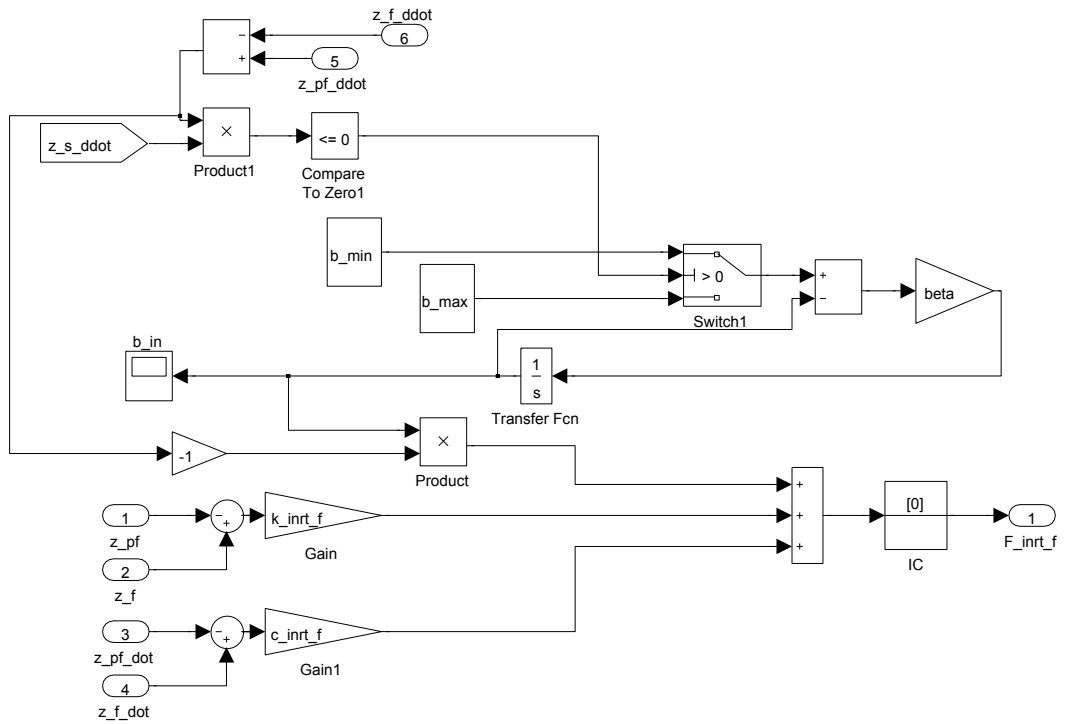


Figure A.7: Controller block of half-car model of semi-active serial inerter